NASA TECHNICAL MEMORANDUM

NASA TM X- 62,384

NASA TM X-62,384

OPTIMAL CONTROL THEORY INVESTIGATION OF PROPROTOR/WING RESPONSE TO VERTICAL GUST

Juanita K. Frick and Wayne Johnson

Ames Research Center
and
U. S. Army Air Mobility R&D Laboratory
Moffett Field, Calif. 94035

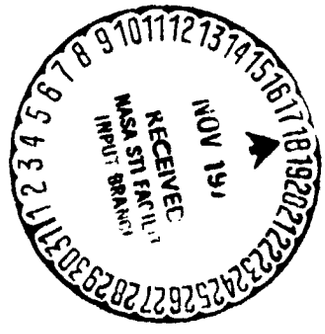

September 1974

NOMENCLATURE

A	matrix of coefficients of equations of motion
B	control matrix in equations of motion
C	gust input matrix in equations of motion
H	system transfer function
J	quadratic performance index
K	linear state variable feedback gain matrix
L	gust correlation length
p	wing torsion degree of freedom
q_1	wing vertical bending degree of freedom
q_2	wing chordwise bending degree of freedom
Q	matrix of weights on state variables in quadratic performance index (normally diagonal)
R	matrix of weights on control inputs in quadratic performance index (normally diagonal)
R	rotor radius
S_w	gust spectrum
S_β	spectrum of state variable response to gust, $S_\beta = \|H\|^2 S_w$
u	gust input vector
v	control vector
V	forward speed
x	state variable vector
β	blade flap degree of freedom; or amplitude of tip path plane tilt response, $(\beta_{1c}^2 + \beta_{1s}^2)^{1/2}$
β_o	rotor coning degree of freedom
β_{1c}	rotor tip path plane pitch degree of freedom

β_{1s} rotor tip path plane yaw degree of freedom

γ blade Lock number

δ_F wing flap input

δ_3 pitch/flap coupling

ζ blade lag degree of freedom; or amplitude of cyclic lag response, $(\zeta_{1c}^2 + \zeta_{1s}^2)^{1/2}$

ζ damping ratio of eigenvalue, $- \mathrm{Re}\lambda/|\lambda|$

ζ_o rotor collective lag degree of freedom

$\dot{\zeta}_o$ time derivative of ζ_o — rotor speed perturbation for windmilling rotor case

ζ_{1c} rotor cyclic lag degree of freedom

ζ_{1s} rotor cyclic lag degree of freedom

θ_o rotor collective pitch input

θ_{1c} rotor lateral cyclic pitch input

θ_{1s} rotor longitudinal cyclic pitch input

λ eigenvalue (root) of system

ν_β rotating natural frequency of blade flap motion

ν_ζ rotating natural frequency of blade lag motion

σ_w rms gust velocity

σ_β rms response of state variable

$\sigma_{\dot{\beta}}$ rms velocity of state variable

$\sigma_{\ddot{\beta}}$ rms acceleration of state variable

ω frequency (in transfer function or spectrum)

Ω rotor rotational speed

$(\dot{})$ time derivative

OPTIMAL CONTROL THEORY INVESTIGATION OF PROPROTOR/WING RESPONSE TO VERTICAL GUST

Juanita K. Frick* and Wayne Johnson*

U.S. Army Air Mobility R&D Laboratory
Ames Research Center
Moffett Field, California

SUMMARY

Optimal control theory is used to design linear state variable feedback to improve the dynamic characteristics of a rotor and cantilever wing representing the tilting proprotor aircraft in cruise flight. The response to a vertical gust and system damping are used as criteria for the open and closed loop performance. The improvement in the dynamic characteristics achievable is examined for a gimballed rotor and for a hingeless rotor design. Several features of the design process are examined, including: using only the wing or only the rotor dynamics in the control system design; the use of a wing flap as well as the rotor controls for inputs; and the performance of the system designed for one velocity at other forward speeds.

INTRODUCTION

The tilting proprotor aircraft is a promising concept for short haul, V/STOL missions. The successful application of this concept will require an aircraft with good ride qualities. The combination of large flapping rotors operating at high inflow ratio on the tips of flexible wings leads to increased response to atmospheric turbulence (compared to a conventional aircraft of equivalent size), and hence increases the desirability for an automatic control system to improve the dynamic characteristics. This report is an examination of the basic features of the control systems and design techniques required for this vehicle.

To represent the tilting proprotor aircraft in cruise flight, a mathematical model for a rotor in axial flight on the tip of a cantilever wing is used. While the design of actual control systems will of course require a model of the complete aircraft dynamics, the proprotor and cantilever wing model includes the basic features of the dynamic behavior and hence is satisfactory for an investigation of the basic control system characteristics. Optimal control theory is used to design linear state variable feedback to minimize a quadratic performance index. As a criterion for the open and closed

---

*Research Scientist, Large Scale Aerodynamics Branch, NASA-Ames Research Center

loop performance of the system, the response to a vertical gust is examined. Of specific interest are the flap and lag response of the rotor blades, and the vertical acceleration of the wing. The damping of the wing modes is also a critical indicator of the dynamic characteristics. The improvement of the dynamic characteristics achievable with such control systems is examined for two proprotor designs — a gimballed, stiff-inplane rotor and a hingeless, soft-inplane rotor. Then several features of the design process are investigated, including: the effect of considering just the rotor or just the wing dynamics in the control system design; the use of a wing flap as well as the rotor controls for inputs; and the performance of the system designed for one velocity at other cruise speeds.

PROPROTOR AND CANTILEVER WING THEORETICAL MODEL

The theory developed in reference 1 will be used for the mathematical model of the proprotor and cantilever wing dynamics.

Figure 1 shows the proprotor configuration considered for the theory. The rotor is operating in high inflow axial flight on a cantilever wing. This configuration incorporates the features of greatest importance to the aircraft: the high inflow aerodynamics of a flapping rotor in axial flow and the coupled dynamics of the rotor/pylon/wing aeroelastic system. Many features of the aircraft-coupled wing and rotor motion may be studied with such a model, theoretically and experimentally, with the understanding that the model must eventually incorporate the entire aircraft.

The theoretical model of the proprotor consists of nine degrees of freedom: the first mode flap (out of disk plane) and lag (inplane) motion for each of three blades; and vertical bending, chordwise bending, and torsion for the cantilever wing. The degrees of freedom of the individual rotor blades are combined into degrees of freedom representing the motion of the rotor as a whole in the nonrotating frame. Thus the rotor flap motion is represented by the tip path plane pitch and yaw (β_{1c} and β_{1s}) and coning (β_0) degrees of freedom. The rotor lag motion is represented by cyclic lag (ζ_{1c} and ζ_{1s}, the lateral and vertical shift of the rotor net center of gravity) and collective lag (ζ_0). Wing vertical and chordwise bending (q_1 and q_2) and torsion about the elastic axis (p) complete the nine degrees of freedom.

The rotor blade motion is represented by first mode flap and lag motion and is assumed to be pure out-of-plane and pure inplane deflections, respectively, of the blade spar. For the gimballed and hingeless rotor blades considered here (except for the flap mode of the gimba-led rotor), there is, in fact, some elastic coupling of the flap and lag modes, so that both out-of-plane and inplane motion participate in each mode. In the coefficients giving the aerodynamic forces on the rotor, it is further assumed that the mode shapes are proportional to the radial distance from the hub, i.e., equivalent to rigid body rotation about a central hinge. The model based on these two assumptions, which considerably simplify the aerodynamic and structural terms of the rotor equations, proves to be an adequate representation of the fundamental proprotor dynamics.

The theoretical results presented here will be for the rotor operating unpowered, i.e., windmilling or autorotation operation. An important element of autorotation dynamic behavior is the rotor speed perturbation. With no restraint on the rotor shaft rotation, this degree of freedom has considerable influence on the aeroelastic behavior of the proprotor and wing. The rotor speed perturbation is modeled by using the collective lag mode ζ_0. By setting the rotating natural frequency of this mode to zero, i.e., no spring restraint, ζ_0 becomes equivalent to the rotor speed perturbation (the natural frequencies of the cyclic lag modes, ζ_{1c} and ζ_{1s}, are not set to zero).

The proprotor operating in high inflow has simpler aerodynamics than the helicopter rotor in forward flight. As in the case of low inflow (i.e., the hovering helicopter rotor), the symmetry of axial flow results in a corresponding symmetry in the equations of motion; it also means that the equations of motion have constant coefficients. In high inflow there is the additional fact that both out-of-plane and inplane motions of the blade produce significant angle-of-attack changes at the sections, and the resulting lift increment has significant components both normal to and in the disk plane. Hence the rotor aerodynamic forces are primarily due to the lift changes produced by angle of attack changes, i.e., the C_{ℓ_α} terms in the aerodynamic coefficients. This is in contrast to low inflow, where, for example, the inplane blade motion produces significant contributions to the forces by the lift and drag increments due to the dynamic pressure changes, i.e., the C_ℓ and C_d terms in the aerodynamic coefficients. As a result, high inflow aerodynamics are well represented by considering only the C_{ℓ_α} forces. If, in addition, the lift curve slope is assumed constant, then the aerodynamic coefficients depend only on two parameters, the Lock number γ and the inflow ratio $V/\Omega R$.

This nine degree of freedom model will have nine roots or eigenvalues (really nine pairs of complex roots) and nine corresponding eigenvectors or modes. Each mode involves motion of all nine degrees of freedom. The modes are identifiable by their frequencies (which are near the nonrotating uncoupled natural frequencies for the rotor modes), and also by the participation of the degrees of freedom in the eigenvector. The nine modes will be denoted as follows (the approximate uncoupled, nonrotating frequency of the mode is given in parentheses):

p	wing torsion (ω_p)
q_1	wing vertical bending (ω_{q_1})
q_2	wing chordwise bending (ω_{q_2})
β	coning (ν_β)
β+1	high frequency flap ($\nu_\beta + \Omega$)
β-1	low frequency flap ($\nu_\beta - \Omega$)
ζ	collective lag (ν_ζ)
ζ+1	high frequency lag ($\nu_\zeta + \Omega$)
ζ-1	low frequency lag ($\nu_\zeta - \Omega$)

The basic theoretical model will consist of all degrees of freedom, autorotation operation, and just the C_{ℓ_α} rotor aerodynamic forces. The wing aerodynamic forces are also included, based on a strip theory calculation.

The theory described above will be applied to two full-scale proprotors. The first is a 7.6 m (25 ft) diameter gimballed, stiff-inplane proprotor (designed and constructed by the Bell Helicopter Company and tested in the Ames 40 by 80 Foot Wind Tunnel in July 1970). The second is a 7.9 m (26 ft) diameter hingeless, soft-inplane proprotor (designed and constructed by the Boeing Vertol Company and tested in the Ames 40 by 80 Foot Wind Tunnel in August 1972). As far as their dynamic characteristics are concerned, the two rotors differ primarily in the placement of the nonrotating natural frequencies of the blade flap and lag motions. The Bell rotor has a gimballed hub and stiff-inplane cantilever blade attachment to the hub, hence ν_β = 1/rev (nearly, for it does have a weak hub spring) and ν_ζ > 1/rev; it also incorporates positive pitch/flap coupling (δ_3 < 0) to increase the blade flap/lag stability. The Boeing rotor has a cantilever or hingeless hub with soft-inplane blade attachment, hence ν_β > 1/rev and ν_ζ < 1/rev. The different placement of the blade frequencies at the opposing extremes of the possible choices, results in quite different dynamic characteristics for the two aircraft.

The rotors are described in references 2 to 5. Table 1 gives the major parameters of the rotors and cantilever wings used in the full scale tests (a more complete description of the parameters required by the theory is given in ref. 1). The wing frequencies in the theory were matched to the experimentally measured values by adjusting the spring constants. The typical blade frequencies are shown in figures 2 and 3 for the Bell and Boeing rotors, respectively. The variation of the Bell lag frequency (fig. 2(b)) with $V/\Omega R$ is due to the collective pitch change. The Boeing rotor blade frequencies vary little with collective pitch ($V/\Omega R$) since the blade has nearly isotropic stiffness at the root.

The theory was demonstrated to be an accurate representation of proprotor and cantilever wing dynamics in reference 1, by comparison with full scale wind tunnel test results for the gimballed and hingeless rotors; some of these results are also given in reference 6. References 1 and 6 discuss the basic (uncontrolled) dynamics of the proprotor and cantilever wing configuration. References 1 and 6 also discuss the influence of various elements of the theory, including the modelling used for the wing and rotor blade aerodynamics, the influence of the rotor lag degree of freedom, and the role of the rotor rotational speed degree of freedom (windmilling rotor).

STATE EQUATIONS OF MOTION

The equations of motion describing the proprotor and wing are of the form:

$$A_2\ddot{\vec{x}}_1 + A_1\dot{\vec{x}}_1 + A_0\vec{x}_1 = B_0\vec{v} + C_0\vec{u}$$

where

$\vec{x}_1$ = proprotor degrees of freedom (System State)

$\vec{v}$ = control components (System control)

$\vec{u}$ = gust components (external disturbance)

and A_2, A_1, A_o, B_o, C_o are constant coefficient matrices.

One or more degrees of freedom may be absent from $A_o x$, i.e., a column of A_o may be zero (in this case it occurs for the ζ_o degree of freedom). This means that there is no spring restraint on these degrees of freedom, making the equations for them actually first order, with the results that some of the eigenvalues of the second order equation will be zero. It is convenient to reduce the system to one of first order. When the substitution

$$\vec{x}_2 = \dot{\vec{x}}_1$$

is made, then

$$\dot{\vec{x}}_2 = -A_2^{-1}A_1\vec{x}_2 - A_2^{-1}A_o\vec{x}_1 + A_2^{-1}B_o\vec{v} + A_2^{-1}C_o\vec{u}$$

and the system becomes

$$\begin{bmatrix} \vec{x}_2 \\ \vec{x}_1 \end{bmatrix}^{\cdot} = \begin{bmatrix} -A_2^{-1}A_1 & -A_2^{-1}A_o \\ I & 0 \end{bmatrix}\begin{bmatrix} \vec{x}_2 \\ \vec{x}_1 \end{bmatrix} + \begin{bmatrix} A_2^{-1}B_o \\ 0 \end{bmatrix}\vec{v} + \begin{bmatrix} A_2^{-1}C_o \\ 0 \end{bmatrix}\vec{u}$$

or,

$$\dot{\vec{x}} = A\vec{x} + B\vec{v} + C\vec{u} \qquad (1)$$

For the proprotor and cantilever wing system, the state variable vector $\vec{x}$ is comprised of the displacement and velocity of each of the nine degrees of freedom described above. The input vector $\vec{v}$ is comprised of the rotor collective and cyclic pitch controls (θ_o, θ_{1c}, θ_{1s}). Later a wing flap input (δ_F) will also be included in $\vec{v}$. For the external disturbance $\vec{u}$, only the vertical gust component will be considered here.

SYSTEM PERFORMANCE CRITERIA

The performance of the system is partly determined from computations of its eigenvalues. The system is stable if the real parts of the eigenvalues are negative; as the real parts become more negative, the stability of the system increases. The damping ratio ζ (fraction of critical damping) is

$$\zeta = \frac{-Re(\lambda)}{|\lambda|}$$

or, on a root locus plot, the cosine of the angle between the negative real axis and the line drawn from the eigenvalue to the origin. The system becomes more damped as ζ increases, and is critically damped for $\zeta = 1$.

In addition to the stability and damping of the system, the performance is evaluated by observing the response of the system to excitation by the

vertical component of a gust. The gust used is described by the Von Kármán gust spectrum as

$$S_w(\omega) = \frac{\sigma_w^2 L}{2\pi V} \frac{1 + 8/3\,[1.339\,(\omega L/V)]^2}{\{1 + [1.339\,(\omega L/V)]^2\}^{11/6}}$$

where ω is the frequency (nondimensionalized by Ω); L the gust correlation length (nondimensionalized by R); σ_ω the rms value of the gust velocity (nondimensionalized by ΩR); and V is the aircraft speed (nondimensionalized by ΩR). L is approximately 1524 m (5000 ft) for high altitude and from 120 to 150 m (400 to 500 ft) for low altitude. A lower value of L gives a stronger high frequency content in the gust spectrum; i.e., the break frequency, $\sim V/L$, is larger. For this analysis the L used was 122 m (400 ft). More details of this gust model are given in references 7-10.

The frequency response of the system to vertical gust is given by

$$\dot{\bar{x}} e^{i\omega t} = H(\omega)\alpha_G e^{i\omega t}$$

with the transfer function for frequency ω,

$$H(\omega) = [-A(A^2 + \omega^2 I)^{-1}C] + i[-\omega(A^2 + \omega^2 I)^{-1}C]$$

where A and C are matrices of (1). The static response is obtained by calculating $H(\omega)$ for $\omega = 0$ [$H(0) = -A^{-1}C$].

The power spectrum of the response of the state variable β is $S_\beta = |H(\omega)|^2 S_w$, hence the rms response σ_β is given by

$$\sigma_\beta^2 = \int_{-\infty}^{\infty} S_\beta \, d\omega = \int_{-\infty}^{\infty} |H(\omega)|^2 S_w d\omega$$

(see refs. 7-9). Since S_β is an even function,

$$\int_{-\infty}^{\infty} S_\beta \, d\omega = 2\int_{0}^{\infty} S_\beta \, d\omega \quad .$$

Computational values for the integration limits 0 and ∞ were numerically determined to be $e^{-6}(V/L)$ and $e^{8}(V/L)$, respectively, as using more extreme limits did not contribute significantly to the value of the integral.

The rms levels of velocity $\sigma_{\dot\beta}$ and acceleration $\sigma_{\ddot\beta}$ are similarly given by

$$\sigma_{\dot\beta}^2 = \int_{-\infty}^{\infty} \omega^2 S_\beta \, d\omega$$

$$\sigma_{\ddot{\beta}}^2 = \int_{-\infty}^{\infty} \omega^4 S_\beta \, d\omega$$

Also, the number of peaks, or zero crossings with positive slope, per rotor revolution is calculated by

$$N = \frac{\sigma_{\dot{\beta}}}{\sigma_\beta}$$

This equation for N comes from the expression for the expected number of crossings of the threshold α per revolution, assuming a Gaussian probability distribution,

$$E[N_+(\alpha)] = \frac{\sigma_{\dot{\beta}}}{\sigma_\beta} e^{-1/2(\alpha/\sigma_\beta)^2} \quad ,$$

with $\alpha = 0$ for threshold level of zero. The ratio of the number of crossings of the level α to the number of zero crossings gives the fraction of cycles in which the response β exceeds threshold level α:

$$f = e^{-1/2(\alpha/\sigma_\beta)^2}$$

So, to determine the fraction of cycles in which the response β exceeds the rms level σ_β,

$$f = e^{-1/2} = 60.7\% \text{ of the cycles.}$$

Similarly, to find the percent cycles in which the response β exceeds n multiples of the rms response

$$f = e^{-n^2/2}$$

is computed. For example, for $n = 2$, β exceeds $2\sigma_\beta$ 13.5% of the cycles; for $n = 3$, β exceeds $3\sigma_\beta$ 1.1 percent of the cycles.

OPTIMAL CONTROL PROBLEM

Given the system (1), the control $\vec{v}$ is input to the system whose output is then measured by the response to an external disturbance $\vec{u}$; a system of this form is open loop. In a closed loop system, a control $\vec{v}^*$, based on the response of the system is input, or fed back to reduce the response and increase the system stability; i.e., the feedback control $\vec{v}^*$ links the output and the input of the system, closing the loop. The system then becomes

$$\dot{\vec{x}} = A\vec{x} + B(\vec{v} + \vec{v}^*) + C\vec{u} \qquad (2)$$

The control $\vec{v}^*$ to be determined here will be an optimal control law, optimal in the sense that the maximum displacements of state and control are bounded, thus minimizing the measure of performance, or performance index,

$$J = \int_0^\infty (\vec{x}^T Q \vec{x} + \vec{v}^{*T} R \vec{v}^*) dt \qquad (3)$$

The weighting matrices Q and R are somewhat arbitrary, as the magnitudes of the elements are not important; however, the size of R relative to Q, or the 'gain' = $\sqrt{Q/R}$, determines the level of feedback control. If R is large relative to Q, i.e., small gain, then to minimize J, control $\vec{v}$ must be small. This allows large values of $\vec{x}$ and is therefore loose control. If R is small relative to Q, i.e., large gain, then control $\vec{v}$ must be large for minimum J, allowing only small values of $\vec{x}$ and, hence, is tight control. Also important are the magnitudes of the elements of Q (and R) with respect to each other. If one state degree of freedom is to be controlled more than another, then its corresponding element of Q will be larger. Similarly, if one control is to be applied more than another, its corresponding element of R will be smaller. For this study, Q and R were chosen for simplicity to be diagonal matrices. In addition, the elements of Q corresponding to the derivative degrees of freedom are set to zero, since attempting to control the velocities while already controlling the displacements is redundant; it also amounts to a constraint on the frequency content of the state response as well as its magnitude, thus introducing the complexity of an additional parameter determining Q. Using the maximum displacement interpretation, Q and R may be represented by

$$Q = \begin{bmatrix} 0 & 0 \\ 0 & \ddots \\ & & \frac{1}{(x_{max})^2} \end{bmatrix}$$

$$R = \begin{bmatrix} \ddots & \\ & \frac{1}{(v_{max})^2} \end{bmatrix}$$

In the presentation of the optimal control results to follow, numbers will be given for Q and a gain. For example, the control for a nine degree of freedom system may be

Q = 5*.1, 4*1. (equivalent to .1, .1, .1, .1, .1, 1., 1., 1., 1.)

and GAIN = 10.

The numbers given for Q are the diagonal elements of the matrix Q corresponding to the displacement states; all other elements of the Q matrix are zero, including the diagonal elements corresponding to the velocities of the degrees of freedom.

For the matrix R, each control variable is given the weight $(GAIN)^{-2}$; hence R is a diagonal matrix

$$R = \frac{1}{(GAIN)^2} I$$

where I is the identity matrix.

Given Q and R, the optimal control problem is to find the control v^* for the system (2) which minimizes the performance index J, equation (3). Details of the formulation of the optimal control problem and its solution are given in references 11 and 12. This optimal control law is found to be linear feedback of the state:

$$\vec{v}^* = -K\vec{x} \quad \text{with} \quad K = R^{-1}B^T\bar{P}$$

The patrix $\bar{P}$ is the solution of the matrix Riccati equation

$$\bar{P}A + A^T\bar{P} - \bar{P}BR^{-1}B^T\bar{P} + Q = 0$$

Following references 11 and 12, to solve the Riccati equation for $\bar{p}$, the matrix

$$M = \begin{bmatrix} A & -BR^{-1}B^T \\ -Q & -A^T \end{bmatrix}$$

is constructed from the known matrices A, B, Q, and R. M has the property that its eigenvalues occur in pairs of equal magnitude but opposite sign. With the eigenvectors of M as columns, the matrix

$$T = \left[\begin{array}{c:c} T_- & T_+ \end{array}\right]$$

is constructed where the columns of T_- are the eigenvectors corresponding to the eigenvalues of M with negative real parts, and the columns T_+ are the eigenvectors corresponding to the eigenvalues with positive real parts. Since there are equal numbers of the eigenvalues having negative and positive real parts, T_- and T_+ have the same dimensions. T_- can be further partioned

$$T_- = \begin{bmatrix} X_- \\ \hdashline Y_- \end{bmatrix}$$

with X_- and Y_- having the same number of rows. The solution $\bar{P}$ is then

$$\bar{P} = Y_-X_-^{-1}$$

Now having solved for $\vec{v}^* = -Kx$, the closed loop system (2) becomes

$$\dot{\vec{x}} = A\vec{x} + B\vec{v} - BK\vec{x} + C\vec{u}$$

or

$$\dot{\vec{x}} = (A - BK)\vec{x} + B\vec{v} + C\vec{u} \ .$$

The matrix (A - BK) then replaces the A of (1) and the performance of the closed loop system may be evaluated and compared to the open loop performance.

RESULTS AND DISCUSSION

The optimal control theory methods will be used to design linear state variable feedback for two proprotor/cantilever wing designs -- a gimballed, stiff-inplane rotor and a hingeless, soft-inplane rotor. The rotors are assumed to be in windmilling operation. That should be a good model for the dynamics considered here since the engine/drive-train/governor dynamics will have a long time constant compared to the proprotor and wing modes. For the frequency range of interest here the rotor should behave as if windmilling even with a rotor-speed governor operating. This assumption may be less valid for the system longitudinal dynamics, where the rotor rotational speed degree of freedom has a particularly important role. Therefore this analysis is concerned primarily with the lateral/vertical dynamics of the proprotor and cantilever wing system – for example, the response of the wing vertical bending (q_1), tip path plane tilt (β_{1c} and β_{1s}), and cyclic lag (ζ_{1c} and ζ_{1s}) to vertical gusts. It should be noted however that the optimal control solution includes feedback and control of the longitudinal dynamics as well; the vertical gust input enters only in examining the system performance, not at all in the optimal control solution.

The primary criteria for the system performance will be the root mean square (rms) response of the rotor motion (σ_β and σ_ζ), the rms acceleration of the wing motion ($\sigma_{\ddot{q}_1}$, $\sigma_{\ddot{q}_2}$, and $\sigma_{\ddot{p}}$), and the damping ratio of the wing modes (q_1, q_2, p). The first is a measure of the rotor motion for an articulated rotor, or of the 1/rev blade loads for a hingeless rotor; the second is a measure of the airframe vibration due to the gust; and the last is a measure of the overall system dynamic stability. Normally the rms response and acceleration will be given as a ratio of closed loop to open loop values; occasionally the absolute magnitudes of the motion will also be examined. For the rotor motion, the rms value of the amplitude of the cyclic flap and lag motion is given – the square root of the sum of the squares of the 1C and 1S degrees of freedom ($|\beta| = (\beta_{1c}^2 + \beta_{1s}^2)^{1/2}$ and $|\zeta| = (\zeta_{1c}^2 + \zeta_{1s}^2)^{1/2}$. In addition to the damping ratio of the wing modes, complete root loci diagrams for the system will be given.

First, the optimal control results will be examined for a standard case to determine the improvement in the dynamics possible. Then the results will be examined for cases when the controller is designed considering only the wing or only the rotor. Next the effect of adding a wing flap to the available controls will be considered. Finally, the effect of cruise speed on the

control system design will be investigated, considering the performance with an optimal controller designed for each speed, and the performance with a controller designed for a single speed but operated for all speeds.

Open Loop Transfer Functions

Figures 4 and 5 show the open loop transfer functions for the Bell and Boeing rotors respectively (at $V/\Omega R = 0.7$, windmilling rotor). The magnitude of the response of each of the nine degrees of freedom to a vertical gust angle α_G is given. Also shown are the transfer functions multiplied by $\sqrt{S_w/S_w(0)}$ (where S_w is the gust spectrum, given above). The square of $|H| * \sqrt{S_w}$ is the spectrum of the response of the system to the gust, and its integral is the rms response. Note the prominence of the wing vertical bending mode resonance in the transfer function, even when multiplied by the gust spectrum. This implies that the wing and rotor dynamics have a significant role in the response, and hence in the control required. Figure 6 shows the gust spectrum, $\sqrt{S_w/S_w(0)}$ for $V/\Omega R = 0.7$. The gust spectrum has a very low corner frequency (around 0.025/rev) even at this high speed (i.e., the gust wavelength is very long). However, the square root of the gust spectrum only falls off as $S_w^{1/2} \sim \omega^{5/6}$. Hence the high frequency response — the resonances in the transfer function — contributes significantly to the gust response.

Gimballed, Stiff-Inplane Rotor

For the gimballed stiff-inplane rotor (Bell) and wing, Q = 5*.1, 4*1 and $V/\Omega R = 0.7$ was taken as the standard case. The values of Q were chosen so that the rms acceleration due to vertical gust achieved a fractional reduction that was roughly the same for both the wing and rotor degrees of freedom. The gain was varied from 0 to 40 with most of the effect occurring by 10 and leveling off from there. Figure 7 shows the results of this case. Part 7(a) shows that a substantial reduction in rms flap and lag motion is possible by applying suitable control. The reduction in the rms flap response is from 0.74 deg/deg at zero gain to around 0.17 deg/deg at high gain, indicating a 77 percent reduction in flap amplitude; so then, for a 6 m/sec (20 fps) rms gust (strong turbulence), the reduction in rms flap response is from 2 deg to 0.46 deg. Figure 7(b) shows that the number of peaks/revolution for β and ζ remain about the same order as the gain increases; however, there is some increase due to σ_x being reduced faster than $\sigma_{\dot{x}}$.

For wing vertical bending q_1, the dominant wing mode, figure 7(c) shows that the rms response achieves about a 45 percent reduction which for a 6 m/sec (20 fps) gust would correspond to reducing the rms vertical motion at the wing tip from about 4 cm (1.5 in.) to about 2 cm (0.8 in.). Also shown is the number of peaks/revolution (also in cycles/hour) and its corresponding reduction. A result of these response and peaks/rev reductions is a decrease in the cumulative wing fatigue. In figure 7(d) is shown a 55 percent reduction in the rms acceleration of q_1 which for a 6 m/sec (20 fps) gust reduces the rms vertical acceleration at the wing tip from about 1.25 g to about 0.57 g.

Figure 7(e) shows that both the wing and rotor rms acceleration due to vertical gust reduces significantly (55 percent to 75 percent) as gain increases. However, while the rotor motion ($\sigma_{\ddot{\beta}}$, $\sigma_{\ddot{\zeta}}$) continuously decreases with increase in gain, the reduction of the wing motion tends to reach an asymptotic limit. This implies that for a given Q, there is a limit to the reduction in wing motion possible, possibly due to the fact that the only controls are to the rotor and the ratio of wing motion to rotor motion is fixed (because of fixed Q). Figure 7 (f) shows that the rms response exhibits similar behavior to the acceleration with a 45 percent to 75 percent reduction achieved. In figure 7(g) there are again significant reductions in the steady state response as gain increases; however, in many cases the reduction is much less than for the rms response or acceleration. In all cases, the static response is not a good measure of rms response to gust, implying that the higher frequency dynamics have a large role in the gust response, especially the wing vertical bending resonance peak.

The damping ratios of the wing modes shown in figure 7(h) indicate a substantial increase; e.g., the wing vertical bending mode (q_1) damping increases from about 3.5 percent to about 12 percent of critical damping. Although the wing modes in particular show a leveling off at higher gain, the limit on wing control may not be a critical factor, as the damping increase achieved is substantial and probably all that would be required. However, this leveling off at high gain may be associated with the type of control and the criterion used, i.e., state variable control and the quadratic performance index.

The feedback gain matrix K in the expression $\vec{v} = -K\vec{x}$ for this case with gain = 10 is shown in table 2.

It was hoped that the matrix would show that measurements of only a few quantities and feedback to only a few inputs would dominate the control, i.e., many of the elements of K would be insignificant compared to a few dominant ones; for then the matrix would suggest a simpler control scheme (smaller matrix). Instead it is found that many of the 51 elements of K are of the same order, and few control elements could be considered unnecessary. Part of this complexity is due to the fact that the whole system is being controlled, not just the dynamics due to the response to vertical gust, which is not a design criterion but a measure of performance. The gain matrix is not without some pattern however; namely, there is some characteristic decoupling into lateral/vertical and longitudinal systems: θ_0, collective control, is obtained mainly from measurements of $\dot{\beta}_0$, $\dot{q}_2$, $\dot{\zeta}_0$, β_0, q_2, the longitudinal degrees of freedom; and θ_{1c}/θ_{1s}, cyclic control is obtained mainly from feedback of $\dot{\beta}_{1c}/\dot{\beta}_{1s}$, $\dot{q}$, $\dot{p}$, β_{1c}/β_{1s}, ζ_{1c}/ζ_{1s}, q_1, p, the vertical/lateral degrees of freedom. Even with this decoupling, the feedback is still quite involved however, but it does suggest the possibility of designing a controller for a reduced system; e.g., analyzing and designing a control system for the longitudinal dynamics on the basis of just the q_2, β_0, and ζ_0 degrees of freedom. A controller of this type must always be checked in operation with the complete system dynamics however.

The root locus in figure 8 further illustrates the effects discussed. There is an increase in the damping of the wing modes, leveling off at high gain. Also there is a continual large increase in the damping of the rotor lag modes but the flap modes show little significant change, though the flap and lag motion are highly coupled by the rotor aerodynamics due to the high inflow ratio. Because of this coupling, the labeling of the β-1 and ζ-1 modes is somewhat ambiguous (on this plot as well as the other root loci) with the further coupling introduced at high gain.

Figure 9 shows the response (transfer functions) of the degrees of freedom to a vertical gust for gains of 0, 2, 10, and 40. There is a general reduction in the magnitude of the response as gain increases; in particular, there is a reduction in the wing vertical bending resonance peak in each degree of freedom. Note also the reduction of the response at high frequencies (around 2/rev) with very high gain.

From the case of Q = 5*.1, 4*1., it is concluded that simultaneous, significant reductions in rotor and wing response with an accompanying increase in dynamic stability of the system is achievable. The feedback control required is not simple as many elements of the state variable feedback gain matrix are of the same order. With only the rotor controls as inputs to the system, there appears to be a limit to both the reduction in wing motion and the increase in wing damping possible (due possibly to the control system design technique used, not the proprotor configuration) for although the rotor response continues to decrease at high gain, the wing motion is asymptotic to nonzero levels. However, the level of reduction of the wing motion possible using just rotor controls may be satisfactory.

The next case examined was for $V/\Omega R = 0.7$ and with Q = 6*1, 3*0, i.e., only the rotor degrees of freedom have constraints on their motion so that the wing motion does not contribute to the quadratic performance index. In figure 10(a) the rms acceleration shows very little reduction is achieved in wing response (q_1, q_2, p) using this performance index, especially for wing vertical bending (q_1) which has a reduction of only 5 percent to 10 percent. In contrast, the reduction of the rotor flap and lag acceleration is greater than for the previous case with the wing motion constrained also; there is about 75 percent reduction at high gain compared to about 65 percent for the previous case. The rms response in figure 10(b) has characteristics similar to those of the acceleration. Wing motion shows little reduction, e.g., q_1 is reduced only 10 percent to 15 percent. However, q_2 actually increases in rms response due to coupling with the β_0 and ζ_0 degrees of freedom (but since the absolute level of the q_2 response is still quite small, this is no real problem). With a slightly greater weight on ζ_0 (smaller corresponding value of Q), the effect could be eliminated. The rotor flap and lag rms response is reduced significantly by elimination of the constraint on the wing motion, with about an 85 percent reduction at high gain compared to about 75 percent for the previous case.

The variation of the damping ratio of the wing modes with gain in figure 10(c) especially shows the effect of eliminating the constraint on the wing motion. The damping of the q_2 and p (wing chordwise bending and wing

torsion) modes change very little and the damping of the q_1 (wing vertical bending) mode actually decreases, from about 3.5 percent for the open (gain = 0) level down to about 2.5 percent at higher gain, as compared to an increase to about 12 percent reduction achieved in the previous case. This decrease in the damping of the wing vertical bending mode is very serious as the dynamic stability of the wing modes is a critical factor in proprotor aircraft design, and implies that a control system designed considering the rotor only will not be satisfactory.

The gain matrix, shown in table 3, as compared to the previous gain matrix (table 1), shows a significant decrease in feedback of wing motion; e.g., the reduction in the $\dot{q}_1$ and q_1 elements. This gain is effectively three times the magnitude of the previous gain matrix (because of the greater weighting of the rotor degrees of freedom) and some of the differences are obscured.

In figure 10(d), the root locus shows a variation of the rotor modes ($\beta \pm 1$, $\zeta \pm 1$, β) with gain that is almost identical to the previous case. But with no constraint, the wing modes (q_1, q_2, p) change very little with gain and do not show the significant increase in damping as with the first Q.

The next case considered used $V/\Omega R = 0.7$ and $Q = 6*0, 3*1$, i.e., constraints are on the wing degrees of freedom only, with no contribution of the rotor motion to the performance index. Figure 11(a) shows that there is a greater reduction in the wing rms response in this case compared to the first case, with about a 65 percent reduction in q_1 compared to about 45 percent for the first Q. Here especially is seen the effect of relaxing the constraint on the rotor motion; there is a 40 percent reduction of the rotor motion response, much less than the 75 percent reduction for the first Q; also at higher gain, the rotor response then increases again and even becomes significantly greater than the open loop (gain = 0) level for gain above 20. Figure 11(b) indicates that a somewhat greater reduction in wing vibration is achieved by relaxing the constraint on the rotor motion, a 65 percent reduction in q_1 compared to 55 percent for the first Q. However, the cost of this increased control of wing motion is a much smaller reduction in the rotor motion.

Figure 11(c) shows that there is a tremendous increase of the damping of the wing modes with increasing gain with no weight placed on the rotor motion, although initially the increase is about the same as with the first Q. The q_1 damping increased from 3.5 percent of critical damping to around 35 percent at high gain, compared to a 12 percent increase achieved with the first Q.

The gain matrix in table 4 shows that there is almost no feedback of the rotor motion at all, just for the wing degrees of freedom, q_1, q_2, and p. The feedback law is then primarily

$$\theta_{1s} = -K_1\dot{q}_1 - K_2\dot{p}$$

$$\theta_o = K_3\dot{q}_2$$

(with some displacement of wing motion feedback as well) which then explains the large wing mode damping increase. This is as expected for increasing the wing damping, but with no constraint on the rotor motion, the rotor response increases with the wing damping.

Figure 11(d) shows that the wing modes (q_1, q_2, p) show dramatic, large increases in damping as gain increases, as compared with the first Q. With no constraint on the rotor modes, their roots do not change much, with the flap mode roots ($\beta \pm 1$) actually showing some decrease in damping which, however, slows down at high gain.

It is seen that relaxing the constraint on the wing motion achieves a larger reduction in the rotor response at the cost of less control of the wing motion (the wing vertical bending mode damping actually decreased) and vice versa for relaxation of the constraint on rotor motion (flap rms response is actually increased). The gains achieved by relaxing the constraint on part of the system are in fact much less than the cost; modest improvement in the response of part of the system is possible but only with a resulting deterioration in the dynamic characteristics of the rest of the system. These results may be taken as limiting cases of possible apportioning of the performance index weight between rotor and wing. The optimal control procedure here provides the means to design a control system considering the entire system, with the first Q selected being a good intermediate case between the two extremes. With a proper apportioning of weight in the quadratic performance index to the wing and rotor, it is possible to simultaneously improve the dynamic behavior of both the rotor and wing, achieving nearly the levels obtained when designing a controller for the rotor or wing alone. So, to improve all the dynamic characteristics of the proprotor aircraft, it is necessary to consider the complete system, both wing and rotor, although the feedback control that results from this analysis is not simple.

The next case considered used Q = 5*.1, 4*1., $V/\Omega R = 0.7$, and a gain range of 0 to 40, as in the first case. Furthermore, added to the controls was a wing trailing edge flap. A 30 percent chord flap was used, extending over the outer 50 percent span of the wing. The effect on the aerodynamic lift and pitching moment on the wing were calculated by strip theory analysis. The control vector for this case now has 4 elements: θ_o, θ_{1c}, θ_{1s}, δ_F.

Figure 12(a) shows that a substantially greater reduction in wing vertical bending rms acceleration is achieved by the addition of the wing flap control, about 85 percent reduction as compared to about 55 percent for the first case (no flap control), with less of a tendency for the wing response to level off at high gain. Comparing the reductions in the case of a 6 m/sec (20 fps) rms gust, the rms vertical acceleration at the tip decreases from 0.57 g in the first case to about 0.18 g with wing flap control (cf. 1.25 g uncontrolled). This reduction in wing response is achieved with even less rotor response, reduced by about 70 percent here as compared to 65 percent reduction for the first case.

The rms response in figure 12(b) again shows a reduction in wing and rotor response of about 85 percent at high gain as compared to about 75 percent

for the first case (only rotor control). For moderate gain levels, about 95 percent reduction is achieved in flap response; applied to a 6 m/sec (20 fps) gust, that gives σ_β = 0.1 degrees as compared to σ_β = 2 degrees in the uncontrolled case.

In figure 12(c) the wing mode damping shows dramatically the effect of including the wing flap control. At high gain the wing vertical bending mode damping is about 50% of critical damping as compared to about 12 percent without flap control, and 3.6 percent uncontrolled. The torsion (p) damping shows a similar increase; however, the wing chordwise bending mode is not affected, as would be expected since the flap gives primarily lift and torsion movement on the wing.

The feedback to the controls shown in table 5 is similar to the case without the flap control, except that there is less feedback of the wing motion, as that feedback now goes to the flap. The flap control is primarily

$$\delta_F = -K_1 \dot{q}_1$$

which directly increases the wing vertical bending damping. So, the flap takes over the primary control of the wing motion (except the chordwise bending which is still controlled by the rotor collective) with little feedback of the rotor motion.

In figure 12(d) the root locus is nearly identical to the case without flap control, except that the wing vertical bending and torsion modes have greatly increased damping.

It has been shown that the wing flap is very powerful for the control of proprotor/cantilever wing motion. The forces due to the flap deflection act directly on the wing to control wing motion, especially the important wing vertical bending motion. Simple feedback of the modal velocities allows a direct increase of damping to very high levels (on the order of 50% critical in this example). By taking over a major role in controlling the wing, use of the flap then allows more control of the rotor for a given level of rotor control deflection (i.e., gain), thus allowing a greater reduction in rotor motion as well as wing motion. Therefore, it is probably desirable to make use of wing aerodynamic control surfaces in the feedback control of proprotor aircraft dynamics. However, the effectiveness of such control surfaces depends on the viscous flow, compressibility, unsteady aerodynamics, three-dimensional aerodynamics; structural and inertial limitations on flap oscillation frequency; and other effects. Hence, such controllers will certainly require experimental verification.

The last case examined for the Bell proprotor used Q = 5*.1, 4*1., and gain = 10 while varying the velocity from 100 to 400 knots. There are two reasons for considering this case; the first is to examine the variation in response of the rotor and wing due to changing cruise speed, both open loop and optimally controlled; secondly, to determine if it is necessary to vary the controller design with speed in order to always achieve the desired

response, i.e., to examine the performance of the controller operating at a speed other than the one at which it was designed, hence the expression, "off design." For this latter case, an optimal controller is designed for a particular speed and the response using that controller at several other speeds is calculated. Compared to that response is the response calculated using the optimal controller for each speed. For this analysis the off design performance of a 250 knot controller will be examined.

Figure 13(a) shows the rms acceleration using the optimum controller for each speed. There is little variation in the percent reduction of the response for a given gain with change in speed, with the exception of the wing vertical bending response which reaches a peak at 200 knots; at that speed there is a resonance of the wing and rotor motion, specifically, between the wing vertical bending mode (q_1) and the rotor low frequency lag (ζ-1) mode. Away from that resonance, which produces substantial coupling of the wing and rotor motion, a greater percent reduction of the q_1 motion is possible for a given gain.

Figure 13(b) shows the rms acceleration due to using the 250 knot controller at each speed instead of the optimal controller (fig. 13(a)); the response is nearly the same for both cases.

The rms response using the optimal controller at each speed in figure 13(c) exhibits similar behavior to the acceleration. Figure 13(d) shows that using the 250 knot controller similarly produces nearly the same response as in figure 13(c), except for the chordwise bending (q_2) response (though the actual magnitude of the response of that mode to vertical gust is small).

Figure 13(e) shows improvement in the wing modes damping levels for all speeds using the optimal controller at each speed. Using the 250 knot controller as shown in figure 13(f), gives about the same results. In both cases (optimal controller and 250 knot controller), the controller is capable of substantially increasing the wing vertical bending mode damping (and other modes) even at high speed, while in the uncontrolled system, the damping decreases as speed increases due to rotor high inflow aerodynamics.

The gain matrices for the optimal controller at 100, 250, and 400 knots in tables 6, 7, and 8 respectively, show very little variation in either absolute or relative magnitudes of the elements, accounting for the success of the 250 knot controller over the entire speed range.

Figure 13(g) shows the root locus plot for both the uncontrolled and the optimally controlled system for varying speed and indicates general improvement of the system stability at all speeds with the optimal controller. In figure 13(h) is shown the root locus for the uncontrolled system and the system using the 250 knot controller for varying speed, demonstrating nearly the same results as with the optimal controller at each speed for both wing and rotor modes.

Figure 13(i) shows the actual magnitudes of the response of the flap and lag motion in deg/fps of gust while varying speed for a) the uncontrolled

system, b) using the optimal controller at each speed, and c) using the 250 knot controller at each speed. The uncontrolled system shows a tremendous increase in rotor response with increasing speed due to the high inflow aerodynamics. While the controlled system also shows an increase in actual magnitude of the response with increasing speed, it does so at a much slower rate. Applied to a 6 m/sec (20 fps) gust, the open loop flap and lag rms response at 400 knots is about 2.5 degrees and is reduced to about 0.5 degrees using a controller (at gain - 10).

Figure 13(j) is similar to 13(i) except that it shows the magnitude of the vertical acceleration of the wing tip in g/fps of gust. The uncontrolled system shows a great increase in q_1 with speed, even faster than the rotor motion increases, while the increase in the controlled system response is much slower (recall that the fractional closed loop/open loop level decreases as speed increases from 200 to 400 knots, figs. 13(a) and (b)). For a 6 m/sec (20 fps) gust then, the rms vertical acceleration at the wing tip for 400 knots is about 2.9 g for the uncontrolled system and is reduced to about 0.9 g with a controlled system (gain = 10).

It can be concluded that a substantial reduction in system response and improvement in dynamic stability over the entire cruise speed range of the aircraft may be achieved with a properly designed controller. The results and conclusions in the rest of this study, for the $V/\Omega R = 0.7$ case may then be applied to the entire speed range. It has been shown that a controller designed for a particular cruise speed (250 knots here) has excellent performance characteristics at all speeds, nearly the same, in fact, at off-design speeds as the performance with the optimal controller for that speed.

Hingeless, Soft-Inplane Rotor

The behavior of the controlled system and the conclusions based on this optimal control analysis for this rotor are much the same as for the gimballed rotor. This discussion therefore will concentrate on those points particular to the case of the Boeing rotor. The differences between the two rotors are primarily the flap and lag frequencies, the Boeing rotor having cantilever, soft-inplane blades, while the Bell rotor has a gimballed hub with stiff-inplane blades. The hub moment capability of the Boeing rotor does have a significant effect on the dynamics, both open loop and closed loop.

For the hingeless, soft-inplane rotor and wing, Q = 5*.2, 10, 1, 10, 1 and $V/\Omega R = 0.7$ was taken as the standard case. The gain was varied from 0 to 40 with most of the effect occurring by 10 and leveling off from there. Figure 14 shows the results of this case. Figure 14(a) shows that the flap and lag rms response achieve a substantial reduction over the closed loop values. The reduction in the rms flap response is from 0.44 deg/deg at zero gain to around 0.15 deg/deg at high gain, about a 65 percent reduction in flap amplitude. Then for a 6 m/sec (20 fps) rms gust, σ_β (rms flap response) is reduced from 1.4 degrees to 0.48 degrees and σ_ζ (rms lag response) is reduced from 3.1 degrees for the uncontrolled system to about 0.28 degrees. Figure 14(b) shows that the number of peaks/revolution remain about the same order as gain

increases, but there is some increase due to σ_x decreasing faster than $\sigma_{\dot{x}}$. Since the number of peaks/rev in the nonrotating frame is low (fig. 14(b)), it follows that the peaks/rev in the rotating frame is dominated by the blade once-per-rev motion, for both the uncontrolled and controlled systems.

Figures 14(c) and (d) show a significant reduction in rms response and acceleration of the wing vertical bending motion as gain increases, with about 60 percent reduction achieved in the rms response and about 70 percent in the rms acceleration. For a 6 m/sec (20 fps) gust, this corresponds to reducing the rms vertical displacement at the wing tip from 5 cm (2.1 in.) to 2 cm (0.8 in.), and the acceleration at the tip from about 1.06 g to about 0.35 g. Also shown is the number of peaks/revolution (and cycles/hour) and the corresponding reduction.

The rms acceleration shown in figure 14(e) achieves a significant reduction in both rotor and wing response to vertical gust. Again, it is seen that while the rotor motion continues to decrease with gain, the wing motion reduction tends to level off at nonzero levels for higher gain. A reduction of 65 percent to 80 percent is achieved (ignoring the q_2 response which is always small for vertical gust). Figure 14(f) similarly indicates a 65 percent to 90 percent reduction achieved in the rms response. The steady state response in figure 14(g) is reduced as gain is increased, but is not at all similar, indicating the important role of the high frequency dynamics in the gust response.

Figure 14(h) shows that there is a substantial increase in the wing modes damping, e.g., wing vertical bending (q_1) damping is increased from about 1.2 percent of critical damping to about 6.7 percent. The open loop (gain = 0, or uncontrolled) low damping level for the q_1 mode is due to the air resonance behavior of this soft-inplane rotor/cantilever wing configuration, but this mode can be significantly stabilized while simultaneously reducing the rotor response by use of the appropriate feedback control.

The feedback gain matrix in table 9 shows the increased importance of the rotor lag mode velocity and displacement in the lateral/vertical dynamics (the feedback to the controls θ_{1c}/θ_{1s}) due to air resonance behavior; i.e., it is the coupling of q_1 with ζ_{1c}/ζ_{1s} which produces low open loop (uncontrolled) stability, so the controller feeds back lag motion as well as wing vertical bending to stabilize this effect. The rms response and acceleration reflect this control, as there is a very large reduction in rotor lag motion.

The root locus shown in figure 15 indicates an increase in the system stability evident in the general movement of the roots to the left. The β-1 and ζ-1 modes are highly coupled and, since the q_1 mode also has about the same frequency, it couples with the other two (more so in other root loci to follow). Consequently, the labeling of these modes at high gain is somewhat arbitrary. The frequency response to vertical gust in figure 16 shows a general reduction in the magnitude of the response as gain increases with a large decrease in the wing vertical bending mode peak and decreases also in the high frequency peaks.

These results indicate that simultaneous, significant reductions in rotor and wing response and an increase in the stability of the system are possible.

The next case considered used $V/\Omega R = 0.7$ with $Q = 6*1., 3*0.$, placing a motion constraint on the rotor degrees of freedom only. The rms acceleration in figure 17(a) shows that little reduction in the wing motion is achieved; particularly, the wing vertical bending is reduced only about 30 percent. There is, however, a greater reduction in the rotor motion in this case than when the constraints were applied to the wing degrees of freedom also, about 75 percent reduction in this case as compared to 65 percent in the first case. Figure 17(b) shows only about 30 percent reduction in the response of q_1, but about 75 percent reduction in flap response compared to 65 percent in the first case. The wing damping in figure 17(c) shows little change with increasing gain. q_1 damping remains at the low level of 1.5 percent critical. The gain matrix shown in table 10 shows a reduction in feedback of the wing motion, especially $\dot{q}_1$ and q_1, compared to the first Q. Figure 17(d) shows that the rotor roots vary nearly the same as for the first case while the wing roots change very little.

Next was considered the case of $Q = 6*0., 3*1.$, having constraints on the wing motion only, and $V/\Omega R = 0.7$. The rms acceleration in figure 18(a) shows that a somewhat greater reduction in wing vibration is achieved, about 75 percent reduction in q_1 compared to 65 percent for the first case. But the cost of this reduction is that the rotor response is not reduced as much as when there are constraints on the rotor motion also. Figure 18(b) illustrates especially the cost of increased control of the wing motion. The rotor flap response decreased by about 55 percent, compared to 65 percent reduction in the case of the first Q; the rotor lag response reaches its maximum reduction of about 40 percent at a gain of 5 as compared to a previous 90 percent reduction, and then increases again at higher gain, becoming greater than the open loop value for gain greater than 25. The wing damping in figure 18(c) experiences a tremendous increase with no constraint on the rotor motion. The q_1 damping increases from around 1.2 percent of critical damping open loop to about 45 percent at high gain, compared to about 7 percent achieved with the first Q. The gain matrix in table 11 shows almost no feedback of the rotor motion. The feedback law is primarily

$$\theta_{1s} = -K_1\dot{q}_1 - K_2\dot{p}$$

$$\theta_o = K_3\dot{q}_2$$

with some feedback of wing displacement as well. In figure 18(d), the root locus indicates a large increase in the damping of the wing modes. Because of their similar frequencies, there is significant coupling of the β-1, ζ-1, and q_1 modes at higher gain.

It has been shown that relaxation of the constraint on the wing motion achieves a larger reduction in the response of the rotor modes, but with a resulting decrease in the control of the wing motion and vice versa for

relaxing the constraint on the rotor motion. Thus it is necessary to consider both the rotor and wing motion when designing a controller so as to simultaneously greatly reduce the response to vertical gust and increase the stability of the system.

In the next case a wing trailing edge flap is added to the controls. As for the first case, $V/\Omega = 0.7$, Q = 5*.2, 10, 1, 10, 1 and the gain ranges from 0 to 40. Figure 19(a) shows that, with this added flap control, there is a substantially greater reduction in wing vertical bending motion, 90 percent reduction at high gain compared to about 70 percent without using the flap control. Applied to a 6 m/sec (20 fps) rms gust, the rms vertical acceleration at the tip is decreased from 0.35 g with no flap control to 0.11 g with flap control (cf. 1.06 g uncontrolled). Shown in figure 19(b) is the reduction in wing response with a simultaneous reduction in rotor motion by using the wing flap control. The reduction is around 85 percent compared to 65 percent without this control. So, using this control for a 6 m/sec (20 fps) rms gust gives $\sigma_\beta = 0.2$ degrees versus 1.4 degrees for the uncontrolled case.

Shown in figure 19(c), wing vertical bending and torsion modes damping experience a dramatic increase (chordwise bending mode damping unchanged); about 55 percent of critical damping is achieved for the wing vertical bending mode at high gain compared to only about 7 percent without wing flap control. The gain matrix in table 12 shows that little of the rotor motion is fed back to the wing flap control, but there is a transfer of the wing q_1 and p feedback from the rotor to the flap control. The root locus in figure 19(d) is nearly identical to the root locus for the case without using the flap, except the greatly increased damping of the wing vertical bending and torsion modes.

It is seen that the wing flap is very effective in controllirg the proprotor/cantilever wing motion, especially the wing vertical bending motion, and allows more control over the rotor for a given gain level, and thus a greater reduction in rotor motion, as well as wing motion.

The last case examined for the Boeing proprotor used Q = 5*.1, 4*1., and gain = 10 while varying the velocity from 100 to 400 knots. The variation of the response with speed was examined, using the optimal controller at each speed and using also a 250 knot controller (optimum at 250 knots) at each speed. In figure 20(a), there is little influence of speed on the effectiveness of the optimal controller. There is some increase in the percent reduction of the q_1 response at low speed where there exists a resonance of this mode with the rotor low frequency lag mode (air resonance behavior). The response with the 250 knot controller shown in figure 20(b) is much the same as with the optimal controller for each speed, except for the wing chordwise bending which has only a small response to vertical gust anyway, and a somewhat increased flapping response at low speed. Figure 20(c) illustrates that the rms response behavior is similar to that of the acceleration when using the optimal controller at each speed. Using the 250 knot controller, it is shown in figure 20(d) that the response is nearly identical as when using the optimal controller for each speed. An exception is the somewhat increased

flapping response at low speed as compared to the optimal controller results, but the actual magnitude of the response is low at that speed.

Shown in figures 20(e) and (f) is a substantial and uniform improvement of the wing mode stability over the entire speed range, with nearly the same performance using the 250 knot controller for all speeds. In tables 13, 14, and 15 are the gain matrices for the optimal controller at 100, 250, and 400 knots respectively. They show little variation, though somewhat more than for the Bell rotor, accounting for a somewhat greater variation in performance especially at low speed. Figures 20(g) and (h) show the root loci for a) the optimal controller at each speed and b) the 250 knot controller. All modes show a consistent and substantial improvement, especially the rotor modes with the 250 knot controller.

Figure 20(i) shows the magnitude of the response of the flap and lag motion in deg/fps of gust with variation in speed for a) no controller, b) the optimal controller, and c) the 250 knot controller. There is a tremendous increase of the response with speed for the uncontrolled system; and while there is some increase for the controlled system, it is much slower. Comparison of the optimally controlled system response with the 250 knot controlled system response shows little difference, indicating that the differences at low speed are unimportant. If the results between the uncontrolled and controlled systems are compared for a 6 m/sec (20 fps) rms gust, the open loop response at 400 knots is about 4.5 degrees for lag and 2.2 degrees for flap, and is reduced to about 0.4 degrees for lag and 0.8 for flap closed loop (for gain = 10). Figure 20(j) is similar to figure 20(i) except that it shows the magnitude of the rms acceleration in g/fps of gust at the wing tip, and it exhibits similar behavior; the uncontrolled response shows a great increase with speed, with a much slower increase using a controller. The 250 knot controller performance is nearly identical to that with the optimal controller at each speed. Applying the results to a 6 m/sec (20 fps) gust, the rms vertical acceleration at the wing tip at 400 knots is about 1.7 g uncontrolled and is reduced to about 0.6 g with a controlled system at gain = 10.

It can be concluded that a properly designed controller is effective and greatly improves the system dynamic performance over the entire cruise speed range. Also a controller designed for a particular cruise speed (250 knots in this case) gives excellent performance, nearly the same as the performance obtained using the optimal controller at each speed.

CONCLUDING REMARKS

The following conclusions are reached from this investigation, based on the proprotor/cantilever wing model and the optimal control theory design technique.

a) Significant and simultaneous reduction in the rotor response, reduction in the wing response, and increase in the dynamic stability of the system is achievable. However, the optimal state variable feedback control required is not simple. It should be noted that these results are based on

feedback of the state variables. In practice the state variables must be estimated from some measurement of the system motion, and so measurement noise and inaccuracies in the mathematical model of the system will reduce the control system performance below the optimum achievable.

b) In the design of control systems to improve the dynamic characteristics of the proprotor aircraft, it is necessary to consider the complete system. Considering just the rotor or just the wing dynamics will not produce a successful design.

c) Using a wing flap in addition to the rotor inputs is very powerful for control of the proprotor/cantilever wing system. The wing flap acts directly to control the wing vertical bending motion, the critical element of the dynamics, and so allows very high levels of wing damping to be achieved while freeing the rotor inputs for more control of the rotor motion.

d) A control system designed for a particular cruise speed (250 knots here) has excellent performance at all forward speeds, nearly the same in fact at off-design speeds as the performance with the optimal controller for that velocity.

REFERENCES

1. Johnson, Wayne: Dynamics of Tilting Proprotor Aircraft in Cruise Flight, NASA TN D-7677, May 1974.

2. Bell Helicopter Company: Advancement of Proprotor Technology Task II — Wind Tunnel Test Results, NASA CR 114363, September 1971.

3. Magee, John P., and Alexander, H. R.: Wind Tunnel Tests of a Full Scale Hingeless Prop-rotor Designed for the Boeing Model 222 Tilt Rotor Aircraft, Boeing Vertol Company Report No. D222-10059-1, July 1973.

4. Bell Helicopter Company: V/STOL Tilt-Rotor Study Task II -- Research Aircraft Design, NASA CR 114442, March 1972.

5. Boeing Vertol Company: V/STOL Tilt-Rotor Aircraft Study Volume II — Preliminary Design of Research Aircraft, NASA CR 114438, March 1972.

6. Johnson, Wayne: Theory and Comparison with Tests of Two Full-Scale Proprotors, AHS/NASA Specialists Meeting on Rotorcraft Dynamics, Moffett Field, California, February 1974.

7. Gaonkar, Gopal H., and Hohenemser, Kurt H.: Flapping Response of Lifting Rotor Blades to Atmospheric Turbulence, J. Aircraft, vol. 6, no. 6, November-December 1969.

8. Gaonkar, Gopal H., and Hohenemser, Kurt H.: Stochastic Properties of Turbulence Excited Rotor Blade Vibrations, AIAA J., vol. 9, no. 3, March 1971.

9. Steiner, Roy, and Pratt, Kermit: Some Applications of Power Spectra to Airplane Turbulence Problems, J. Aircraft, vol. 4, no. 4, July-August 1967.

10. Gault, J. D., and Gunter, D. E., Jr.: Atmospheric Turbulence Considerations for Future Aircraft Designed to Operate at Low Altitudes, J. Aircraft, vol. 5, no. 6, November-December 1968.

11. Bryson, Arthur E., Jr., and Ho, Yu-Chi: Applied Optimal Control, Blaisdell Publishing Co., Waltham, Massachusetts, 1969.

12. Anderson, Brian D. O., and Moore, John B.: Linear Optimal Control, Prentice-Hall, Inc., Englewood Cliffs, New Jersey, 1971.

TABLE 1.- DESCRIPTION OF THE FULL-SCALE PROPROTORS (AS TESTED IN THE AMES 40- BY 80-FT WIND TUNNEL).

	Bell		Boeing	
Rotor				
Type	gimballed, stiff-inplane		hingeless, soft-inplane	
Number of blades	3		3	
Radius, R	3.81 m		3.96 m	
Lock number, γ	3.83		4.04	
Solidity ratio	0.089		0.115	
Pitch/flap coupling, δ_3	-15 deg		0	
Rotor rotation direction, on right wing	clockwise		counterclockwise	
Tip speed, ΩR (cruise mode)	183 m/sec		160 m/sec	
Rotation speed, (cruise mode)	458 rpm		386 rpm	
Wing				
Semispan, y_w/R	1.333		1.281	
Mast height, h/R	0.342		0.354	
Typical frequencies				
Vertical bending	3.2 Hz	0.42/rev	2.3 Hz	0.36/rev
Chordwise bending	5.35	0.70	4.0	0.62
Torsion	9.95	1.30	9.2	1.48

TABLE 2.- GAIN MATRIX FOR BELL PROPROTOR Gain = 10, Q = 5*.1, 4*1., V/ΩR = .7.

State variables	Controls θ_{1c}	θ_{1s}	θ_0
$\dot{\beta}_{1c}$	2.54	-.11	-.02
$\dot{\beta}_{1s}$	.27	2.06	.03
$\dot{\zeta}_{1c}$	.47	-.10	.01
$\dot{\zeta}_{1s}$	-.29	.63	-.02
$\dot{\beta}_0$	-.04	.02	2.28
$\dot{q}_1$	2.15	11.11	1.86
$\dot{q}_2$	-.76	-5.22	-7.01
$\dot{p}$	-5.96	5.12	-.42
$\dot{\zeta}_0$	.06	-.03	2.76
β_{1c}	.72	-2.21	-.03
β_{1s}	2.38	.85	-.07
ζ_{1c}	3.10	.31	-.04
ζ_{1s}	.30	2.90	-.03
β_0	.06	-.00	9.01
q_1	-3.16	3.26	1.23
q_2	-5.51	-.84	-4.72
p	-4.53	5.39	-.10

TABLE 3.- GAIN MATRIX FOR BELL PROPROTOR Gain = 10, Q = 6*1, 3*0, V/ΩR = .7.

State variables	Controls θ_{1c}	θ_{1s}	θ_0
$\dot{\beta}_{1c}$	8.22	-.49	.05
$\dot{\beta}_{1s}$	.20	7.83	.05
$\dot{\zeta}_{1c}$	-1.15	.30	-.01
$\dot{\zeta}_{1s}$	-.09	-1.08	-.03
$\dot{\beta}_0$	-.14	.09	.89
$\dot{q}_1$	-2.73	-5.98	1.00
$\dot{q}_2$	5.57	-16.77	-3.24
$\dot{p}$	-11.30	.22	-1.3
$\dot{\zeta}_0$	.20	-.13	9.58
β_{1c}	3.31	-7.86	-.19
β_{1s}	8.15	3.45	-.17
ζ_{1c}	10.03	1.15	.00
ζ_{1s}	-1.02	9.76	.06
β_0	.19	-.16	9.75
q_1	-.10	.28	2.30
q_2	-13.46	.33	-7.05
p	-5.79	10.45	-1.14

TABLE 4.- GAIN MATRIX FOR BELL PROPROTOR Gain = 10, Q = 6*0, 3*1, V/ΩR = .7.

State variables	Controls θ_{1c}	θ_{1s}	θ_0
$\dot{\beta}_{1c}$	.08	-.01	-.02
$\dot{\beta}_{1s}$	-.02	-.02	-.02
$\dot{\zeta}_{1c}$	.43	-.20	.03
$\dot{\zeta}_{1s}$	-.14	.84	.04
$\dot{\beta}_0$	.05	.03	.43
$\dot{q}_1$	-.63	17.69	-1.20
$\dot{q}_2$	-1.57	-.20	-11.21
$\dot{p}$	-2.52	6.62	.22
$\dot{\zeta}_0$	-.01	.01	.00
β_{1c}	.22	-.05	.01
β_{1s}	.06	.33	.00
ζ_{1c}	.11	.57	-.01
ζ_{1s}	-.07	.48	-.03
β_0	.01	.04	.37
q_1	-1.77	3.04	-.43
q_2	-.76	-.32	-4.21
p	-4.24	1.14	.30

TABLE 5.- GAIN MATRIX FOR BELL PROPROTOR W/FLAP CONTROL Gain = 10, Q = 5*.1, 4*1., V/ΩR = .7.

State variables	Controls θ_{1c}	θ_{1s}	θ_0	δ_F
$\dot{\beta}_{1c}$	2.41	-.03	-.01	-.05
$\dot{\beta}_{1s}$	.01	2.35	.02	.17
$\dot{\zeta}_{1c}$	.38	-.01	.01	.20
$\dot{\zeta}_{1s}$	-.02	.34	-.02	.22
$\dot{\beta}_0$	-.05	.03	2.28	.06
$\dot{q}_1$	-.60	2.77	2.46	25.44
$\dot{q}_2$	-.46	-5.61	-7.04	-.66
$\dot{p}$	-3.30	1.34	-.45	-3.05
$\dot{\zeta}_0$	.08	-.05	2.75	-.18
β_{1c}	.53	-2.28	-.03	.28
β_{1s}	2.41	.59	-.07	.21
ζ_{1c}	3.07	-.12	-.05	.34
ζ_{1s}	.28	2.99	-.03	-.16
β_0	.04	-.00	9.01	.21
q_1	-1.28	2.94	.78	3.41
q_2	-5.50	-.44	-4.69	-.57
p	-1.03	3.56	.04	-7.05

TABLE 6.- GAIN MATRIX FOR BELL PROPROTOR Gain = 10, Q = 5*.1, 4*1., V_{knots} = 100.

State variables	Controls θ_{1c}	θ_{1s}	θ_0
$\dot{\beta}_{1c}$	2.19	-.11	-.06
$\dot{\beta}_{1s}$	.11	2.04	.02
$\dot{\zeta}_{1c}$	.64	.08	.08
$\dot{\zeta}_{1s}$	-.29	.99	.01
$\dot{\beta}_0$	-.06	.03	3.18
$\dot{q}_1$	-1.35	11.47	4.60
$\dot{q}_2$	2.25	-5.08	-10.24
$\dot{p}$	-4.97	4.77	-.27
$\dot{\zeta}_0$	.13	-.02	2.81
β_{1c}	1.36	-2.11	-.06
β_{1s}	2.15	1.38	-.13
ζ_{1c}	2.56	.05	-.02
ζ_{1s}	.47	2.89	.16
β_0	-.04	.05	7.55
q_1	.11	4.97	.88
q_2	-4.32	-.56	-2.33
p	-3.14	2.55	.39

TABLE 7 - GAIN MATRIX FOR BELL PROPROTOR Gain = 10, Q = 5*.1, 4*1., V_{knots} = 250.

State variables	Controls θ_{1c}	θ_{1s}	θ_0
$\dot{\beta}_{1c}$	2.54	-.11	-.02
$\dot{\beta}_{1s}$	.27	2.06	.03
$\dot{\zeta}_{1c}$	.47	-.10	.01
$\dot{\zeta}_{1s}$	-.29	.63	-.02
$\dot{\beta}_0$	-.04	.02	2.27
$\dot{q}_1$	2.10	11.09	1.85
$\dot{q}_2$	-.78	-5.23	-6.98
$\dot{p}$	-5.96	5.12	-.42
$\dot{\zeta}_0$	.06	-.03	2.76
β_{1c}	.72	-2.21	-.03
β_{1s}	2.38	.85	-.07
ζ_{1c}	3.10	.30	-.04
ζ_{1s}	.29	2.90	-.03
β_0	.05	-.00	9.02
q_1	-3.18	3.26	1.23
q_2	-5.52	-.85	-4.73
p	-4.54	5.41	-.10

TABLE 8.- GAIN MATRIX FOR BELL PROPROTOR Gain = 10, Q = 5*.1, 4*1., V_{knots} = 400.

State variables	Controls θ_{1c}	θ_{1s}	θ_0
$\dot{\beta}_{1c}$	2.59	-.29	-.00
$\dot{\beta}_{1s}$	.45	1.88	.03
$\dot{\zeta}_{1c}$	.40	-.02	.00
$\dot{\zeta}_{1s}$	-.21	.48	-.01
$\dot{\beta}_0$	-.06	.01	1.38
$\dot{q}_1$	-2.83	10.05	.77
$\dot{q}_2$	-2.55	-5.76	-4.11
$\dot{p}$	-6.39	4.39	-.41
$\dot{\zeta}_0$	.06	-.01	2.87
β_{1c}	-.02	-2.04	-.00
β_{1s}	2.32	.22	-.07
ζ_{1c}	3.19	.14	-.07
ζ_{1s}	.38	3.01	-.03
β_0	.09	-.04	.71
q_1	-3.66	2.99	.90
q_2	-6.60	-1.78	-4.79
p	-4.89	6.93	-.26

TABLE 9.- GAIN MATRIX FOR BOEING PROPROTOR Gain = 10, Q = 5*.2, 10, 1, 10, 1 V/ΩR = .7.

State variables	Controls θ_{1c}	θ_{1s}	θ_0
$\dot{\beta}_{1c}$	-.80	-.18	.01
$\dot{\beta}_{1s}$	.12	-1.10	-.05
$\dot{\zeta}_{1c}$	4.25	.01	-.01
$\dot{\zeta}_{1s}$	.01	4.34	.03
$\dot{\beta}_0$	.19	.02	5.12
$\dot{q}_1$	-8.83	4.22	-6.55
$\dot{q}_2$	16.61	18.40	-19.23
$\dot{p}$	-4.45	4.71	.57
$\dot{\zeta}_0$	-.23	-.03	4.20
β_{1c}	4.00	1.07	.04
β_{1s}	-.79	4.00	.04
ζ_{1c}	2.56	-4.40	-.03
ζ_{1s}	4.07	2.88	.13
β_0	-.24	-.16	30.68
q_1	-4.07	7.39	-1.26
q_2	12.75	9.12	-4.28
p	-2.96	2.51	-.24

TABLE 10.- GAIN MATRIX FOR BOEING PROPROTOR Gain = 10, Q = 6*1., 3*0., V/ΩR = .7.

State variables	Controls θ_{1c}	θ_{1s}	θ_0
$\dot{\beta}_{1c}$	-3.24	-.35	-.08
$\dot{\beta}_{1s}$	.10	-3.35	-.02
$\dot{\zeta}_{1c}$	8.36	.39	.04
$\dot{\zeta}_{1s}$	.10	8.37	-.03
$\dot{\beta}_0$	.10	-.17	.78
$\dot{q}_1$	-.36	6.52	-1.51
$\dot{q}_2$	7.78	-10.66	-4.19
$\dot{p}$	.13	3.71	2.28
$\dot{\zeta}_0$	-.15	.17	9.60
β_{1c}	7.20	3.55	.06
β_{1s}	-3.01	7.88	.07
ζ_{1c}	7.55	-8.35	.26
ζ_{1s}	8.29	7.58	-.04
β_0	-.53	.26	9.57
q_1	-1.08	3.13	-.96
q_2	-6.07	3.15	-6.35
p	-4.20	-.29	-.44

TABLE 11.- GAIN MATRIX FOR BOEING PROPROTOR Gain = 10, Q = 6*0., 3*1., V/ΩR = .7.

State variables	Controls θ_{1c}	θ_{1s}	θ_0
$\dot{\beta}_{1c}$	.44	-.37	.01
$\dot{\beta}_{1s}$	.02	.27	-.03
$\dot{\zeta}_{1c}$	.59	-.18	-.08
$\dot{\zeta}_{1s}$	-.35	.87	-.03
$\dot{\beta}_0$	-.11	-.06	.38
$\dot{q}_1$	-4.38	19.69	1.40
$\dot{q}_2$	3.64	1.98	-12.28
$\dot{p}$	-5.14	6.48	-.00
$\dot{\zeta}_0$	.01	.01	.00
β_{1c}	1.05	-.93	-.01
β_{1s}	.06	.59	-.06
ζ_{1c}	.04	-.12	-.02
ζ_{1s}	.08	.26	-.04
β_0	-.05	-.05	.33
q_1	-3.83	6.52	.22
q_2	1.57	.31	-3.63
p	-1.77	-.41	.21

TABLE 12.- GAIN MATRIX FOR BOEING PROPROTOR W/FLAP CONTROL Gain = 10, Q = 5*.2, 10, 1, 10, 1, V/ΩR = .7.

State variables	Controls θ_{1s}	θ_{1s}	θ_0	δ_F
$\dot{\beta}_{1c}$	-.97	-.06	.00	.05
$\dot{\beta}_{1s}$	-.05	-.88	-.06	.08
$\dot{\zeta}_{1c}$	4.17	.09	.01	.00
$\dot{\zeta}_{1s}$	.17	4.09	.03	-.15
$\dot{\beta}_0$	.22	.00	5.12	-.09
$\dot{q}_1$	-1.83	.62	-5.56	32.45
$\dot{q}_2$	14.22	20.00	-18.97	5.98
$\dot{p}$	.28	1.19	.48	-1.39
$\dot{\zeta}_0$	-.25	-.02	4.20	.20
β_{1c}	3.93	1.01	.06	-.17
β_{1s}	-.84	4.04	.01	-.05
ζ_{1c}	2.69	-4.19	-.01	.88
ζ_{1s}	4.18	2.72	.16	-.07
β_0	-.16	-.22	30.66	-.94
q_1	-1.96	1.56	-.75	3.04
q_2	12.01	9.84	-4.25	-.03
p	-2.39	.63	-.29	-5.89

TABLE 13.- GAIN MATRIX FOR BOEING PROPROTOR Gain = 10, Q = 5*.2, 10, 1, 10, 1 V_{knots} = 100.

State variables	Controls θ_{1c}	θ_{1s}	θ_0
$\dot{\beta}_{1c}$	.76	-.19	.00
$\dot{\beta}_{1s}$	-.06	.69	-.04
$\dot{\zeta}_{1c}$	5.03	.10	-.09
$\dot{\zeta}_{1s}$	-.06	5.15	.03
$\dot{\beta}_0$	-.02	-.03	7.59
$\dot{q}_1$	.56	15.31	-6.76
$\dot{q}_2$	25.45	17.56	-23.95
$\dot{p}$	-3.74	5.96	.47
$\dot{\zeta}_0$	-.08	-.00	3.96
β_{1c}	4.37	-.86	-.01
β_{1s}	.53	4.12	-.02
ζ_{1c}	.82	-5.08	-.10
ζ_{1s}	4.78	.96	-.00
β_0	-.31	-.20	29.80
q_1	-4.72	10.15	-.52
q_2	4.73	4.36	-2.03
p	-1.02	-.94	-.05

TABLE 14.- GAIN MATRIX FOR BOEING PROPROTOR Gain = 10, Q = 5*.2, 10, 1, 10, 1, V_{knots} = 250.

State variables	Controls θ_{1c}	θ_{1s}	θ_0
$\dot{\beta}_{1c}$	-1.08	-.15	.01
$\dot{\beta}_{1s}$	.13	-1.40	-.06
$\dot{\zeta}_{1c}$	3.96	-.02	.00
$\dot{\zeta}_{1s}$	.07	4.03	.03
$\dot{\beta}_0$	.26	.03	4.44
$\dot{q}_1$	-10.66	2.41	-6.50
$\dot{q}_2$	13.68	18.75	-17.50
$\dot{p}$	-4.56	4.03	.62
$\dot{\zeta}_0$	-.25	-.03	4.31
β_{1c}	3.73	1.41	.04
β_{1s}	-.98	3.81	.05
ζ_{1c}	2.76	-4.18	-.01
ζ_{1s}	3.85	3.13	.15
β_0	-.21	-.13	30.84
q_1	-4.05	6.57	-1.37
q_2	13.64	10.44	-4.61
p	-3.38	3.08	-.26

TABLE 15.- GAIN MATRIX FOR BOEING PROPROTOR Gain = 10, Q = 5*.2, 10, 1, 10, 1, V_{knots} = 400.

State variables	Controls θ_{1c}	θ_{1s}	θ_0
$\dot{\beta}_{1c}$	-1.85	-.01	-.01
$\dot{\beta}_{1s}$	.03	-2.09	-.07
$\dot{\zeta}_{1c}$	2.87	-.08	.02
$\dot{\zeta}_{1s}$	.30	2.87	.01
$\dot{\beta}_0$	.54	.06	1.77
$\dot{q}_1$	-15.52	-1.67	-5.96
$\dot{q}_2$	3.13	19.18	-9.61
$\dot{p}$	-4.53	1.40	.81
$\dot{\zeta}_0$	-.31	-.03	4.70
β_{1c}	2.45	2.21	.06
β_{1s}	-1.31	2.86	.03
ζ_{1c}	3.14	-3.33	.08
ζ_{1s}	3.08	3.67	.16
β_0	-.09	.11	31.17
q_1	-3.84	4.18	-1.49
q_2	14.86	15.40	-4.58
p	-4.92	4.03	-.32

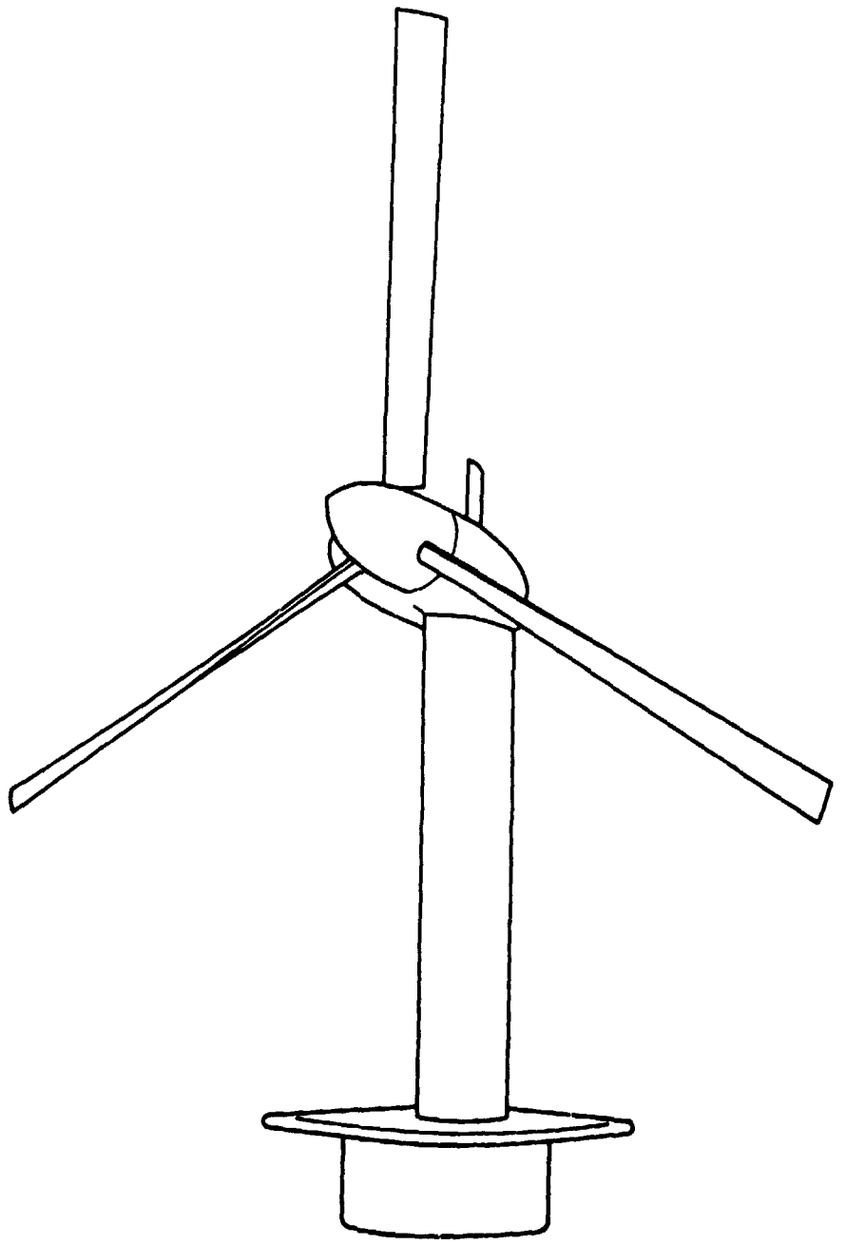

Figure 1.— Configuration of analytical model: proprotor operating in high inflow axial flight on a cantilever wing.

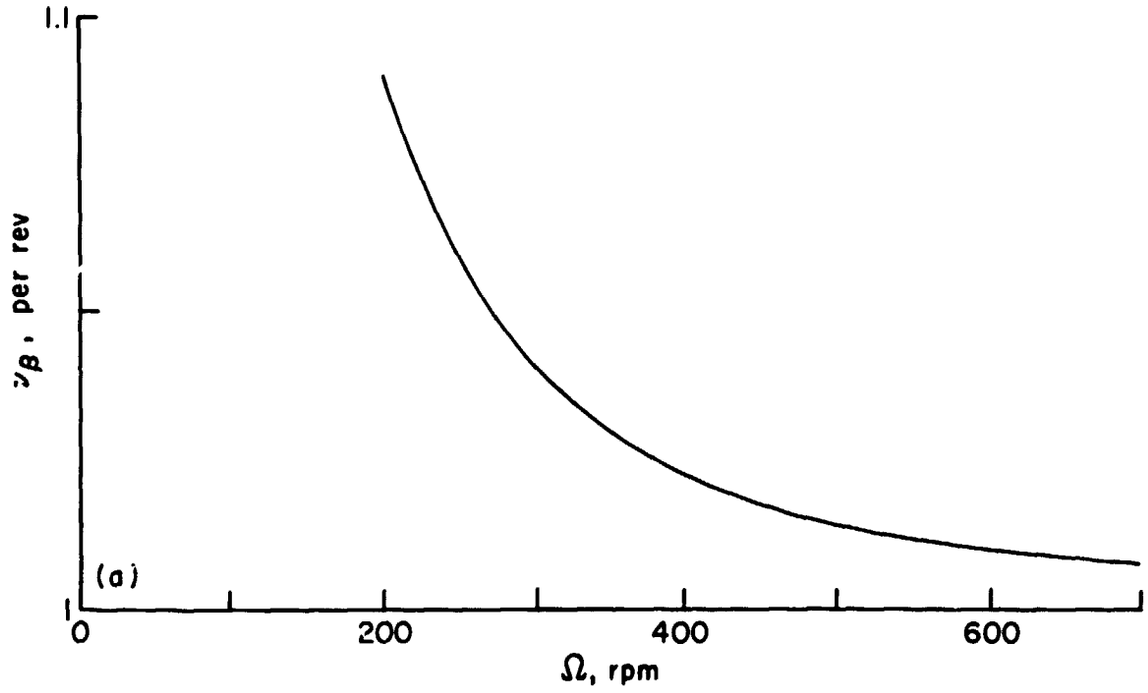

(a) Flap frequency ν_β (normal Ω = 458 rpm).

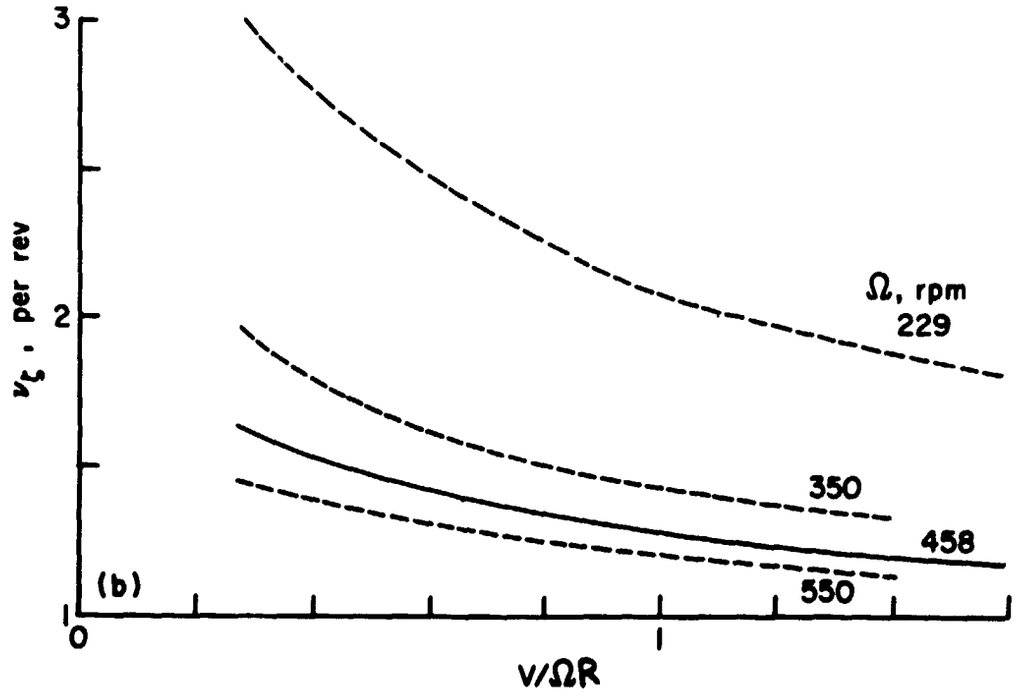

(b) Lag frequency ν_ζ.

Figure 2.– Blade rotating natural frequencies for the Bell rotor.

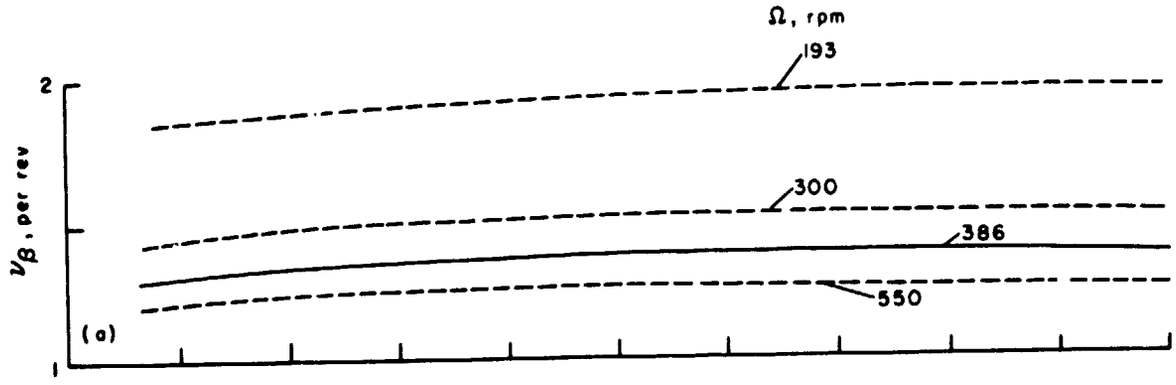

(a) Flap frequency ν_β.

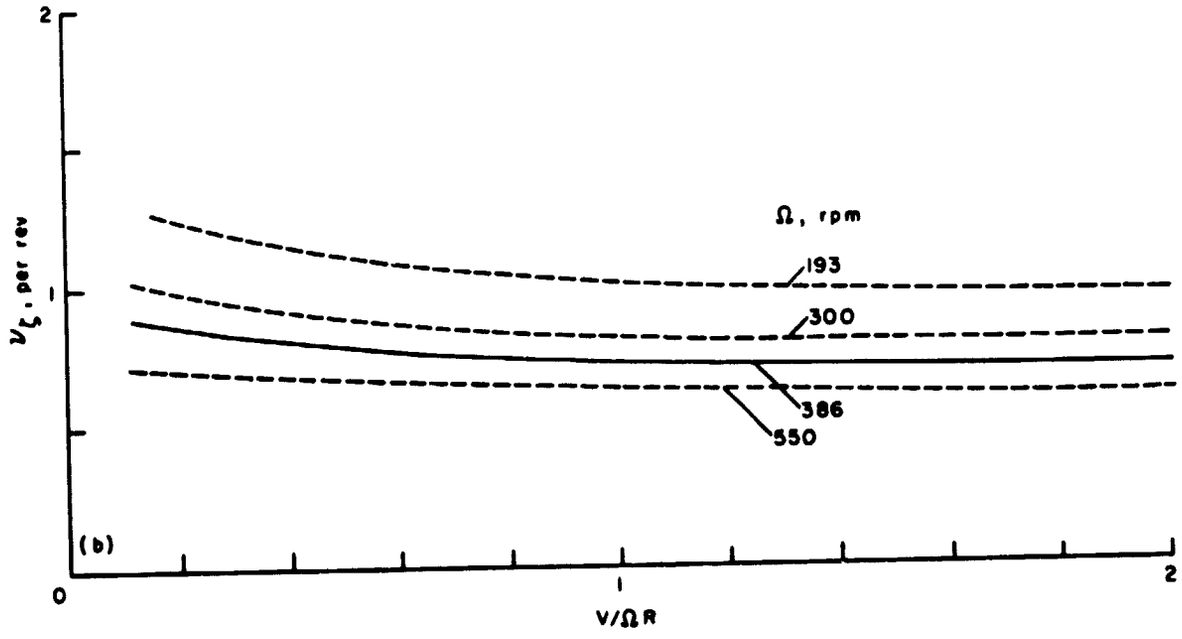

(b) Lag frequency ν_ζ.

Figure 3.— Blade rotating natural frequencies for the Boeing rotor (normal Ω = 386 rpm).

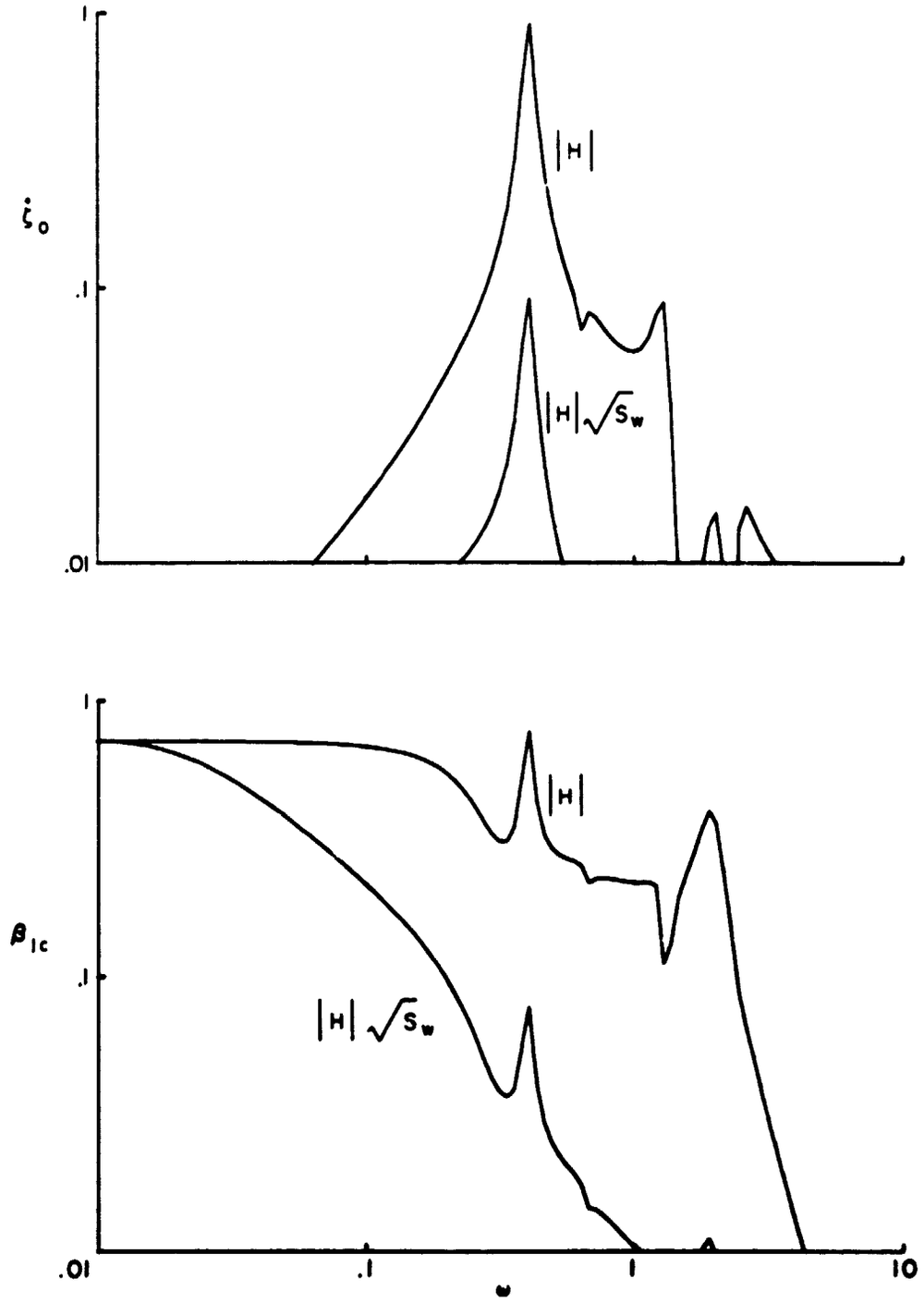

Figure 4.-- Transfer function for Bell rotor at V/ΩR = 0.7: magnitude of response of each degree of freedom to vertical gust at frequency ω; and times the gust spectrum, $\sqrt{S_w/S_w(0)}$.

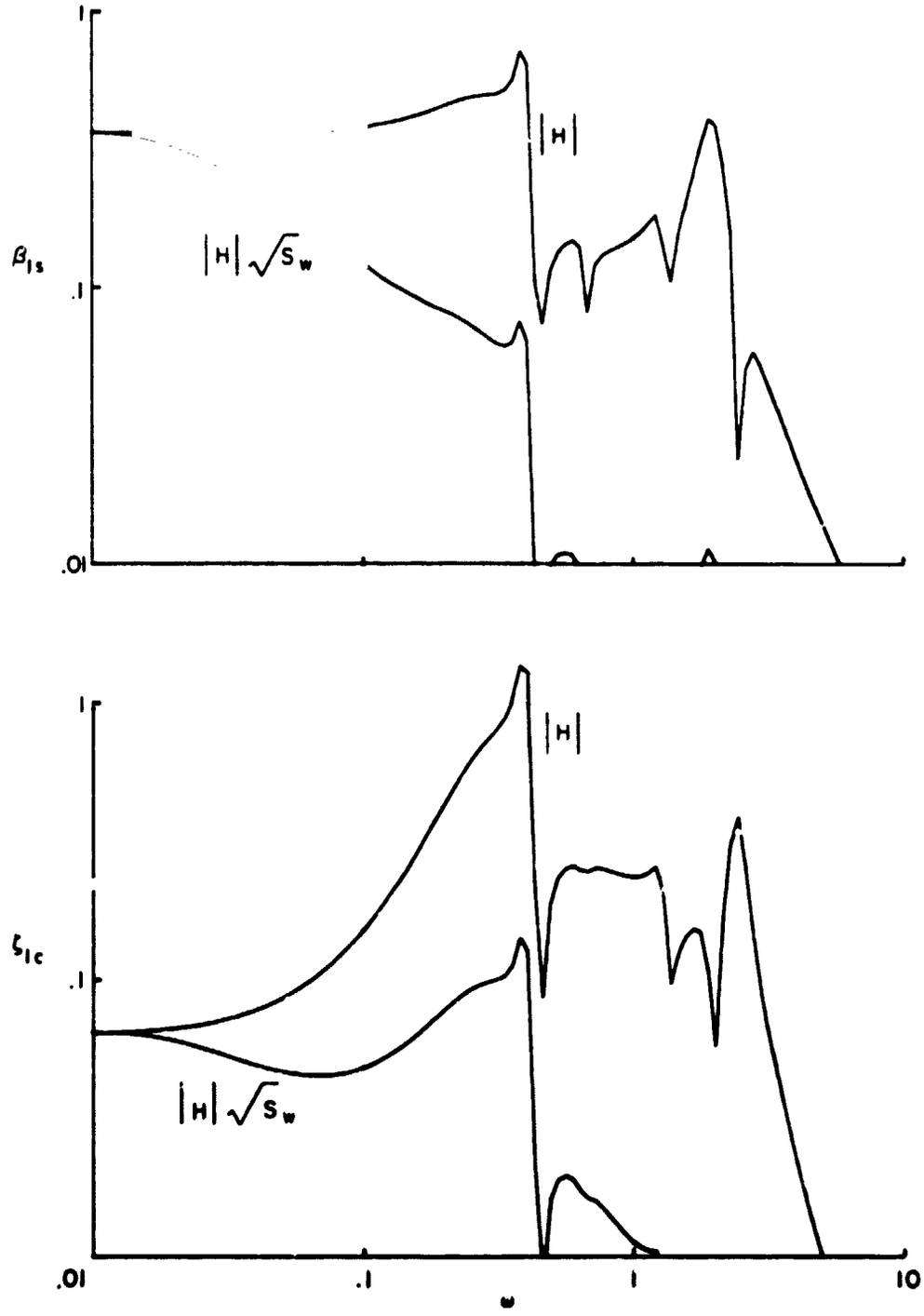

Figure 4.— Continued.

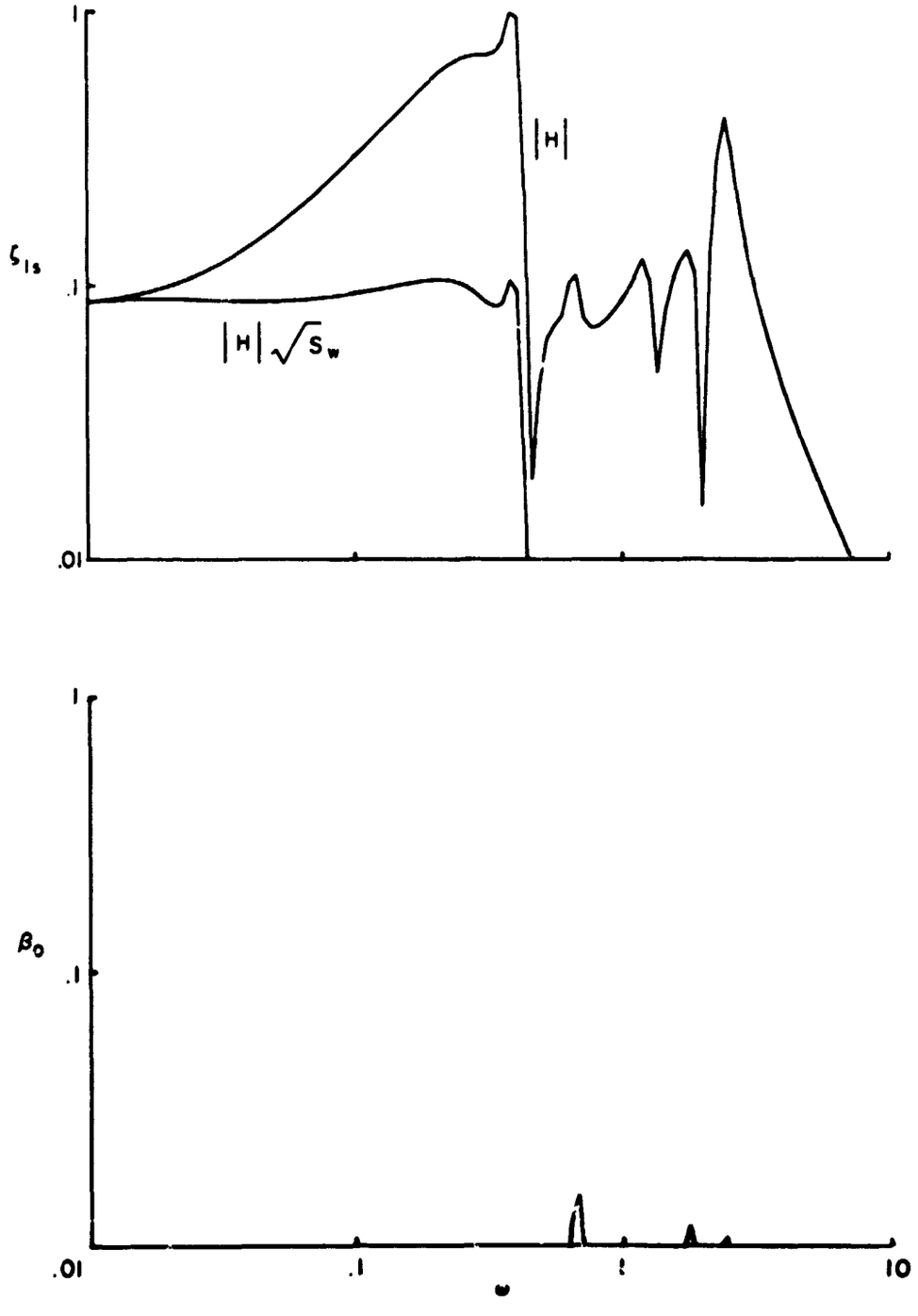

Figure 4.— Continued.

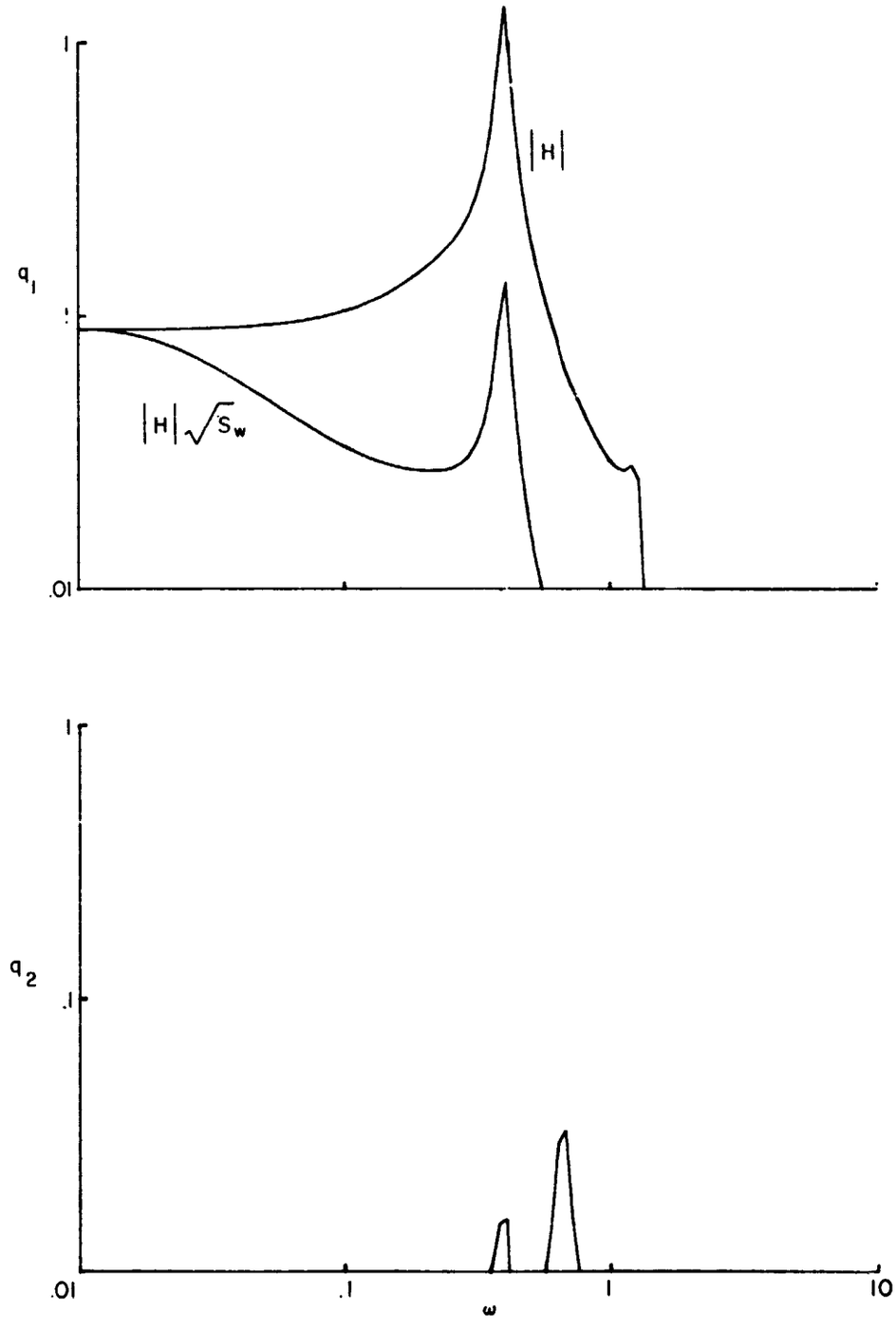

Figure 4.— Continued.

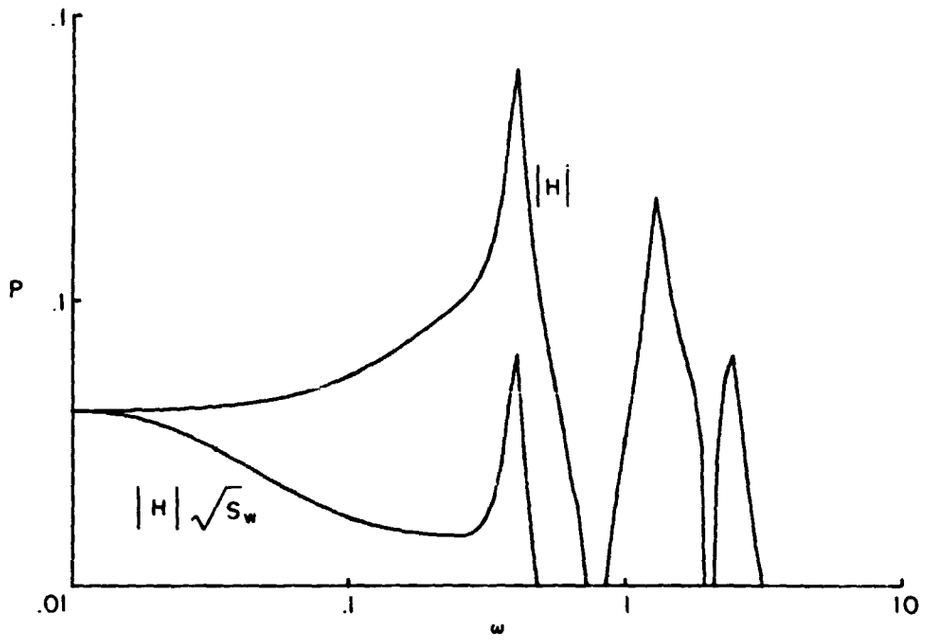

Figure 4.— Concluded.

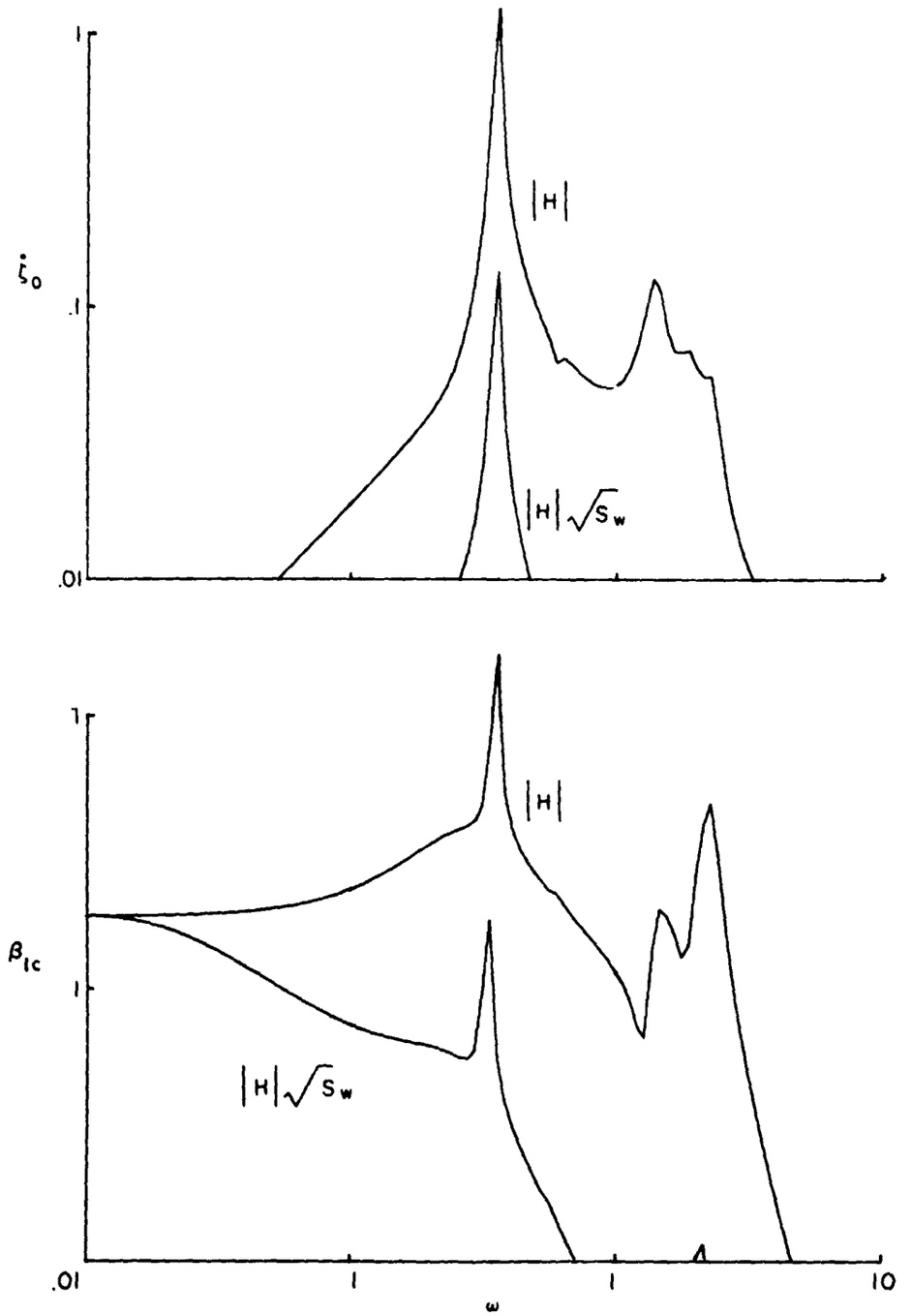

Figure 5.— Transfer function for Boeing rotor at $V/\Omega R = 0.7$: magnitude of response of each degree of freedom to vertical gust at frequency ω; and times the gust spectrum, $\sqrt{S_w/S_w(0)}$.

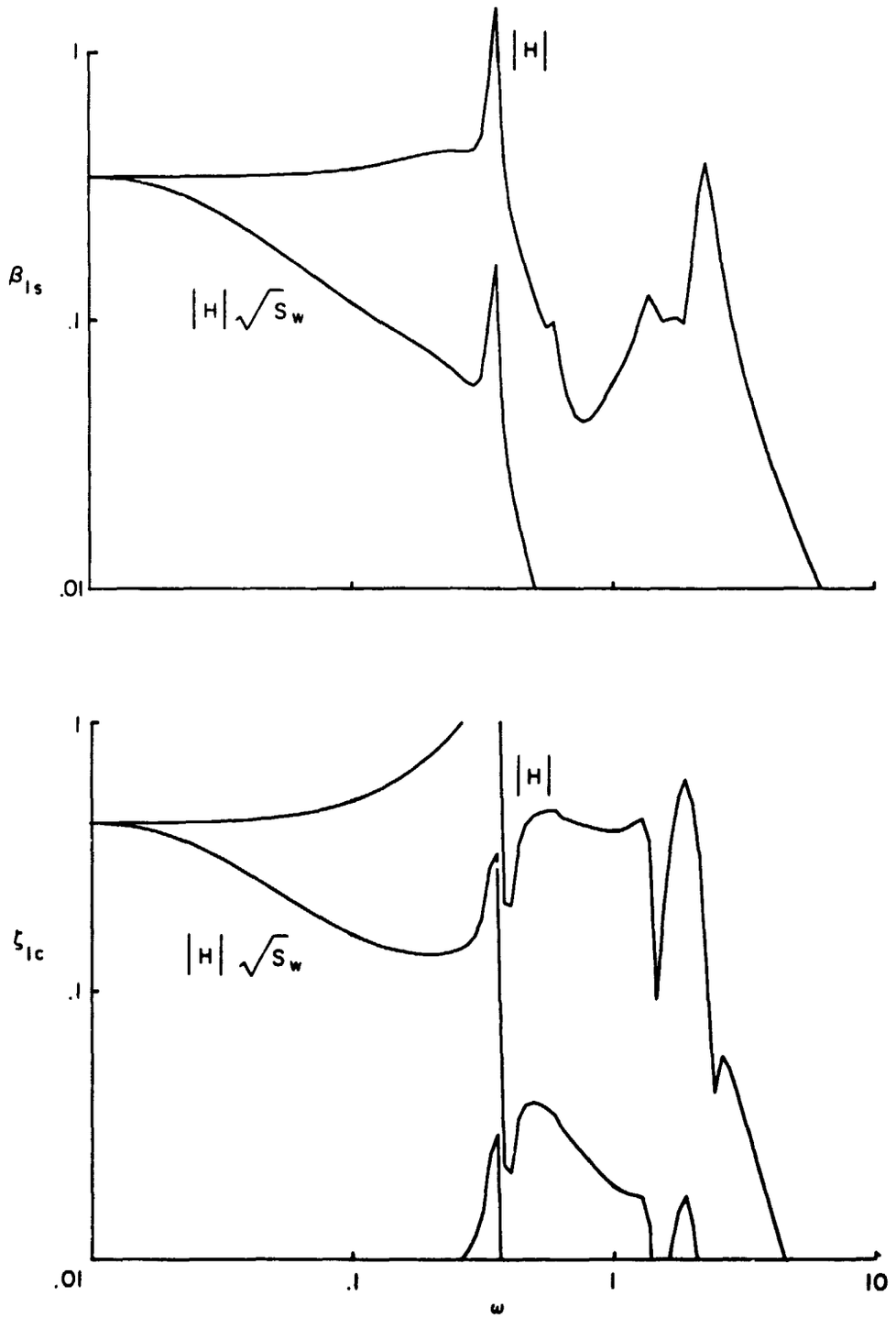

Figure 5.— Continued.

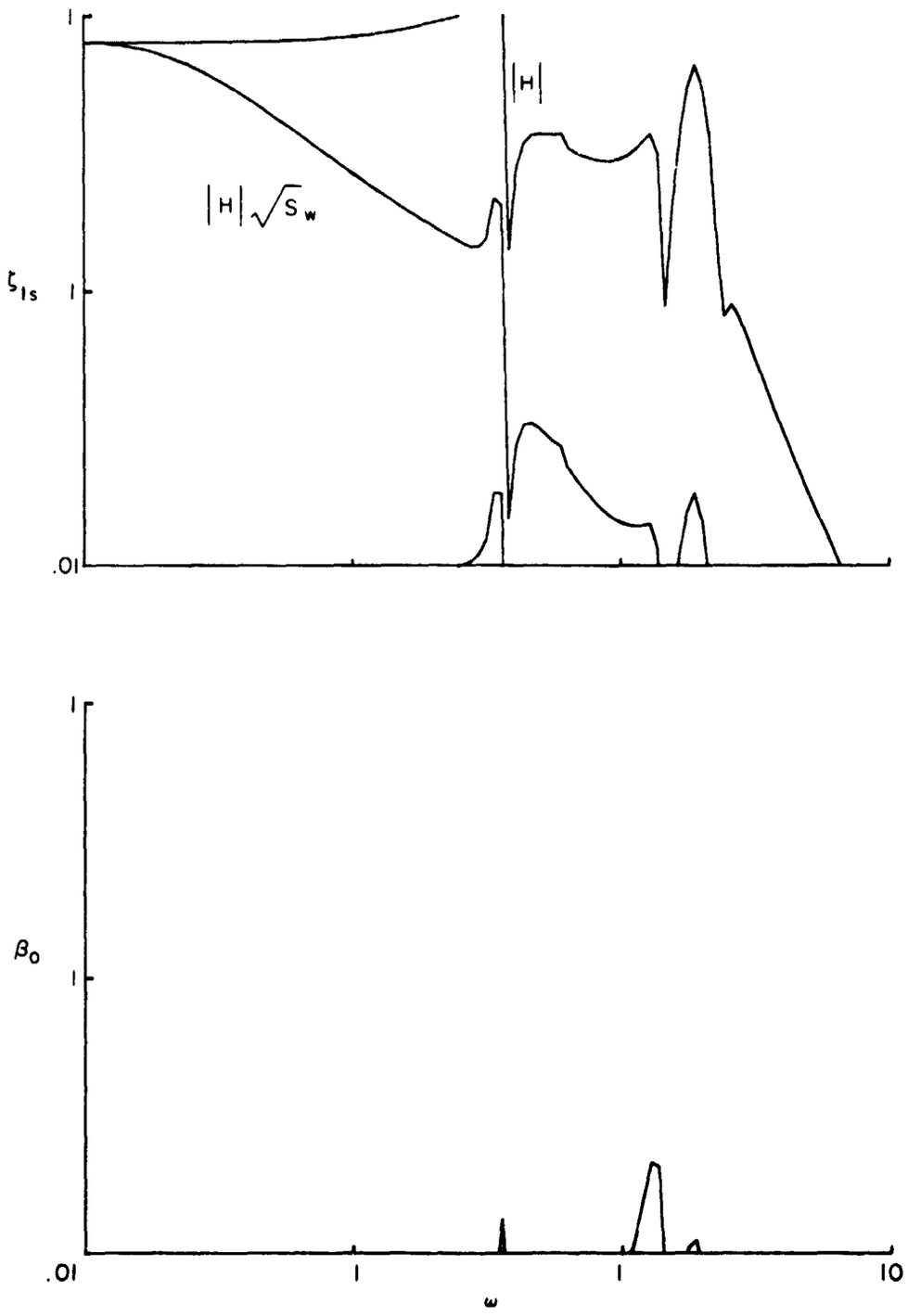

Figure 5.— Continued.

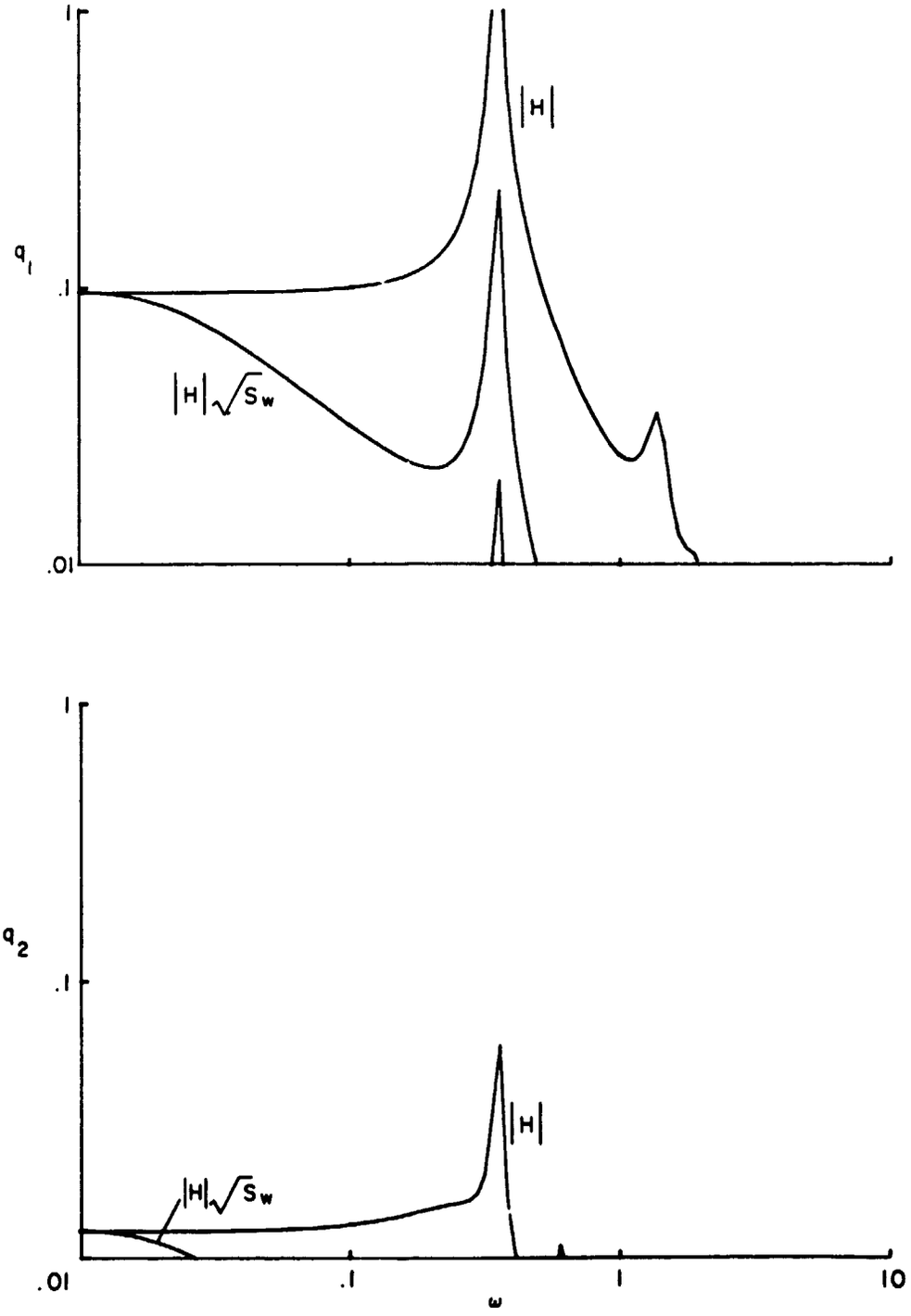

Figure 5.— Continued.

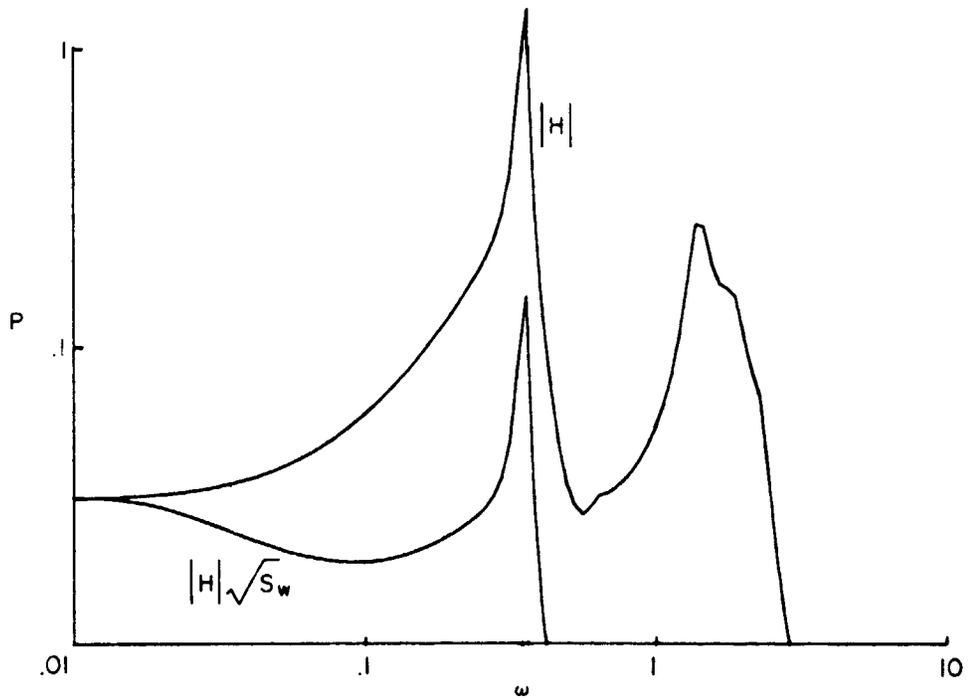

Figure 5.— Concluded.

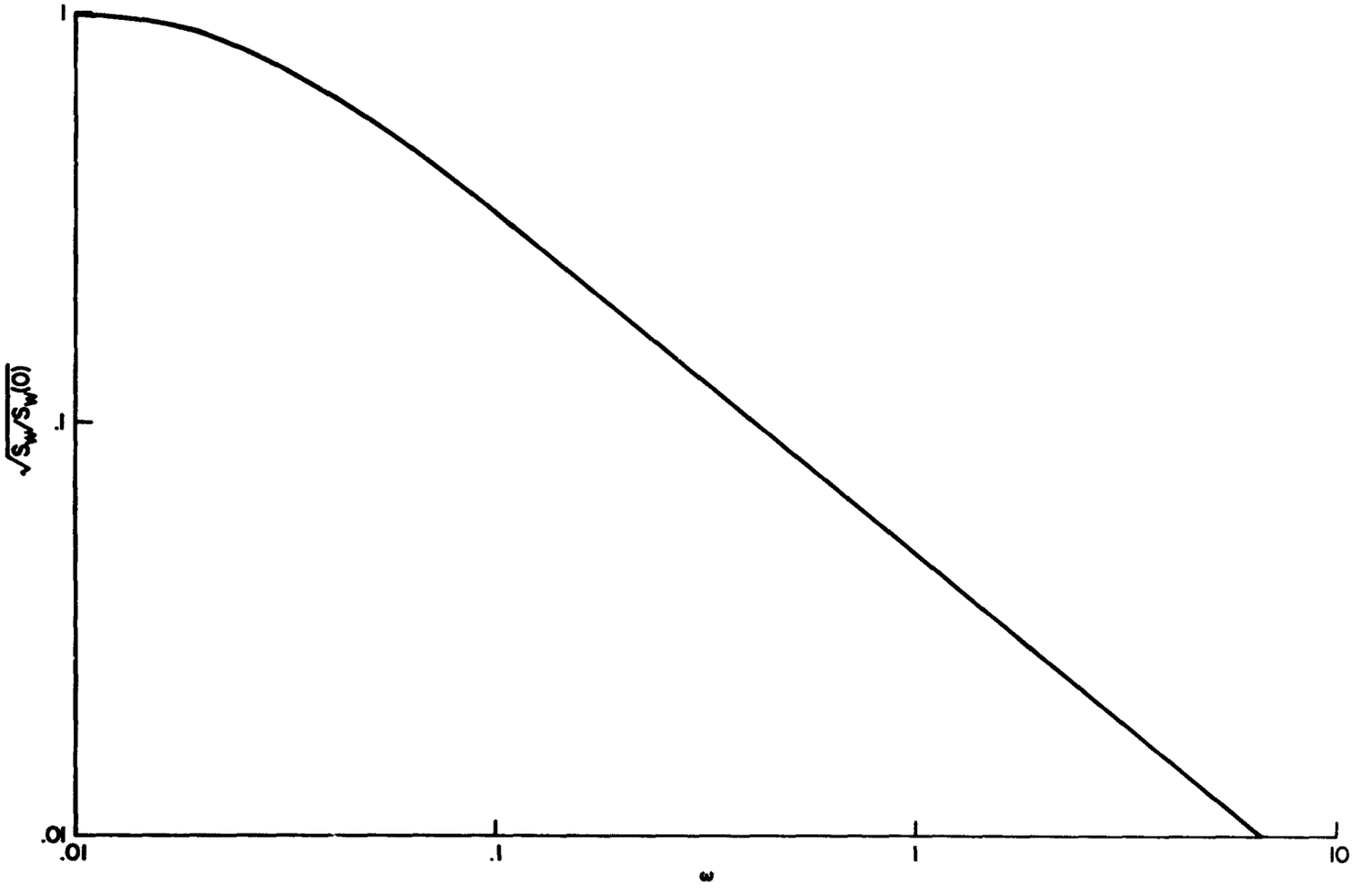

Figure 6.— Gust spectrum, $\sqrt{S_w/S_w(0)}$ for $V/\Omega R = 0.7$.

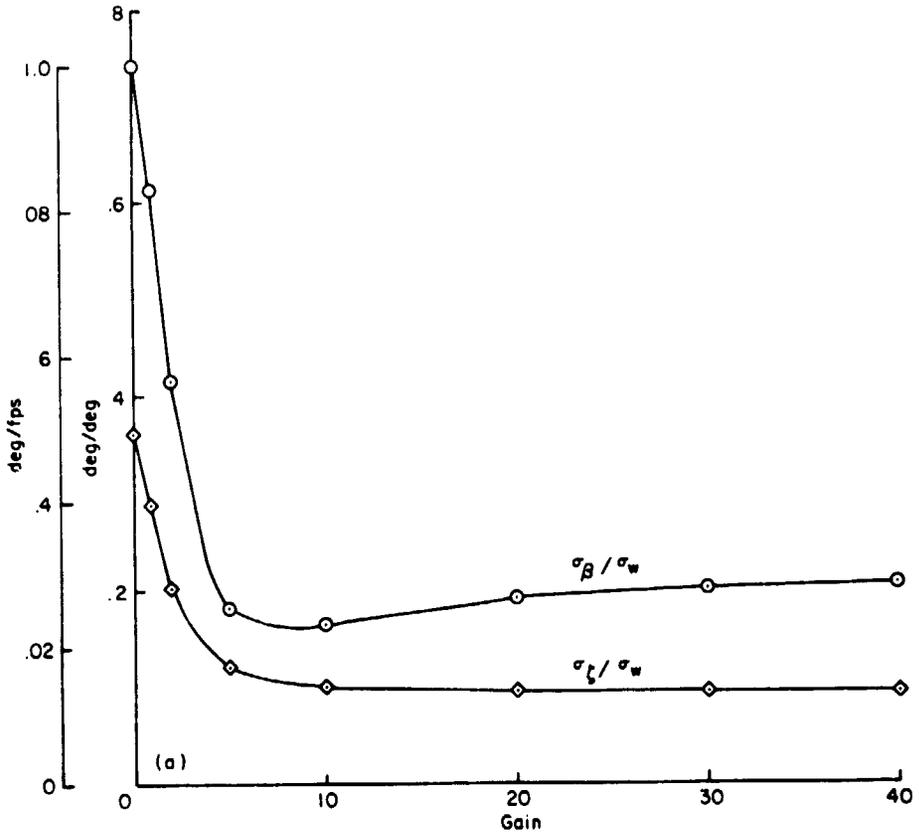

(a) Rms rotor flap and lag response (closed loop/open loop).

Figure 7.— Optimal control for Bell rotor at $V/\Omega R = 0.7$, gain sweep for $Q = 5*.1, 4*1$.

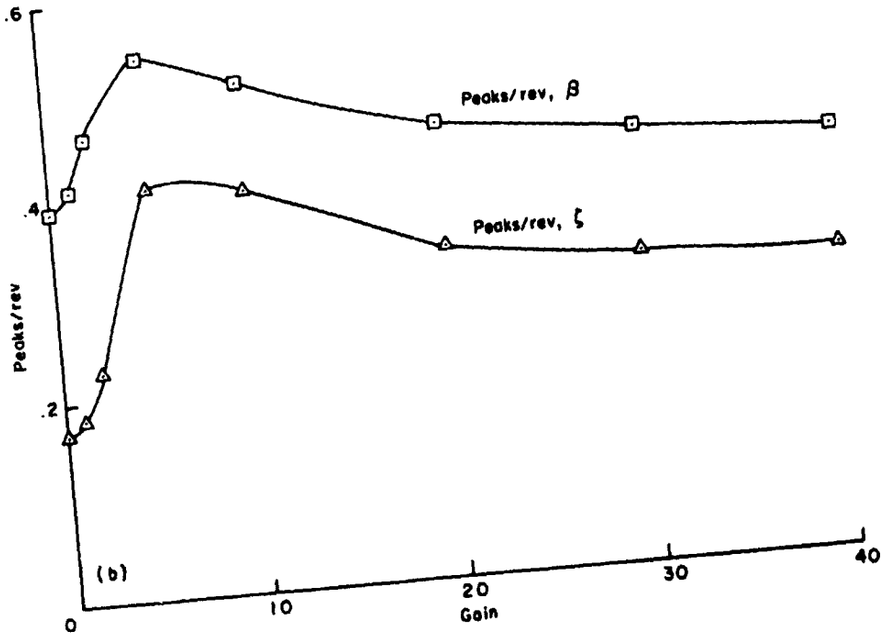

(b) Peaks/rev for flap and lag.

Figure 7.— Continued.

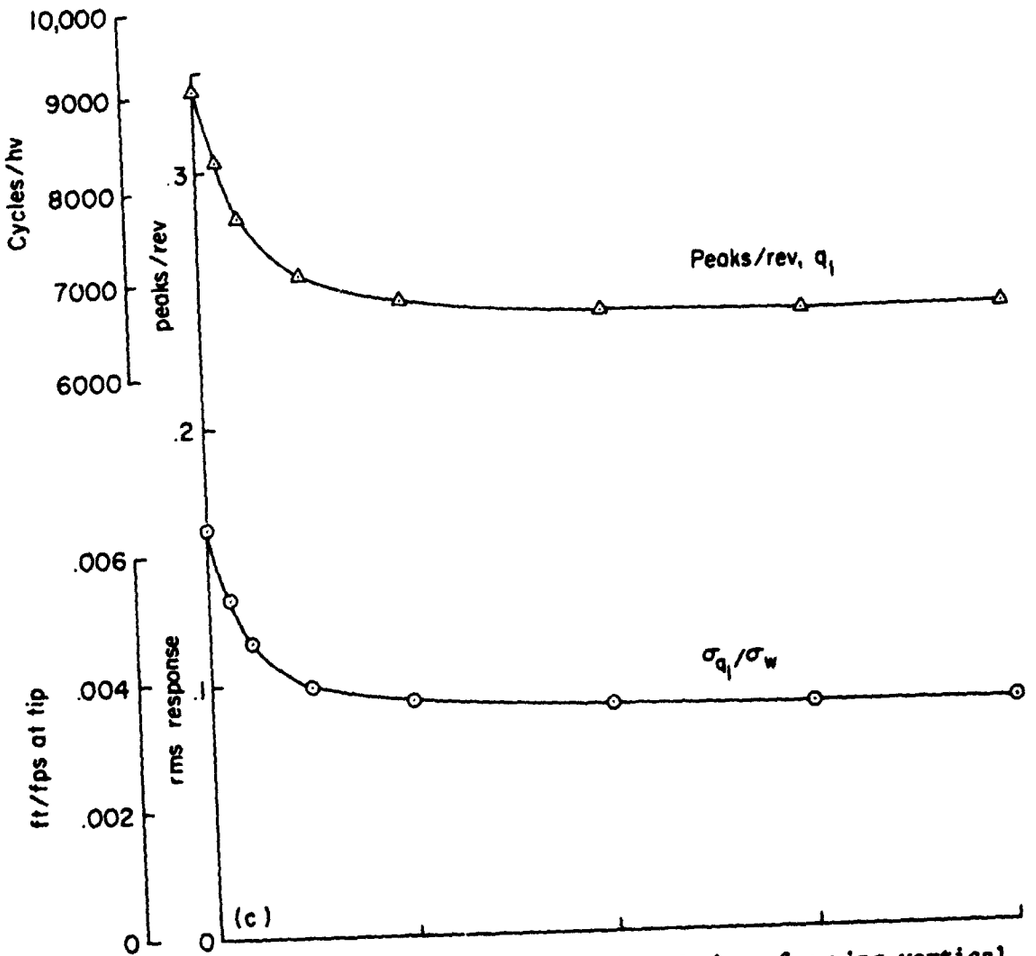

(c) Rms response (closed loop/open loop) and peaks/rev for wing vertical bending (q_1).

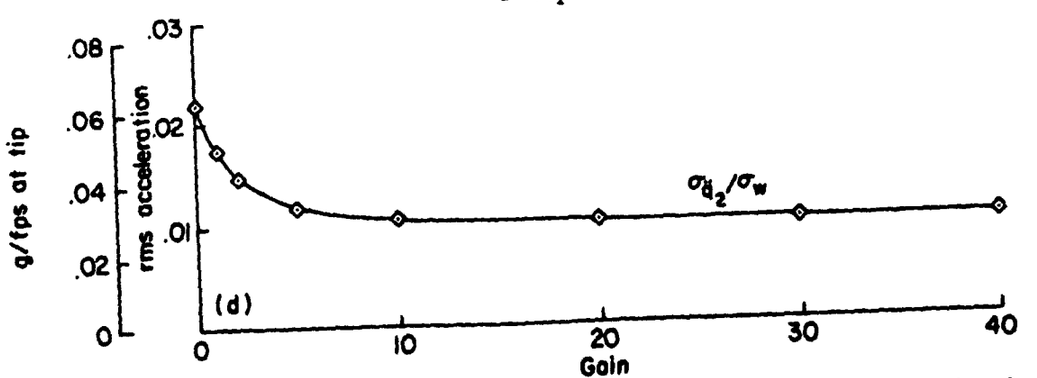

(d) Rms acceleration for wing vertical bending ($\ddot{q}_1$) (closed loop/open loop).

Figure 7.— Continued.

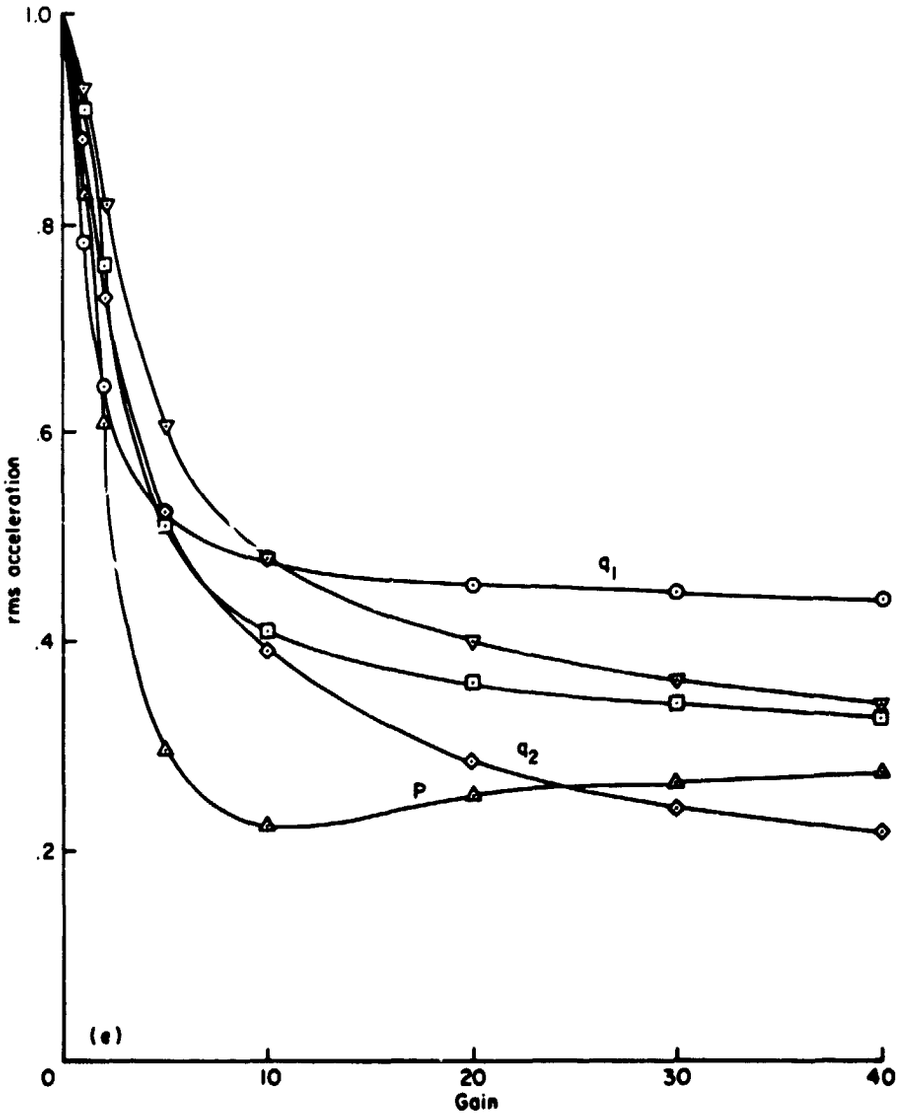

(e) Rms acceleration of wing and rotor motion (closed loop/open loop).

Figure 7.– Continued.

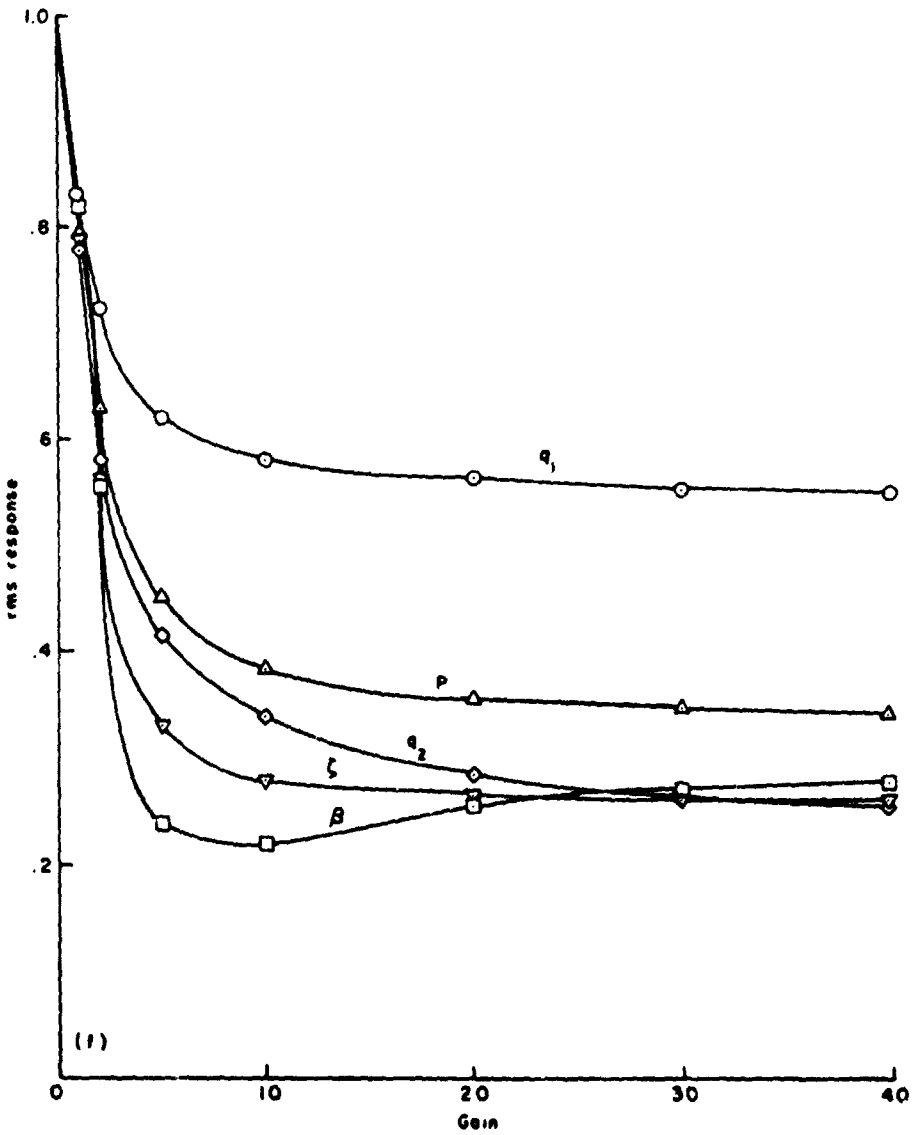

(f) Rms response of wing and rotor motion (closed loop/open loop).

Figure 7.– Continued.

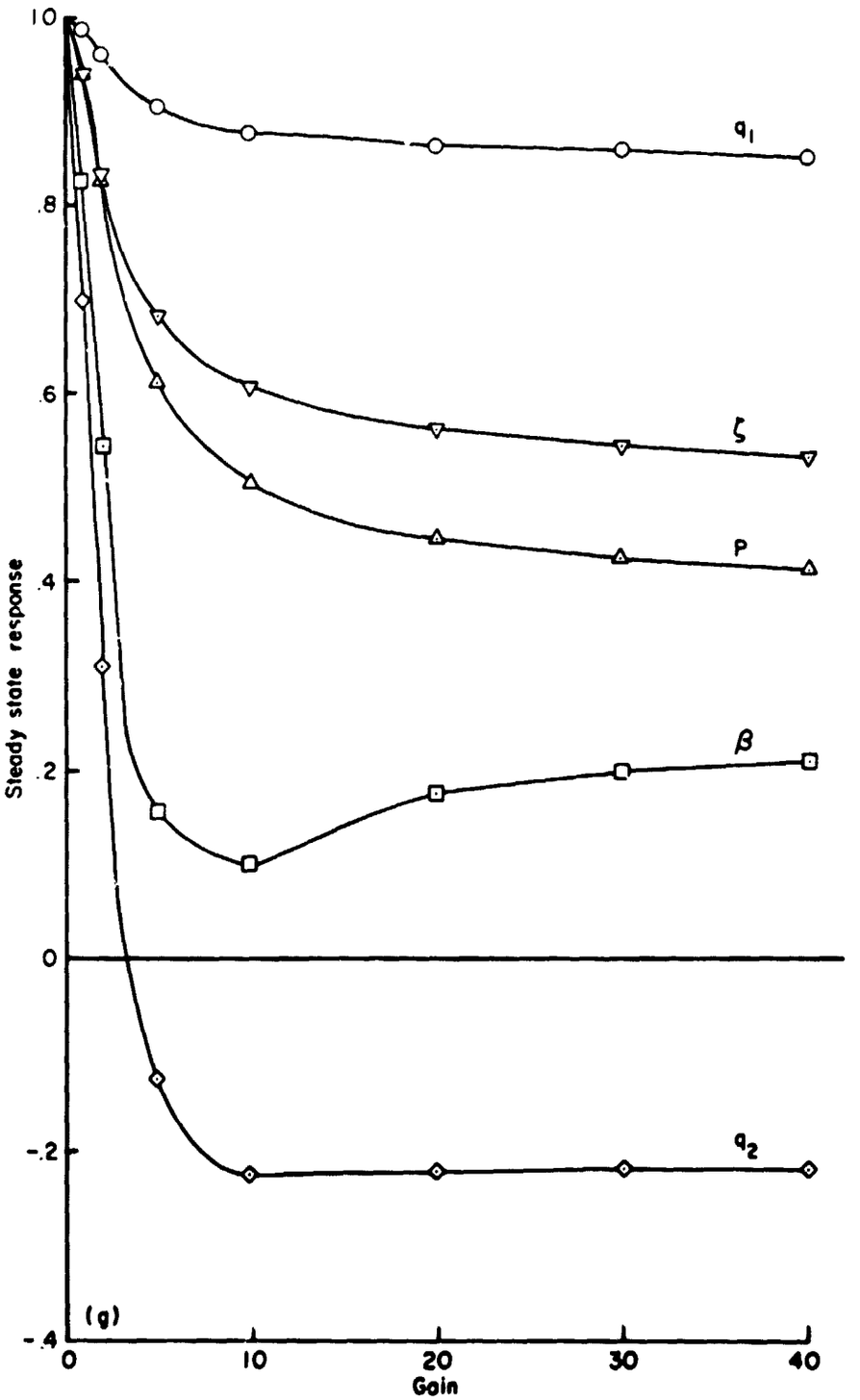

(g) Steady state response of wing and rotor (closed loop/open loop).

Figure 7.– Continued.

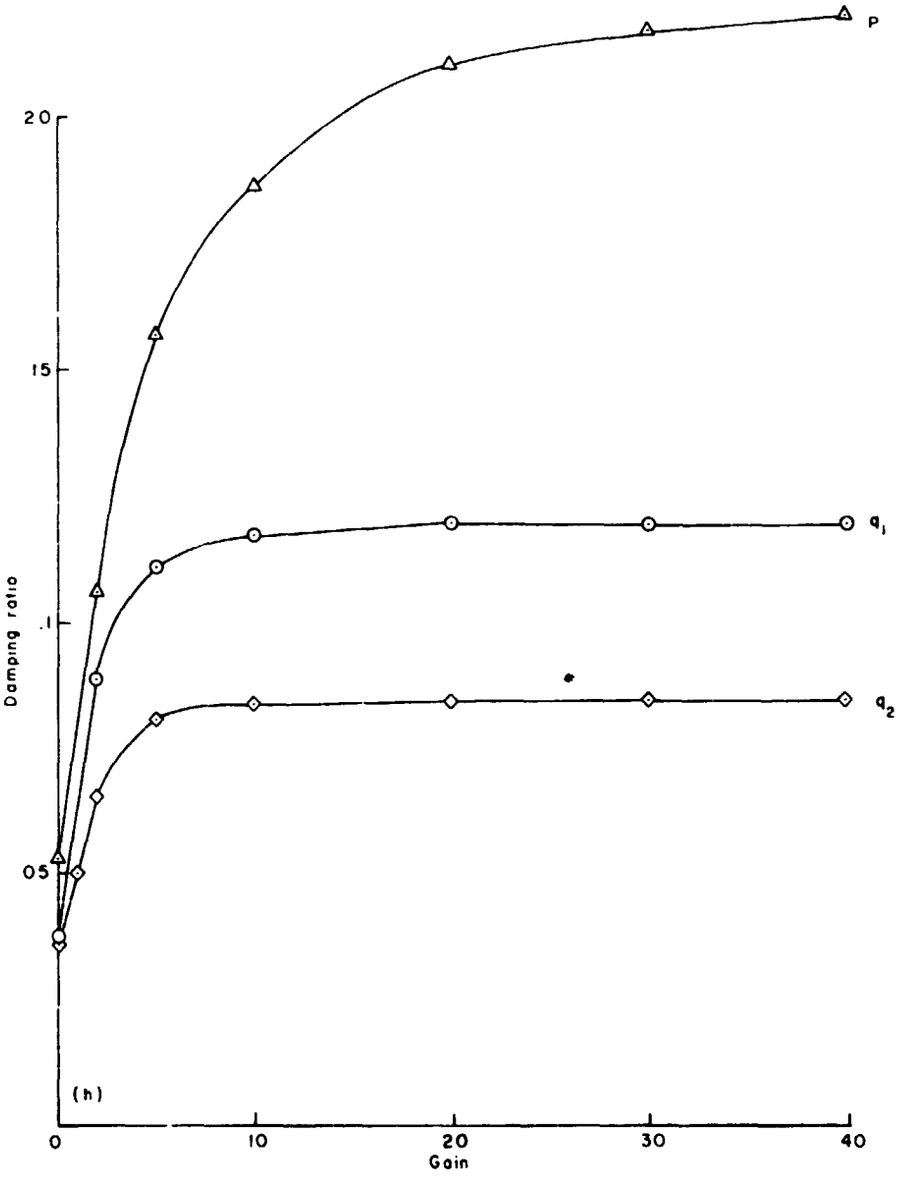

(h) Damping ratio of wing modes.

Figure 7.— Concluded.

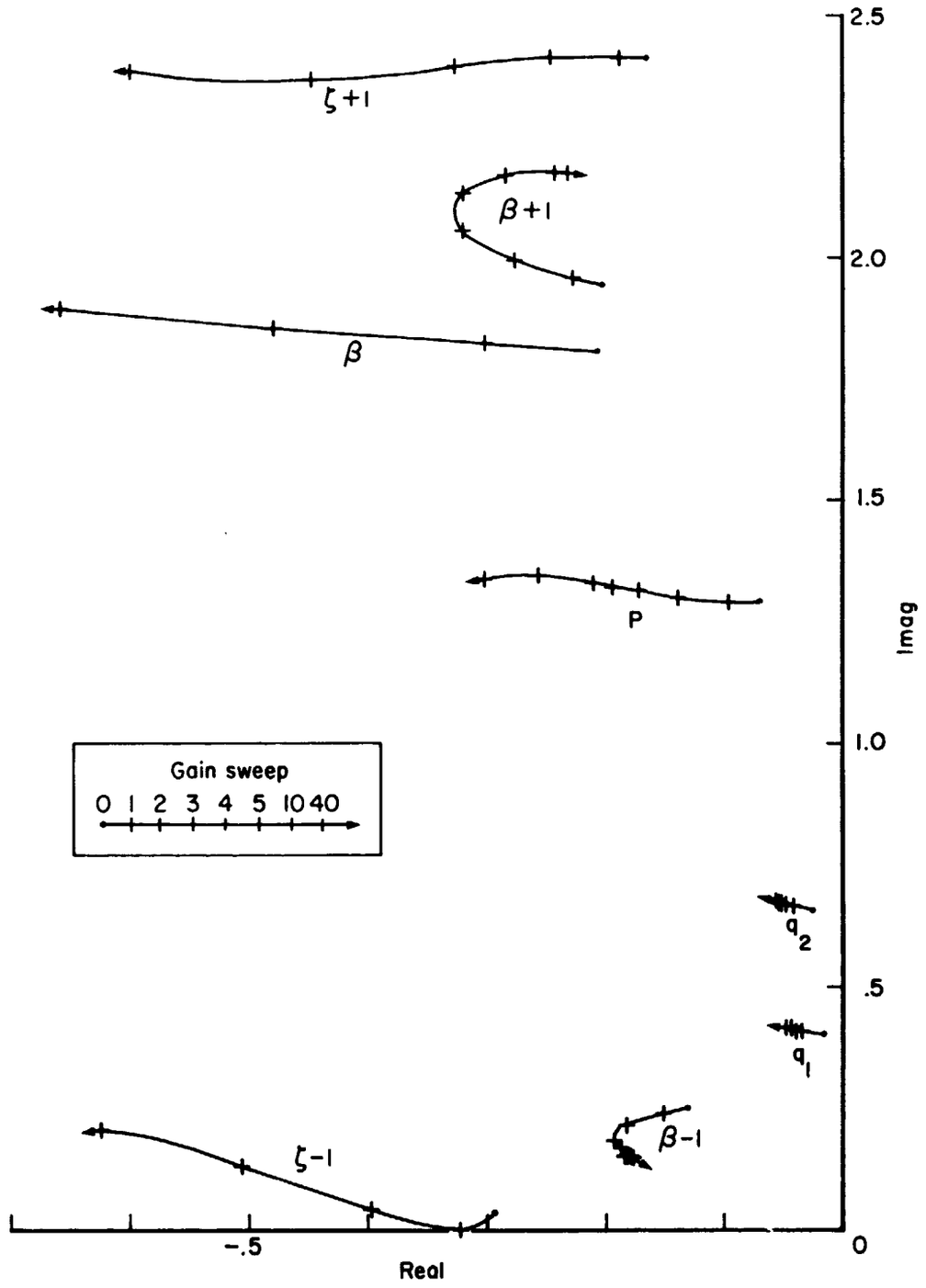

Figure 8.— Root locus for Bell rotor, gain sweep for Q = 5*.1, 4*1.

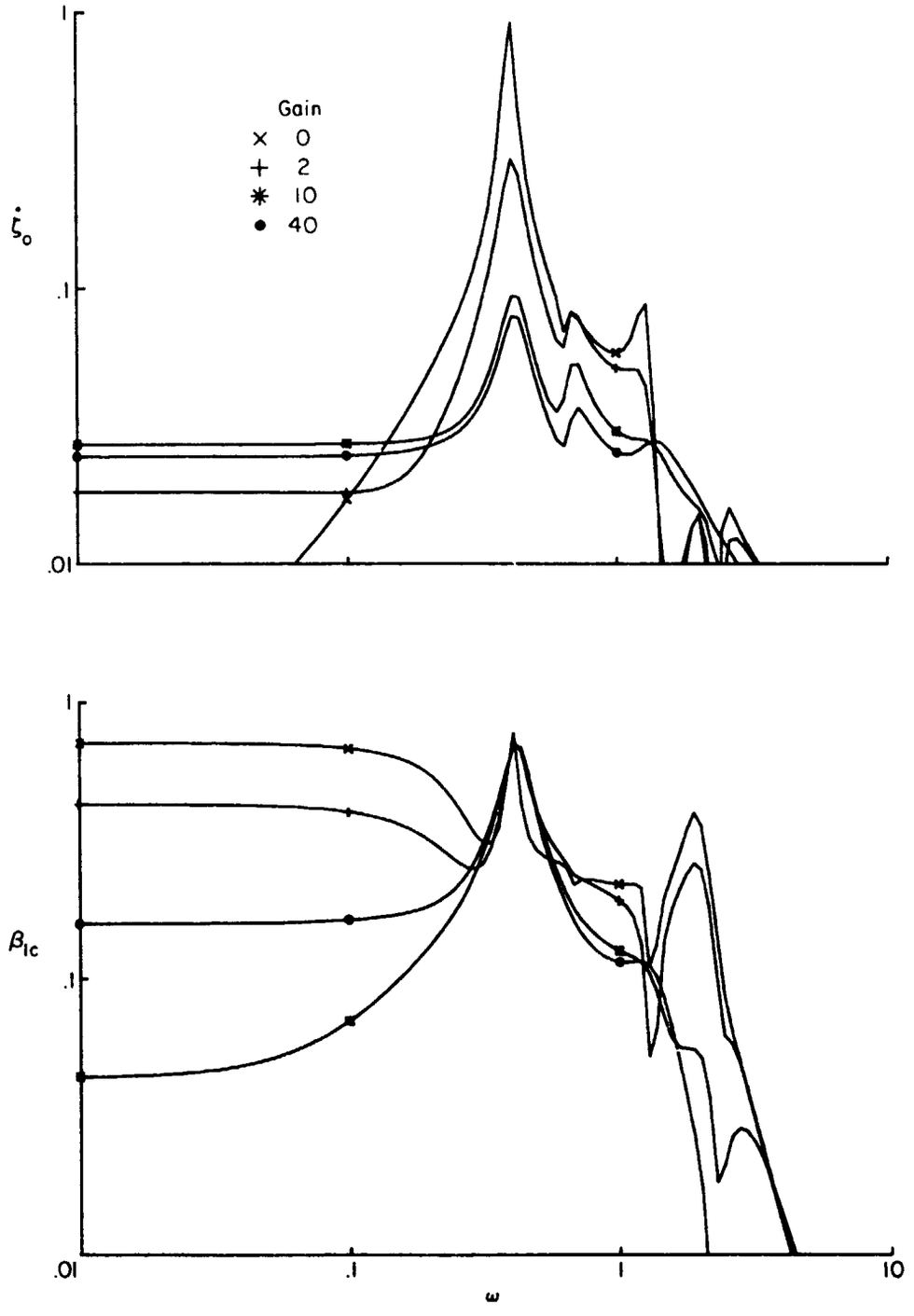

Figure 9.— Transfer function for Bell rotor, gain sweep for Q = 5*.1, 4*1.

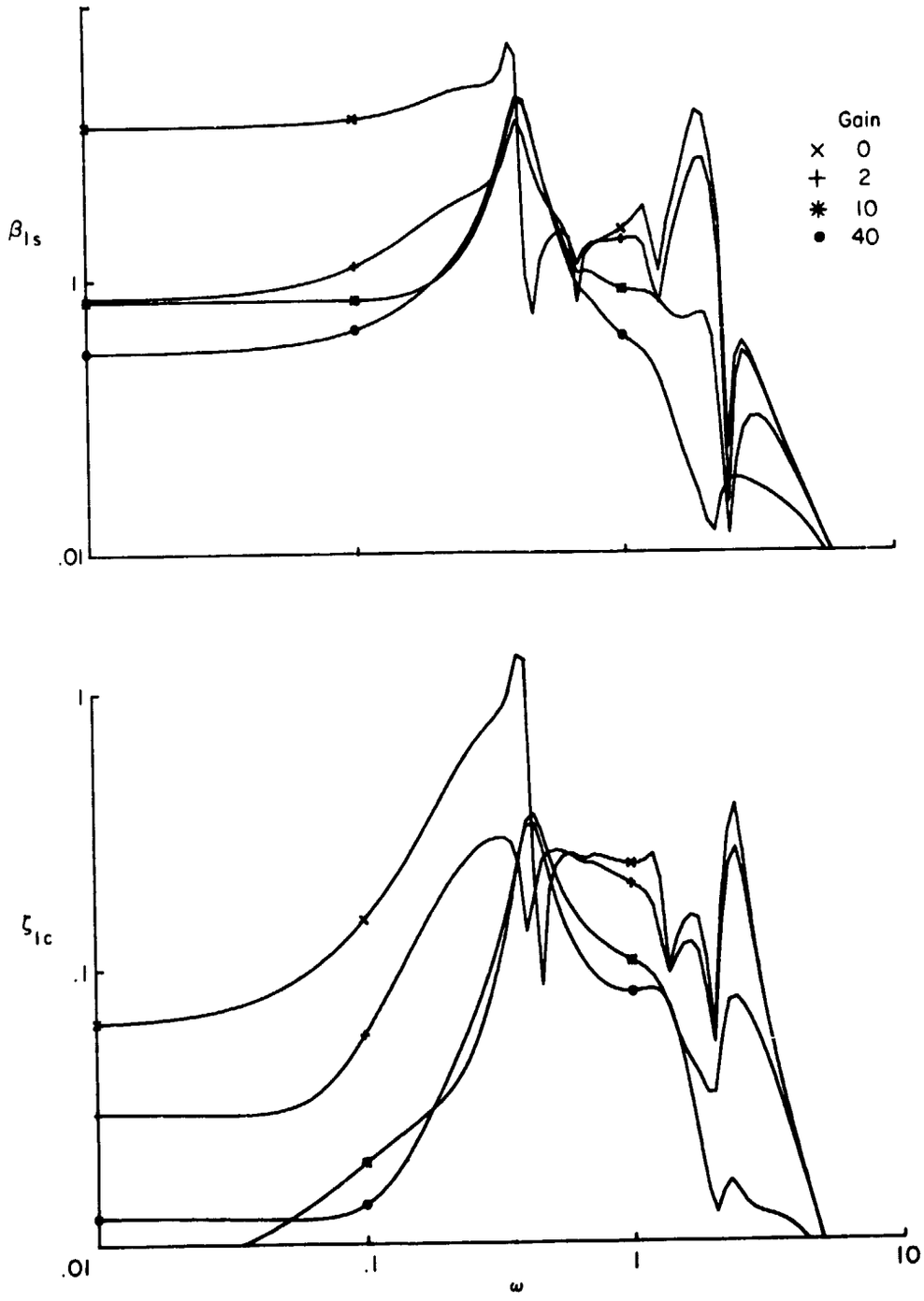

Figure 9.– Continued.

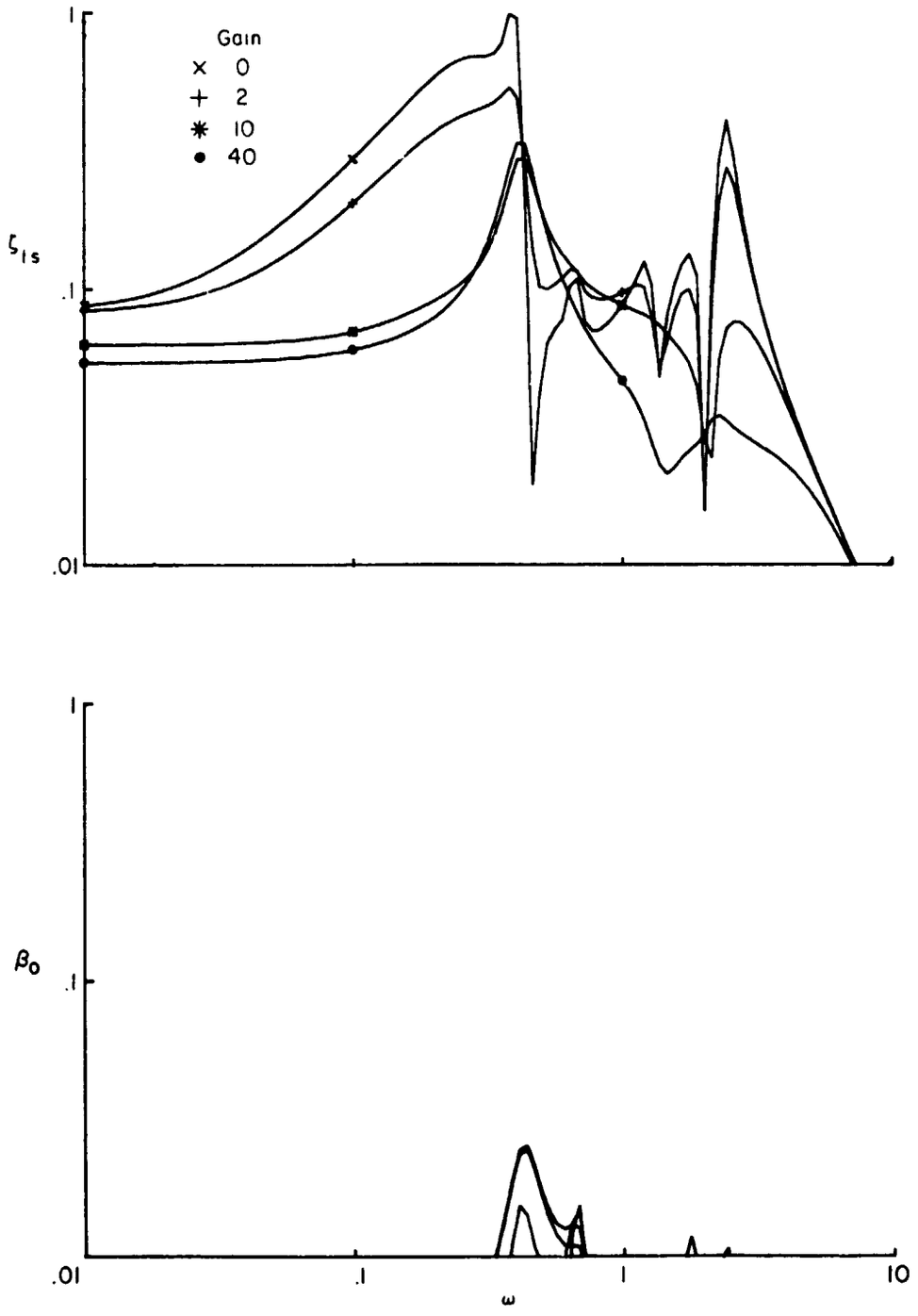

Figure 9.— Continued.

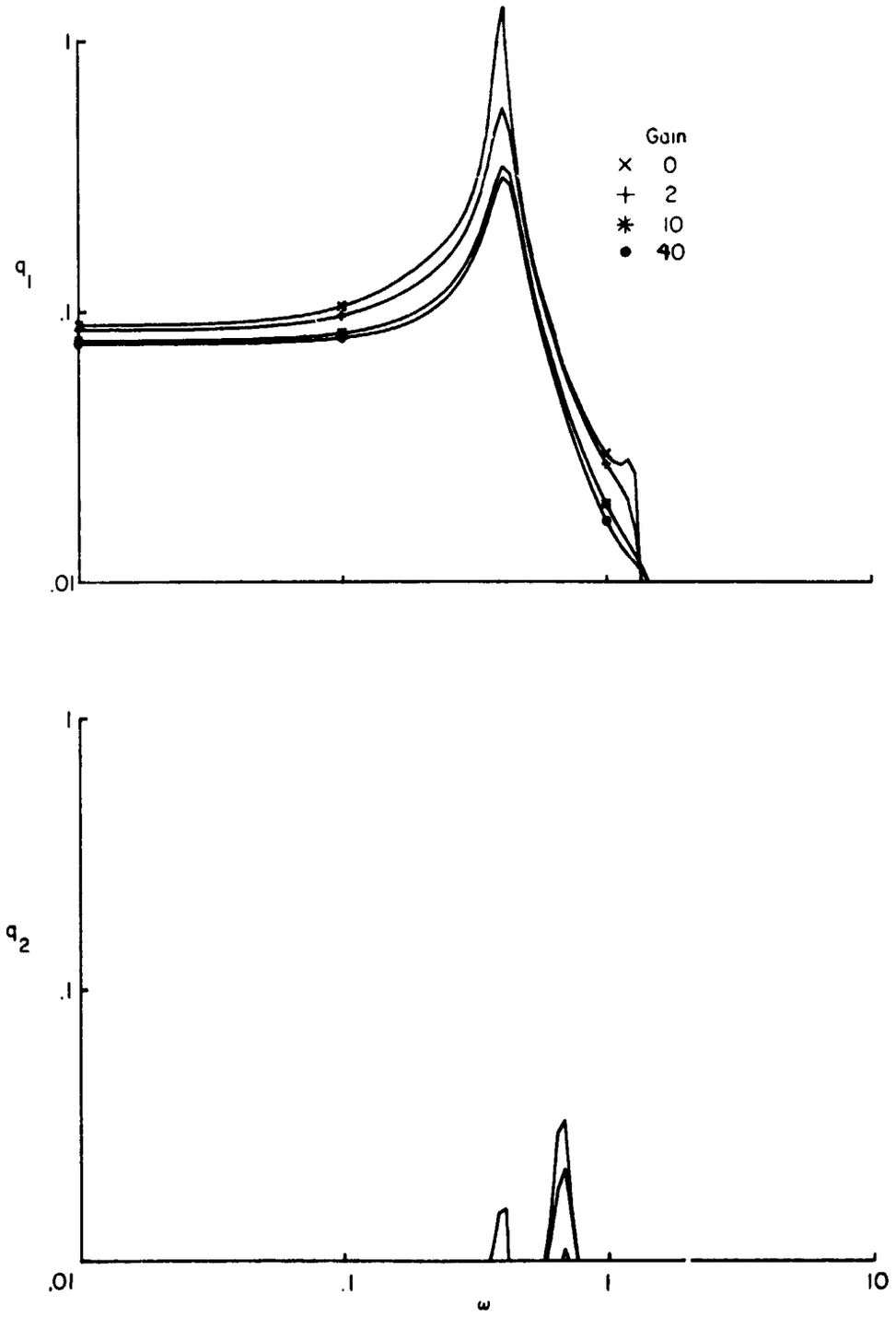

Figure 9.— Continued.

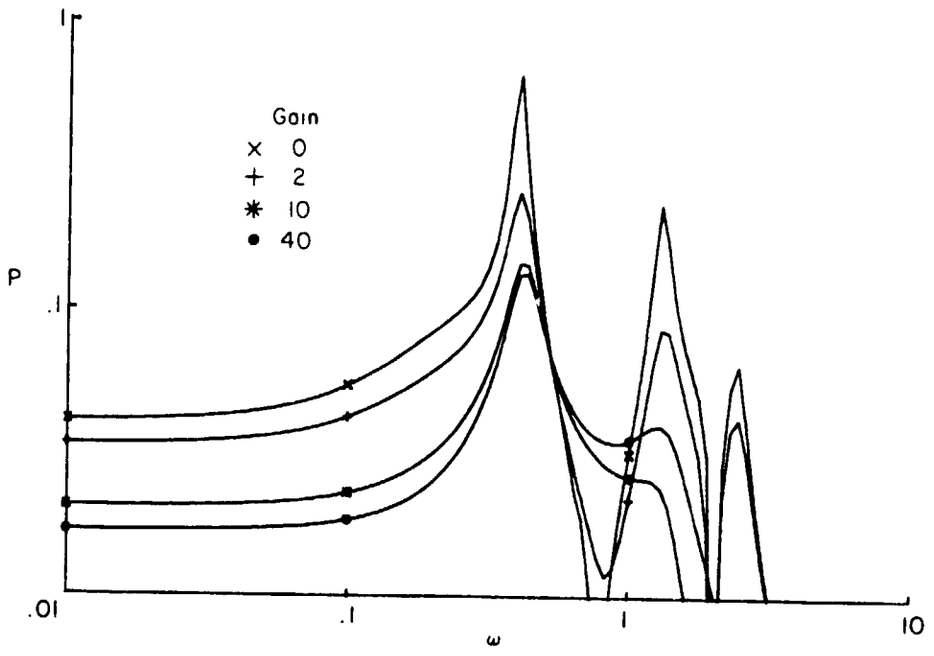

Figure 9.— Concluded.

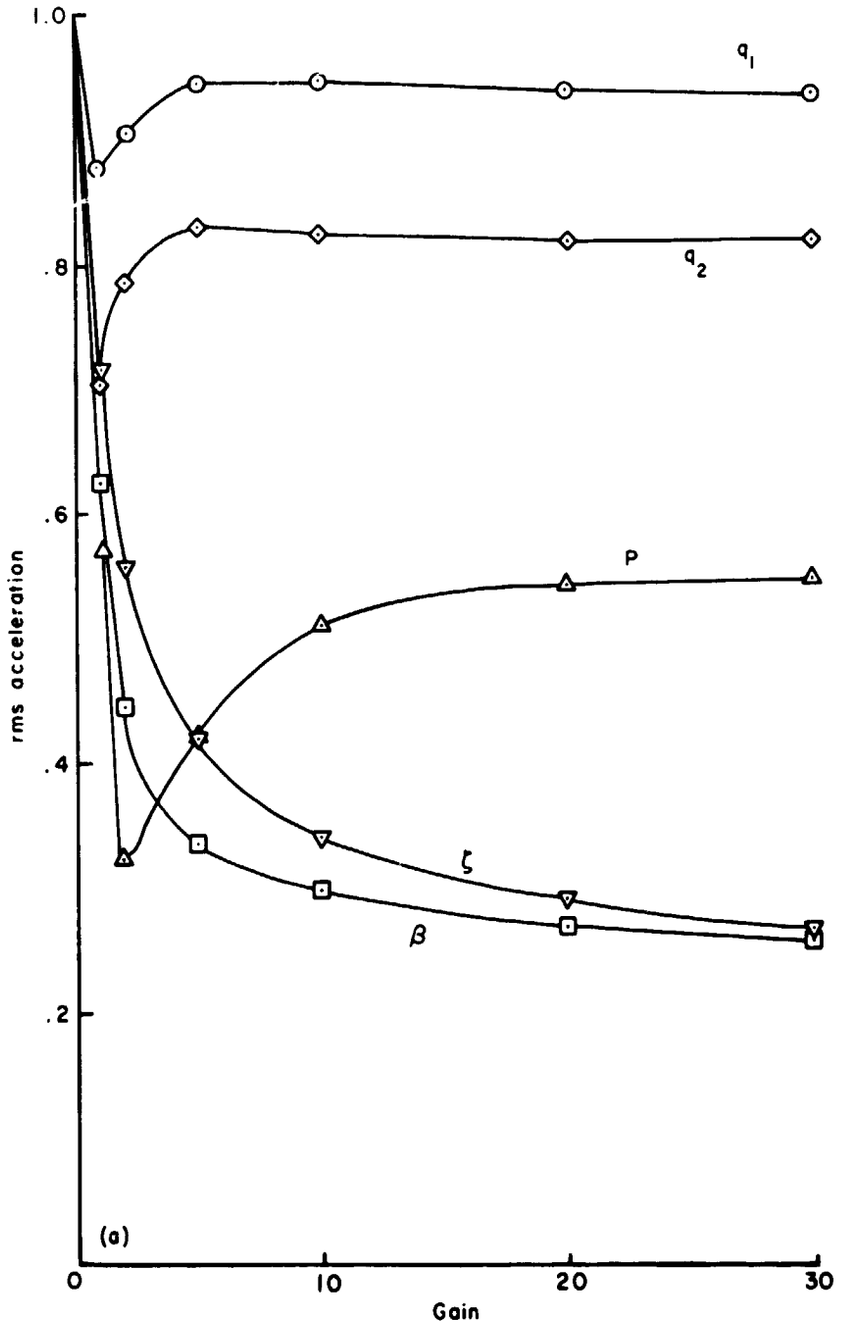

(a) Rms acceleration of wing and rotor motion (closed loop/open loop).

Figure 10.— Control of Bell rotor with constraint on rotor motion only, Q = 6*1, 3*0.

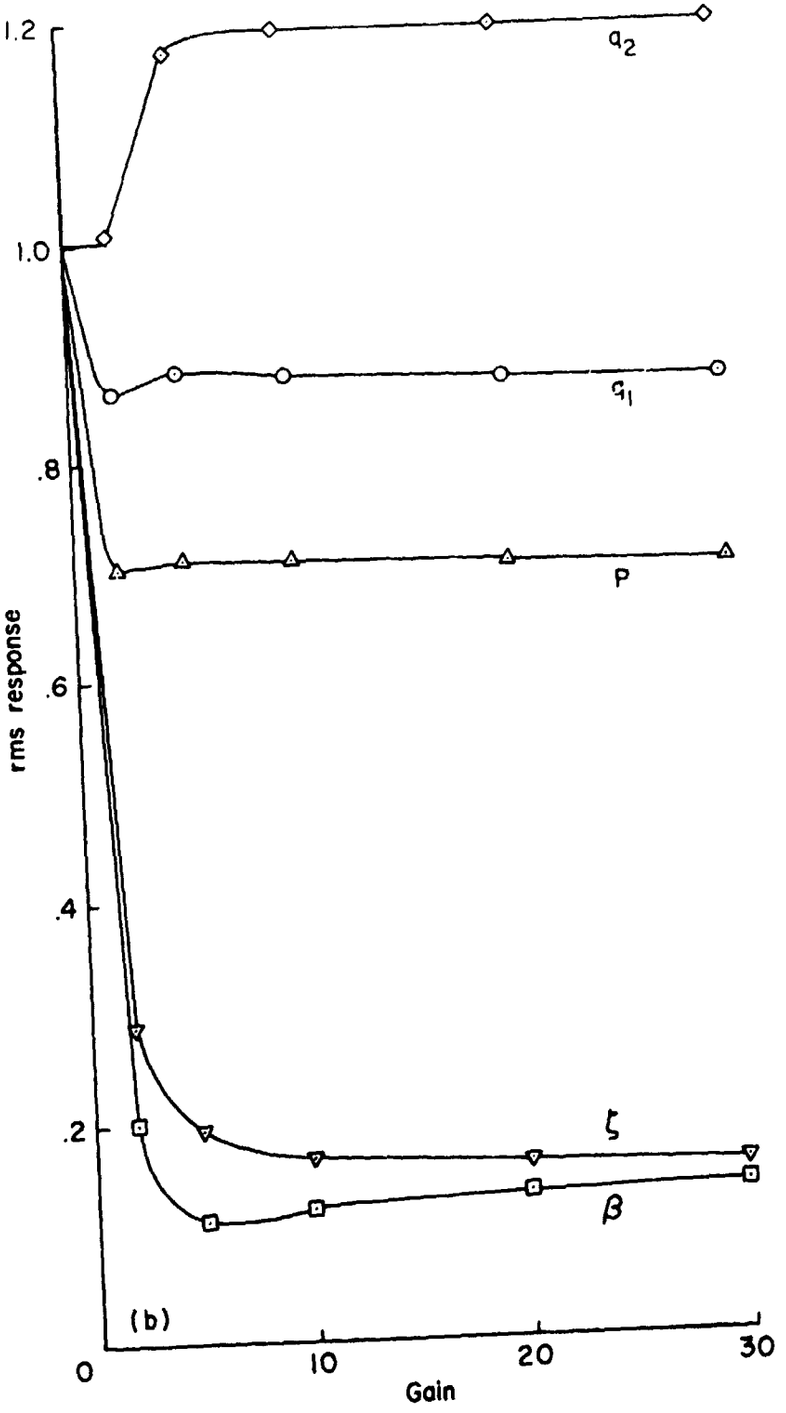

(b) Rms response of wing and rotor motion (closed loop/open loop).

Figure 10.— Continued.

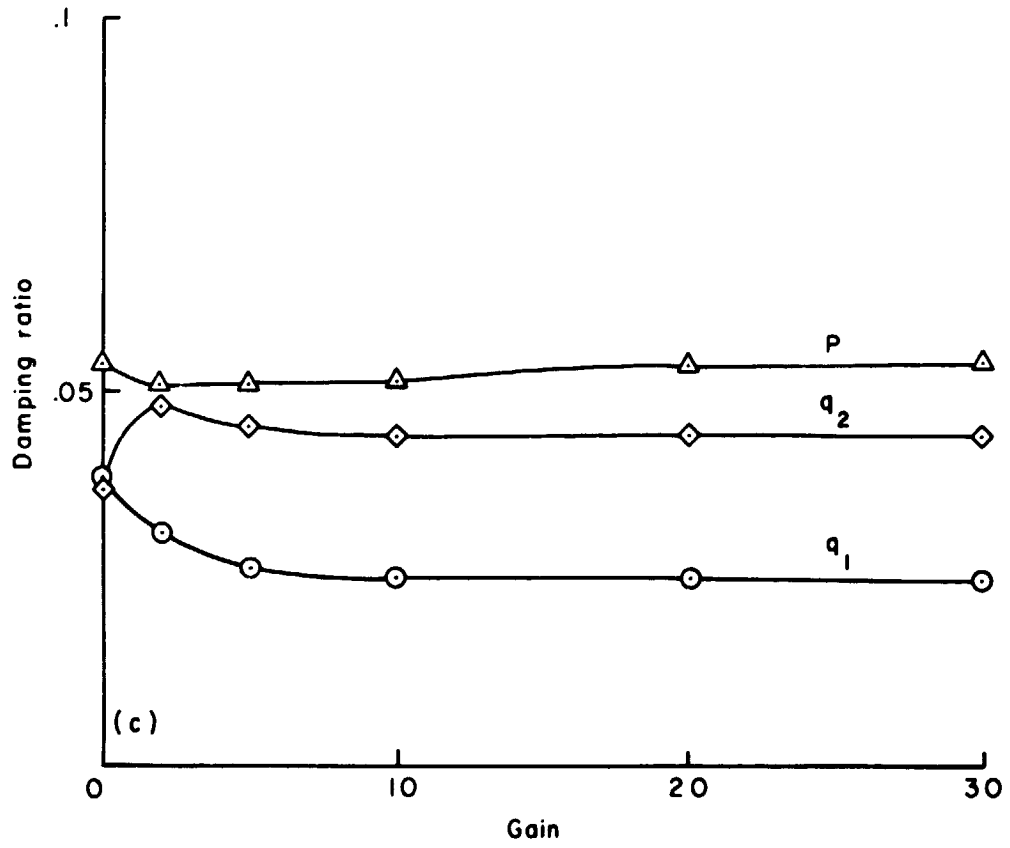

(c) Damping ratio of wing modes.

Figure 10.— Continued.

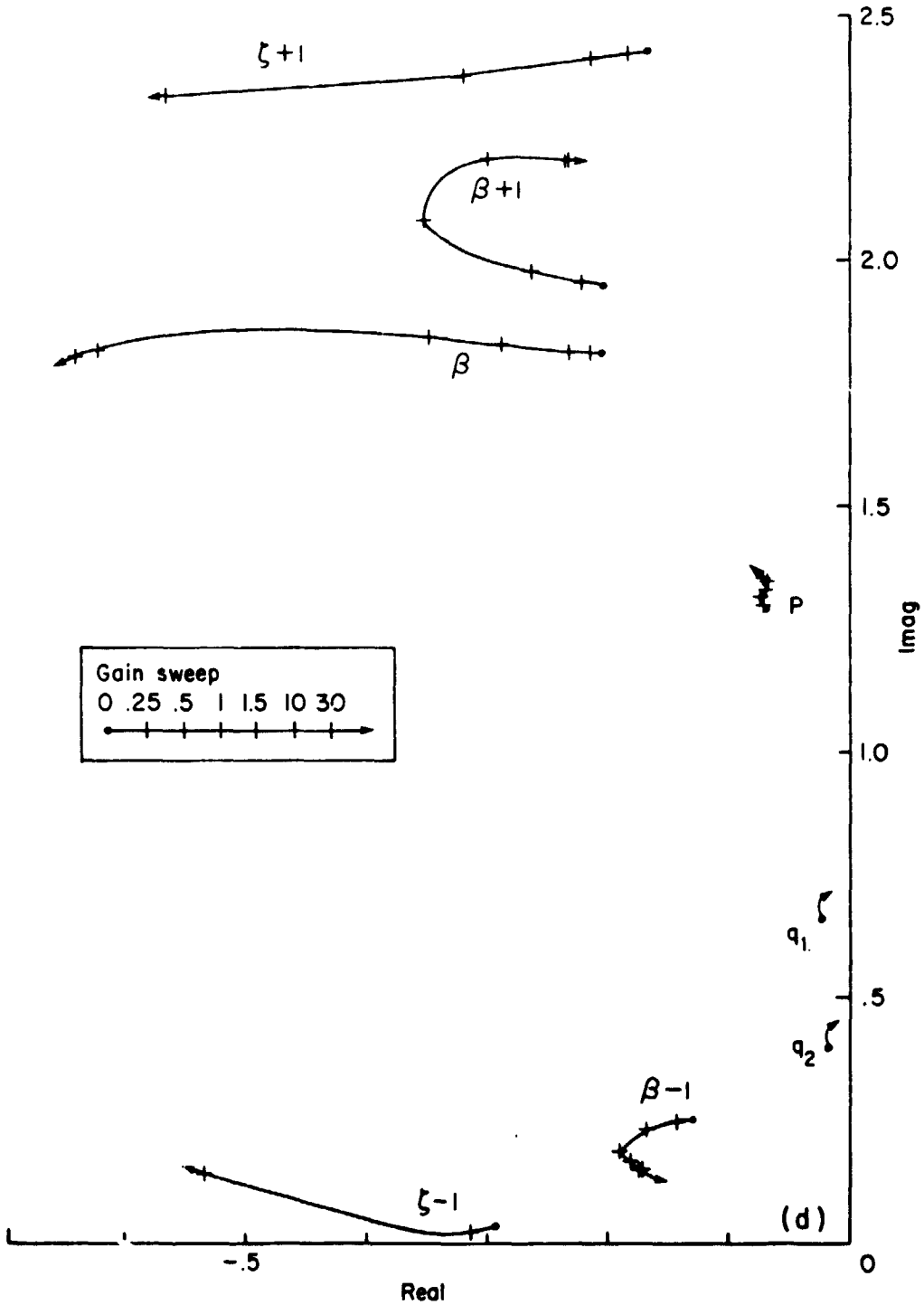

(d) Root locus.

Figure 10.– Concluded.

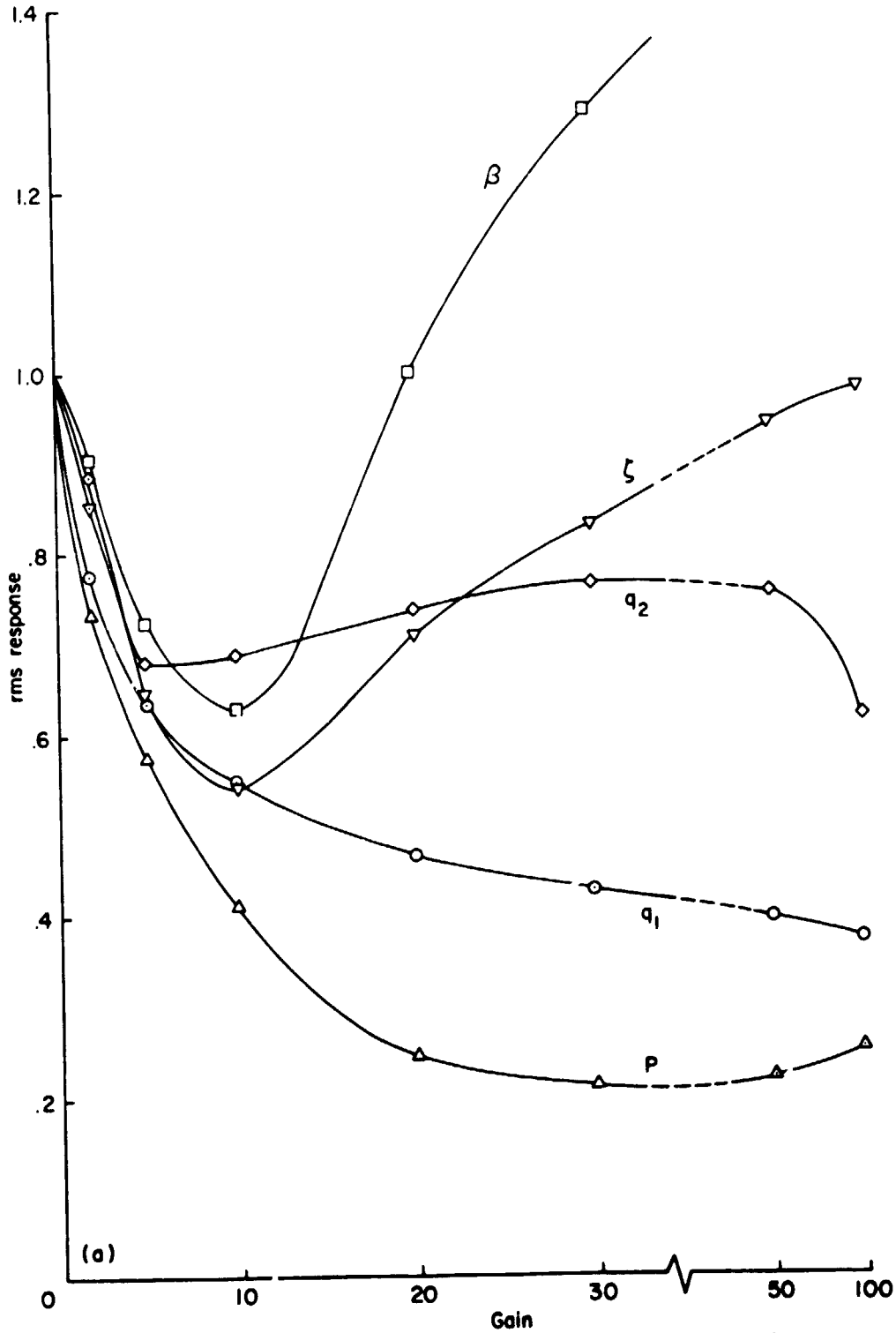

(a) Rms acceleration of wing and rotor motion (closed loop/open loop).

Figure 11.– Control of Bell rotor with constraint on wing motion only, Q = 6•0, 3•1.

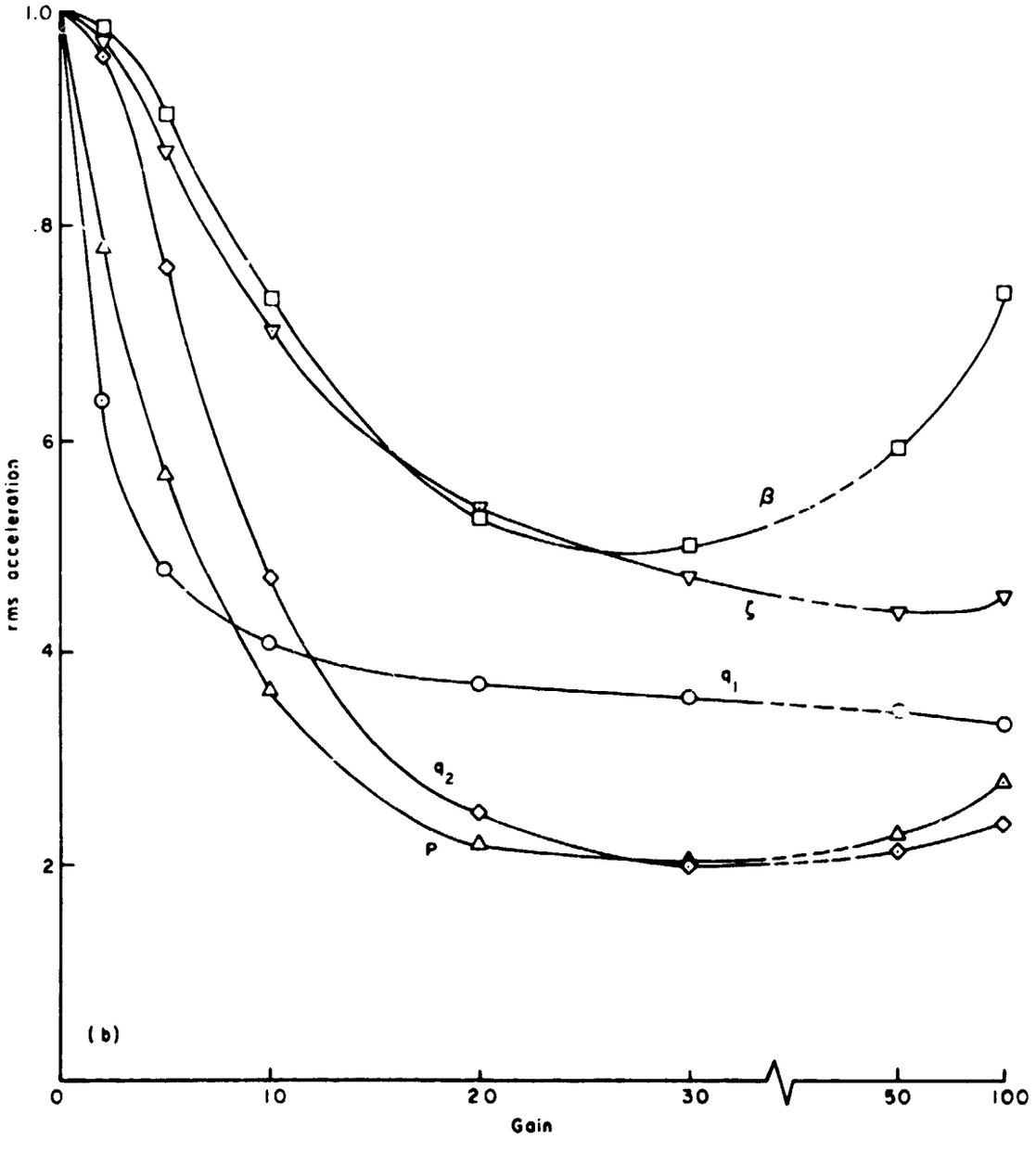

(b) Rms response of wing and rotor motion (closed loop/open loop).

Figure 11.– Continued.

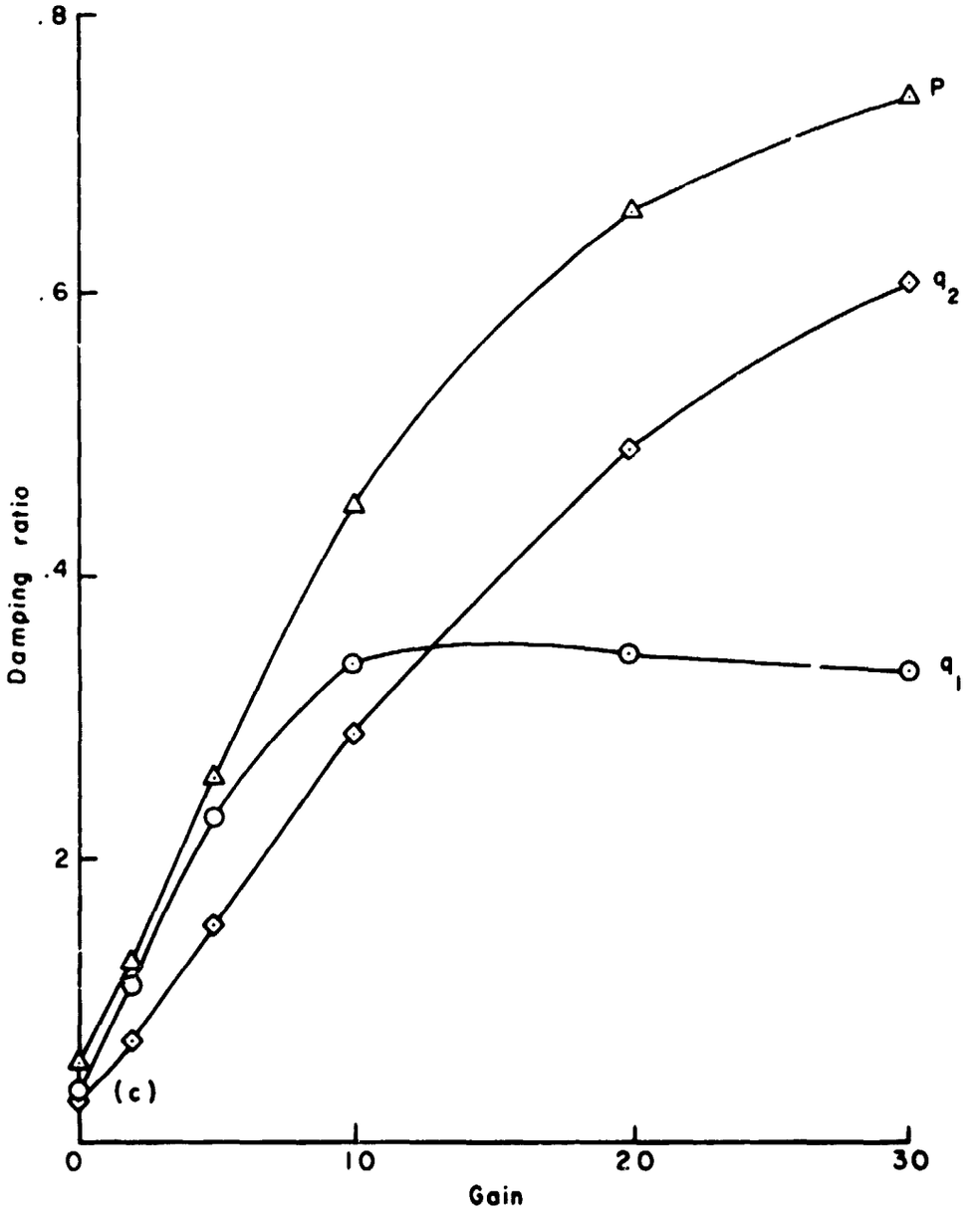

(c) Damping ratio of wing modes.

Figure 11.– Continued.

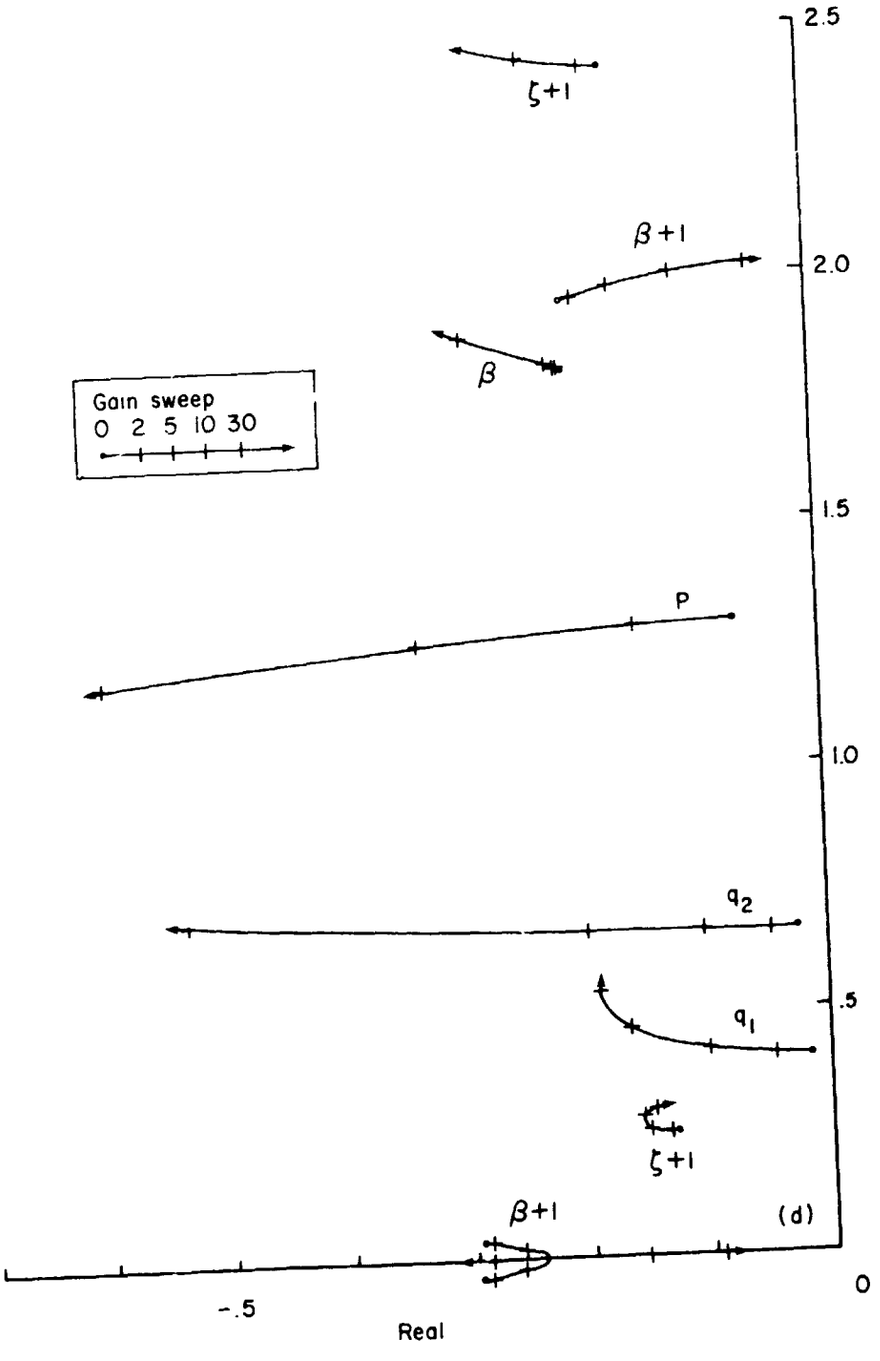

(d) Root locus.

Figure 11.— Concluded.

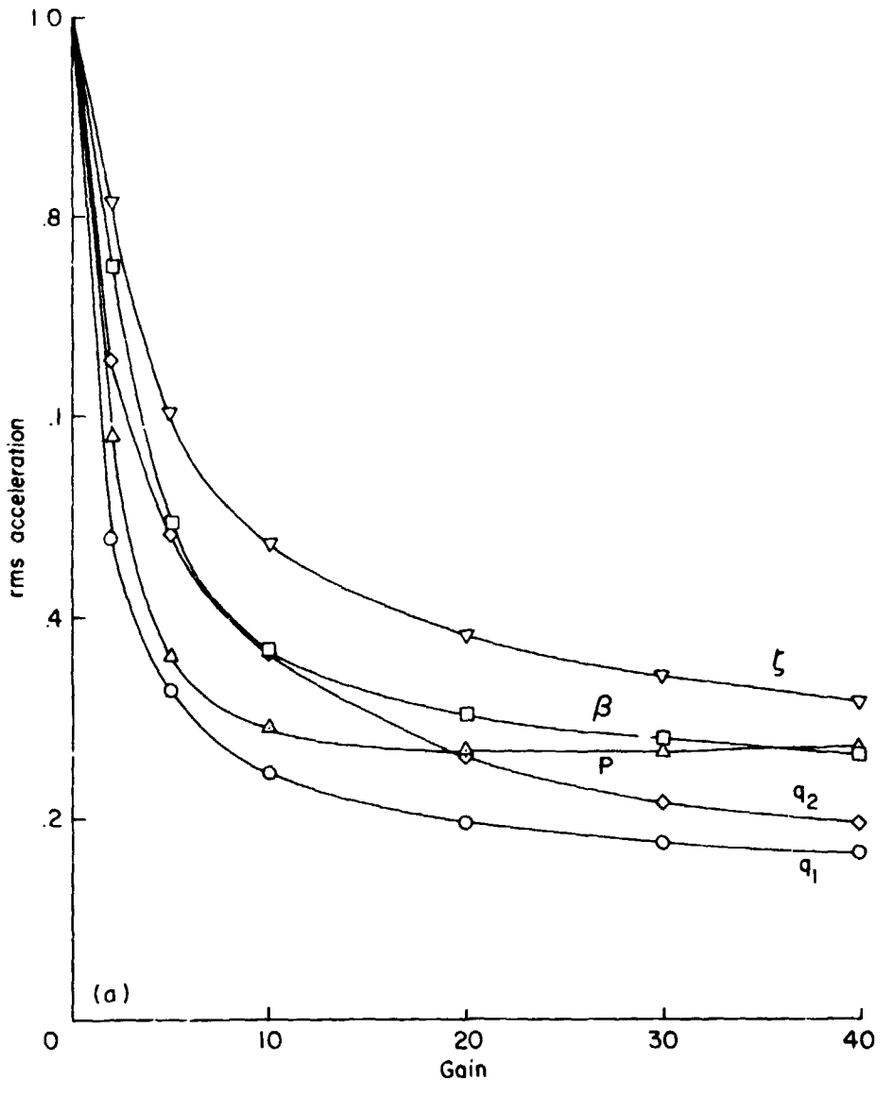

(a) Rms acceleration of wing and rotor motion (closed loop/open loop).

Figure 12.— Optimal control of Bell rotor including wing flap control input, Q = 5*.1, 4*1.

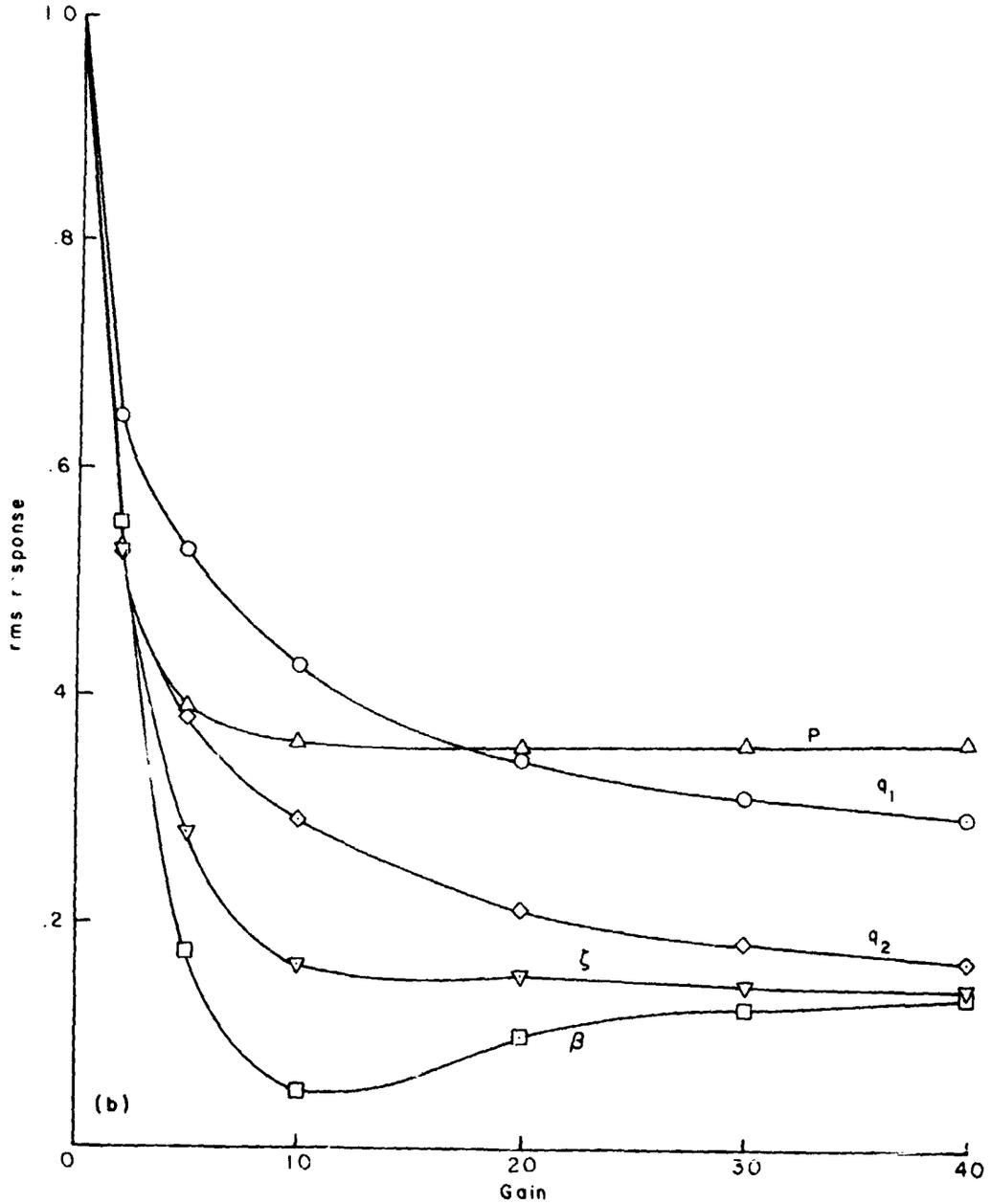

(b) Rms response of wing and rotor motion (closed loop/open loop).

Figure 12.– Continued.

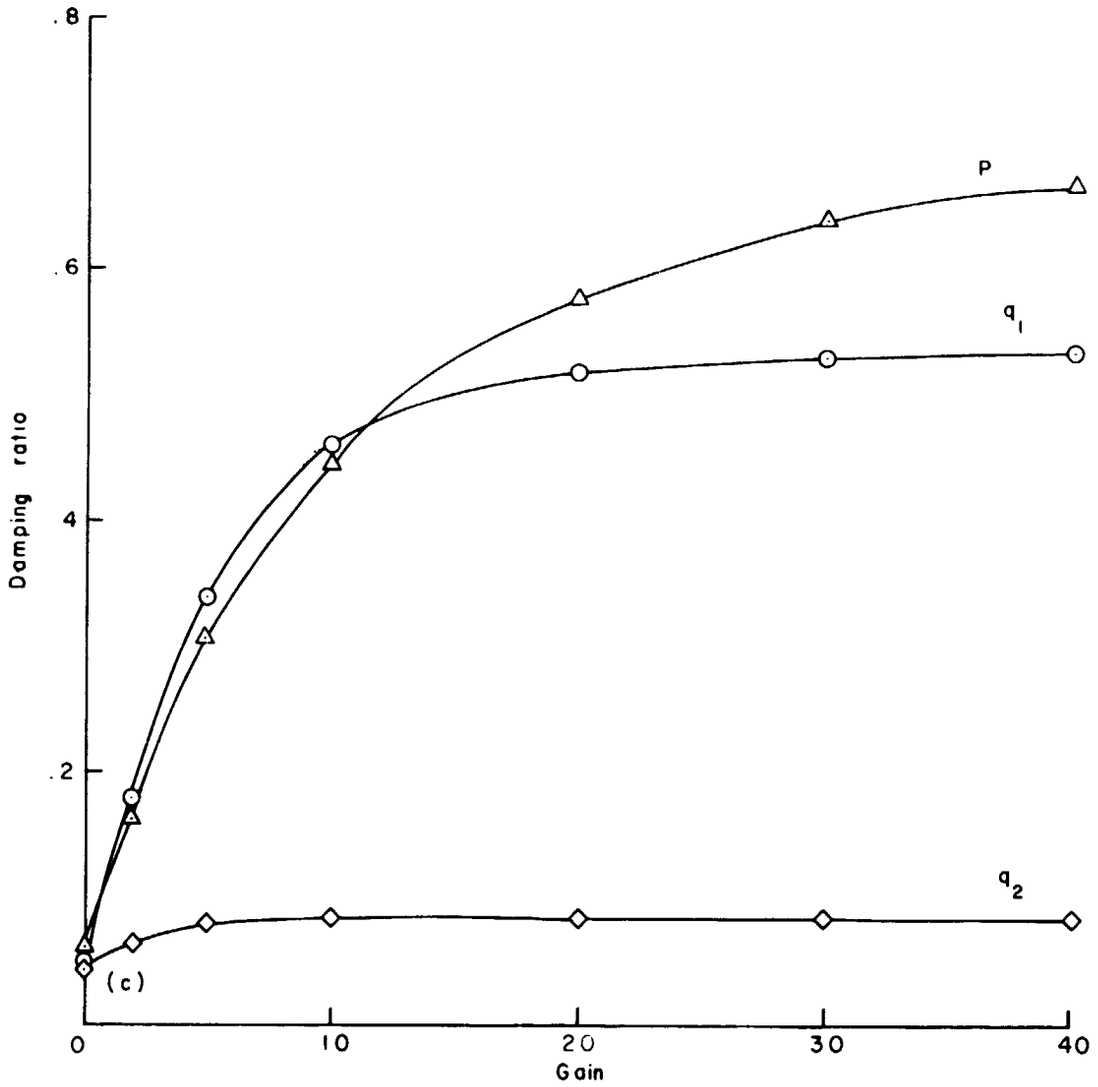

(c) Damping ratio of wing mc

Figure 12.— Continued.

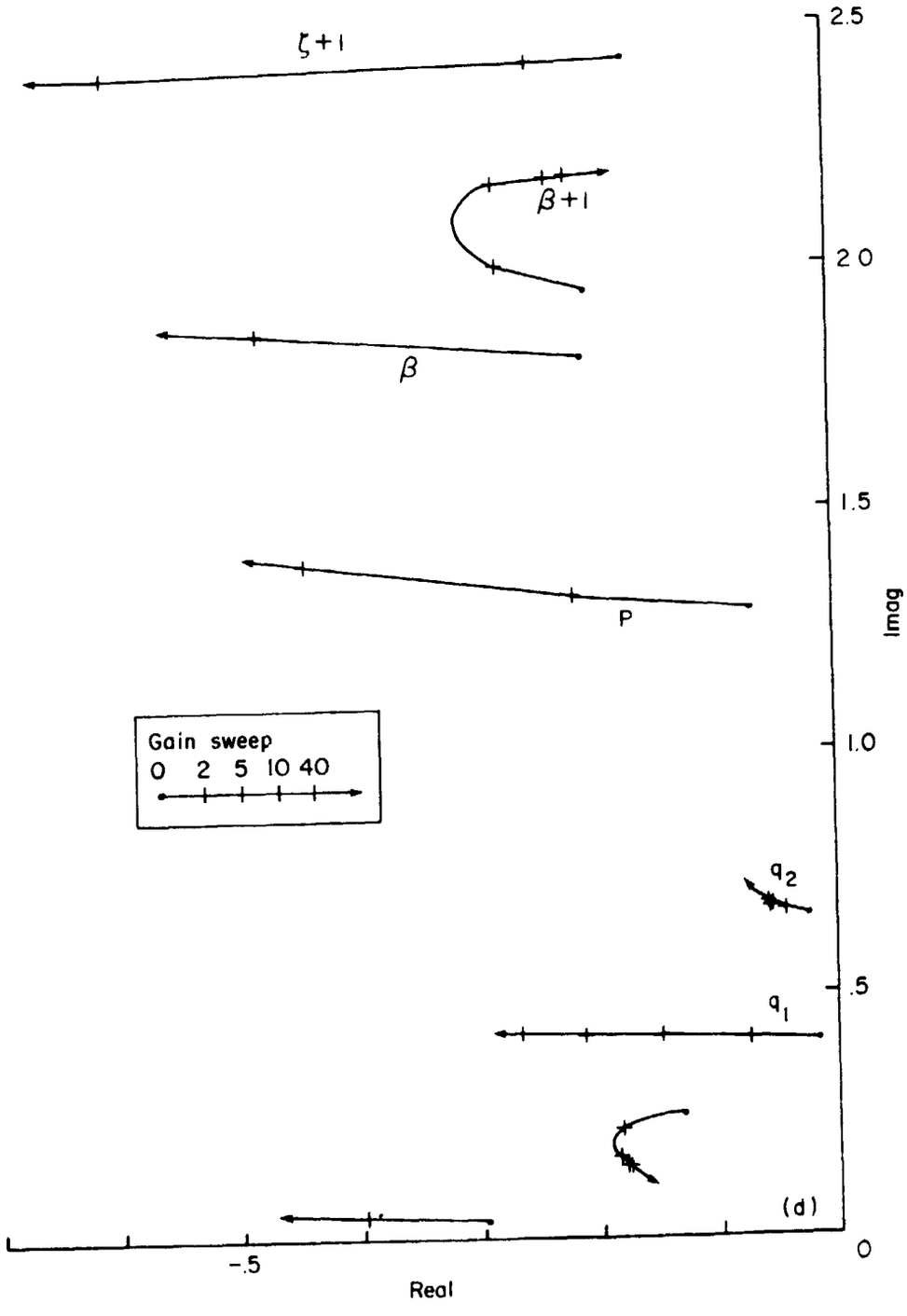

(d) Root locus.

Figure 12.– Concluded.

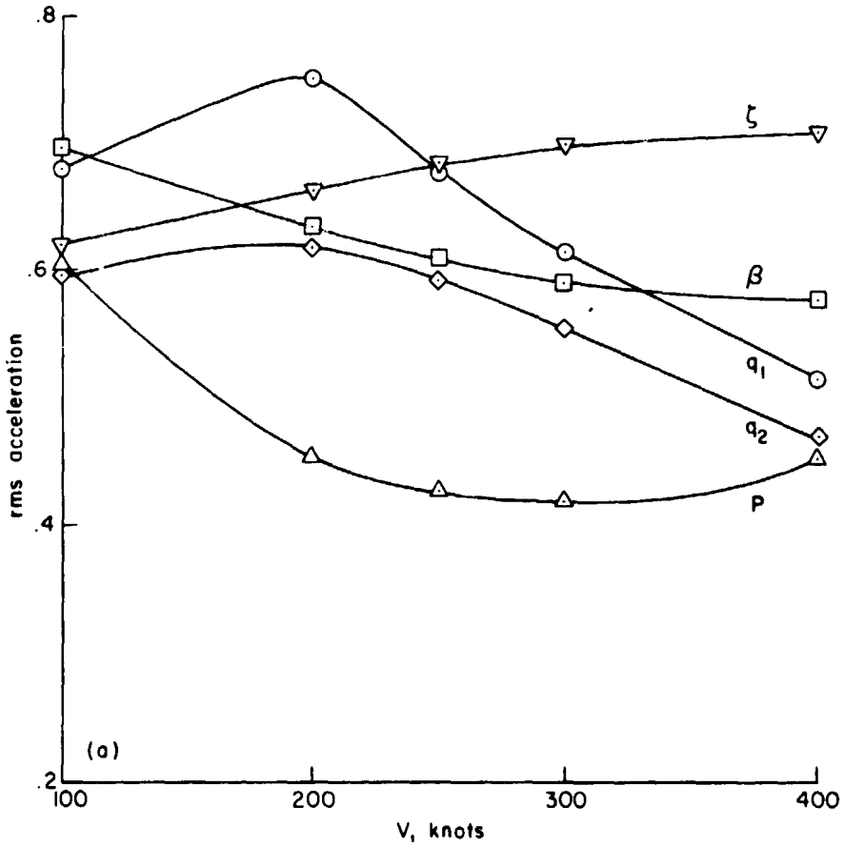

(a) Rms acceleration, optimum controller (closed loop/open loop).

Figure 13.— Control of Bell rotor for velocity sweep, with optimum controller for each speed and with controller designed for 250 knots (Q = 5*.1, 4*1.).

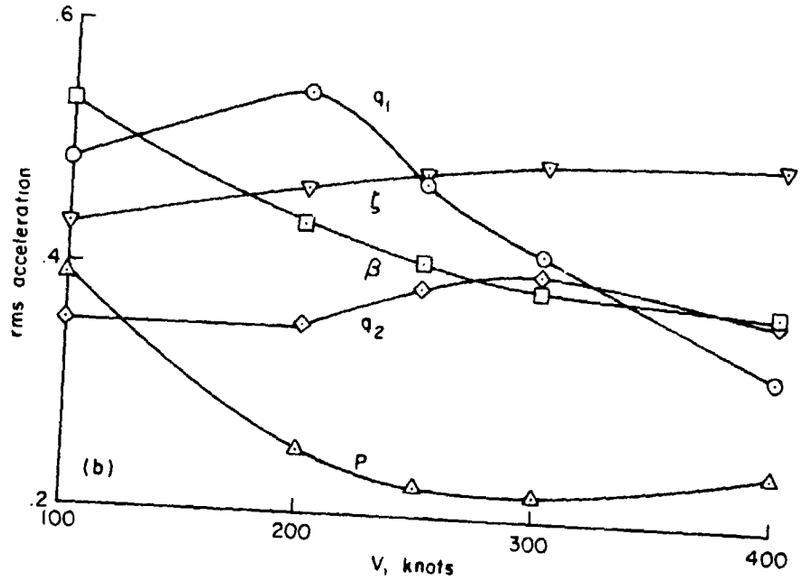

(b) Rms acceleration, 250 knot controller (closed loop/open loop).

Figure 13.– Continued.

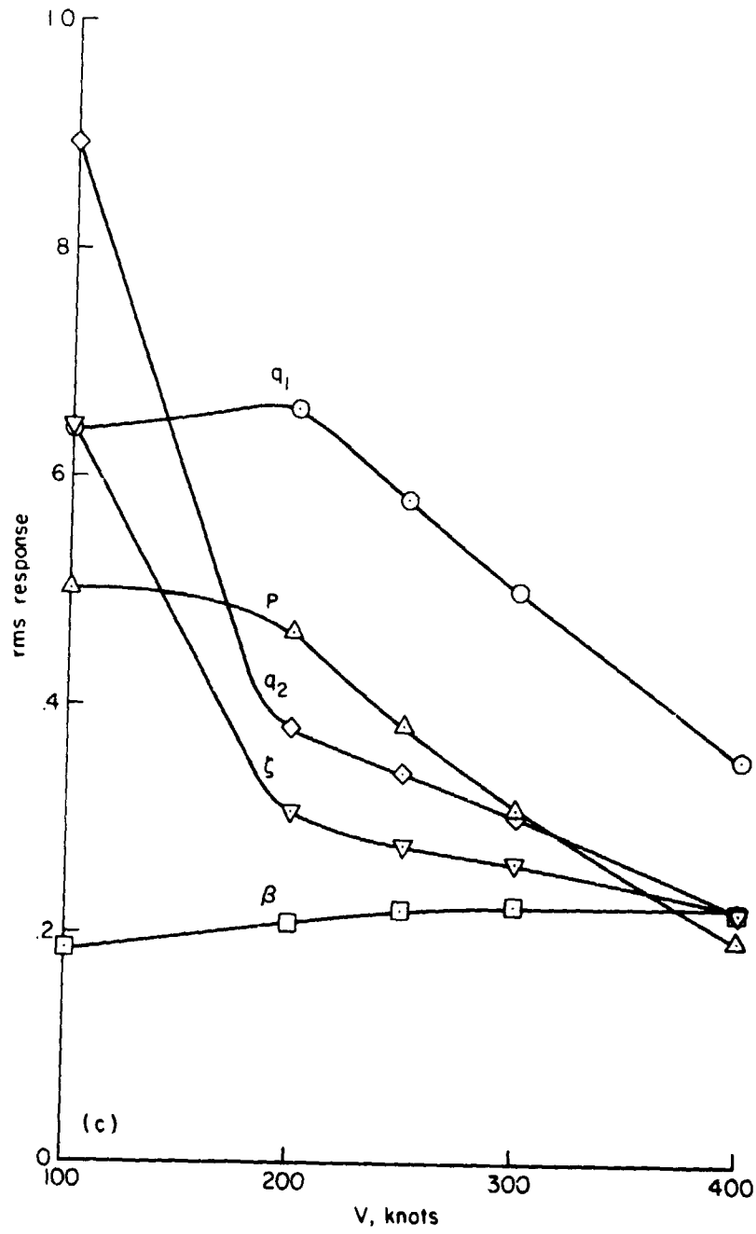

(c) Rms response, optimum controller (closed loop/open loop).

Figure 13.– Continued.

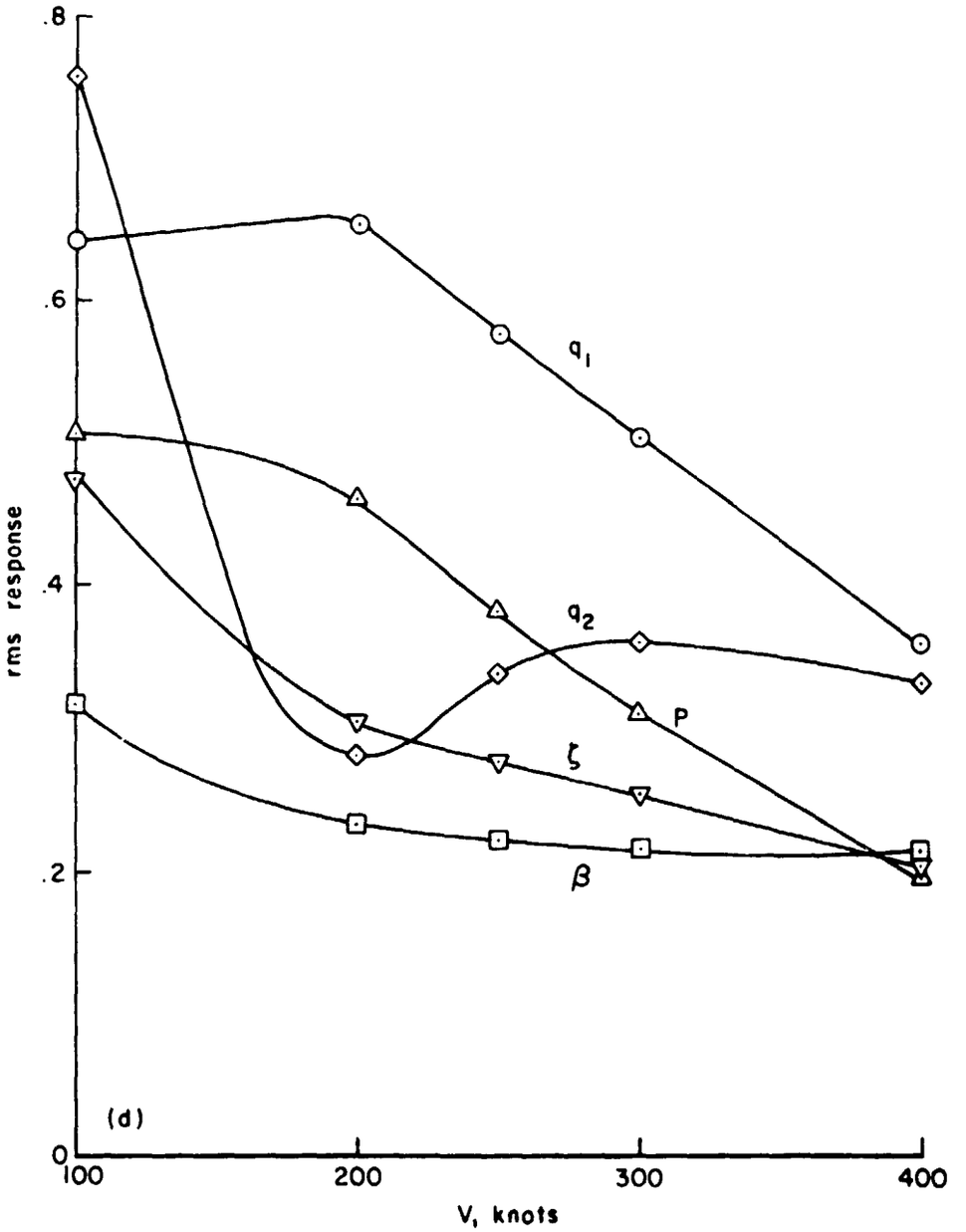

(d) Rms response, 250 knot controller (closed loop/open loop).

Figure 13.– Continued.

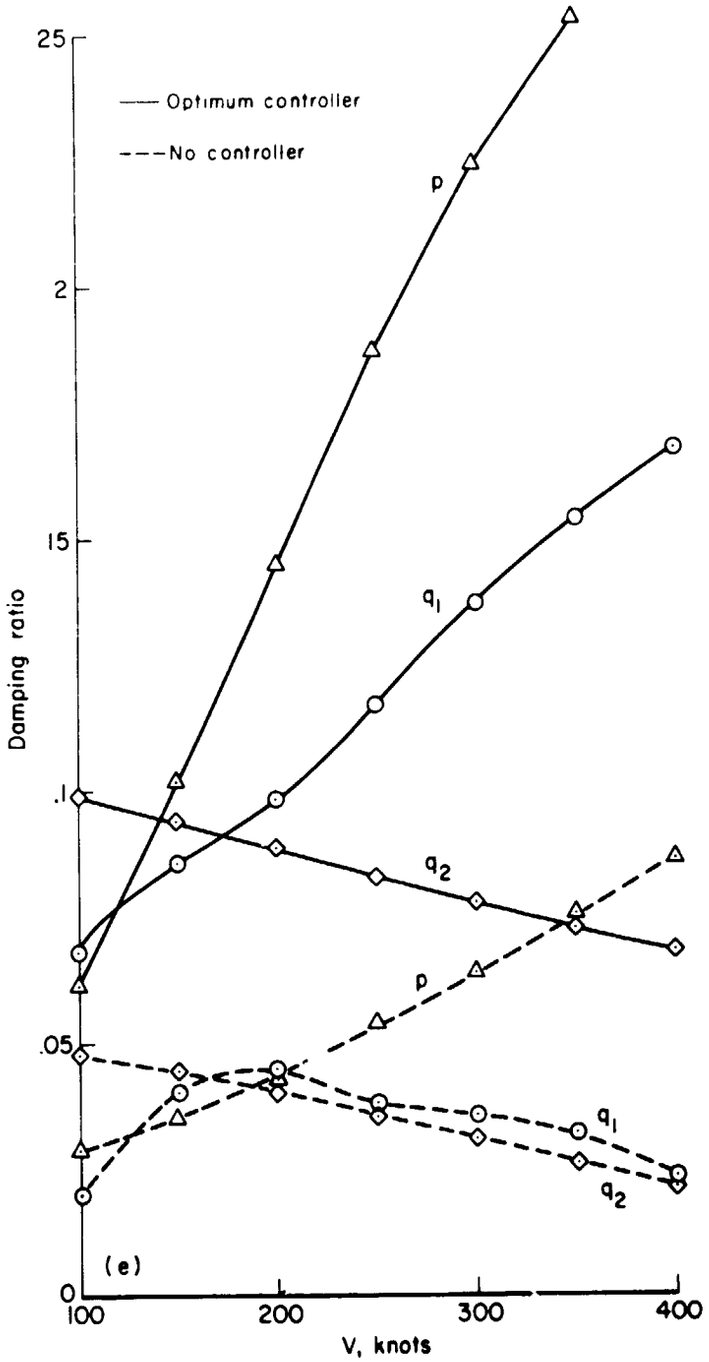

(e) Damping ratio, optimum controller.

Figure 13.– Continued.

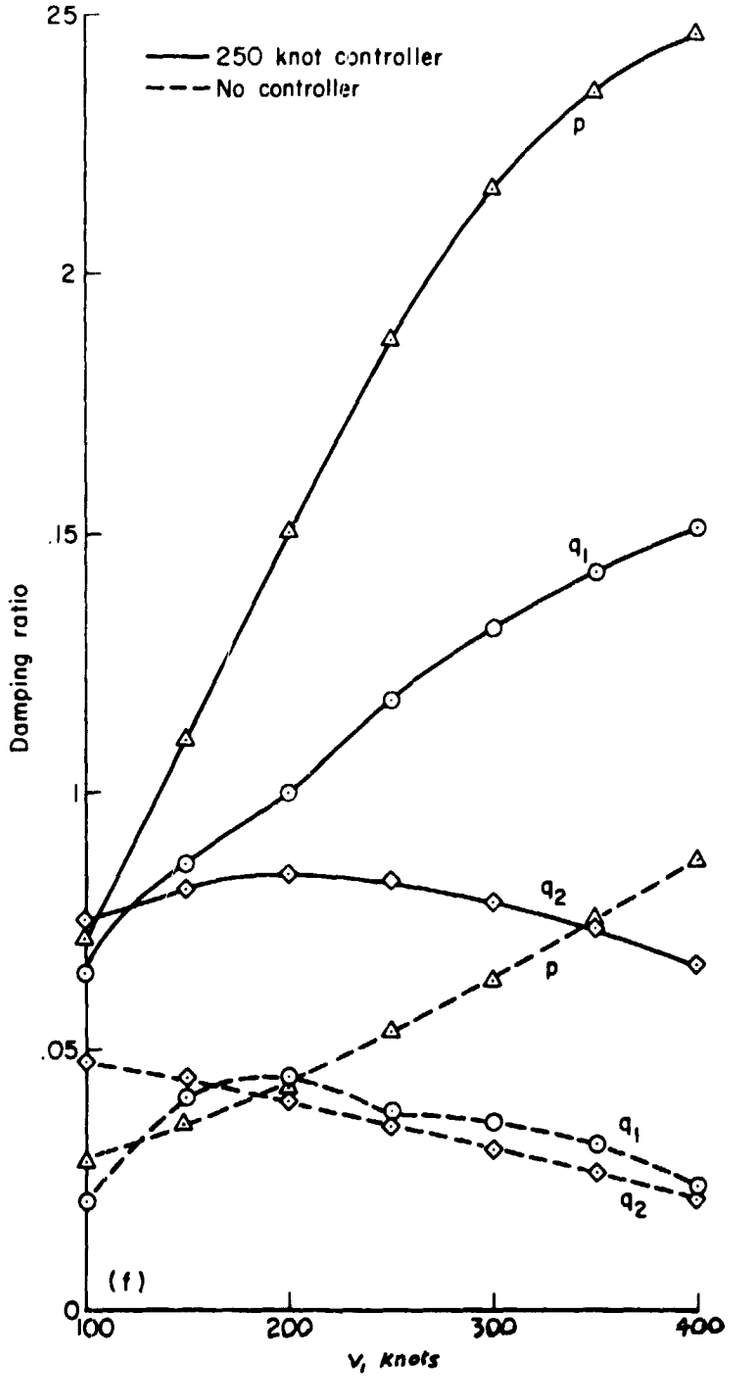

(f) Damping ratio, 250 knot controller.

Figure 13.– Continued.

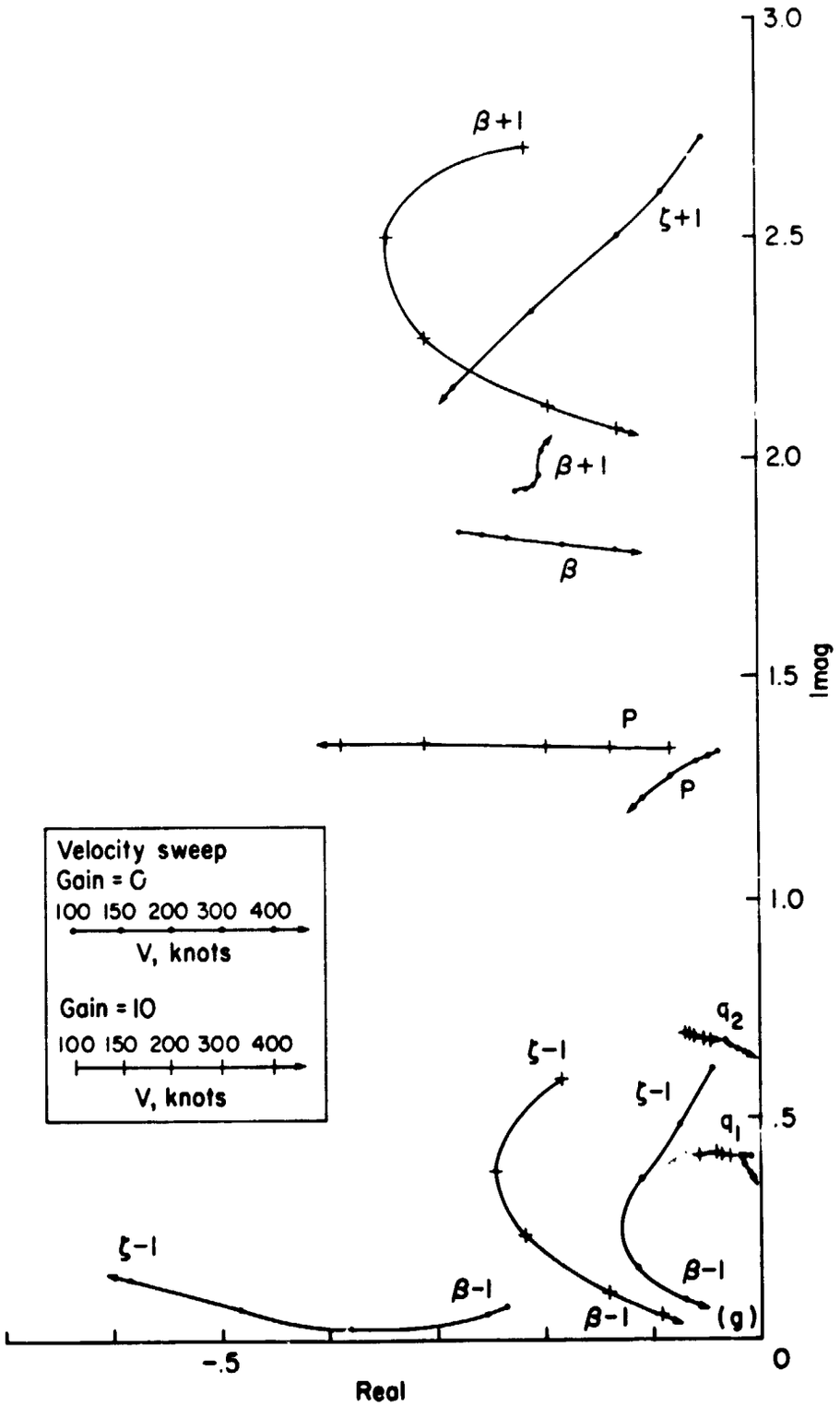

(g) Root locus, optimum controller.

Figure 13.— Continued.

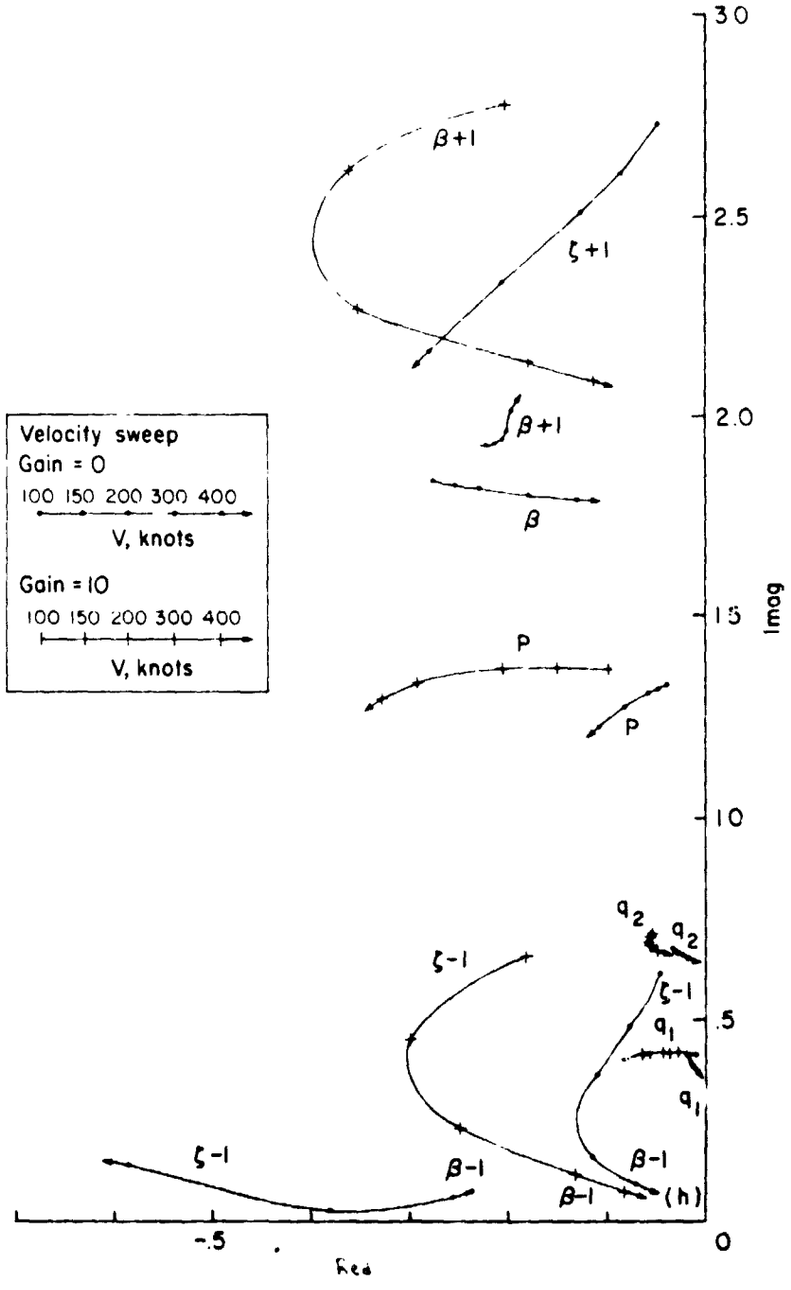

(h) Root locus, 250 knot controller.

Figure 13.– Continued.

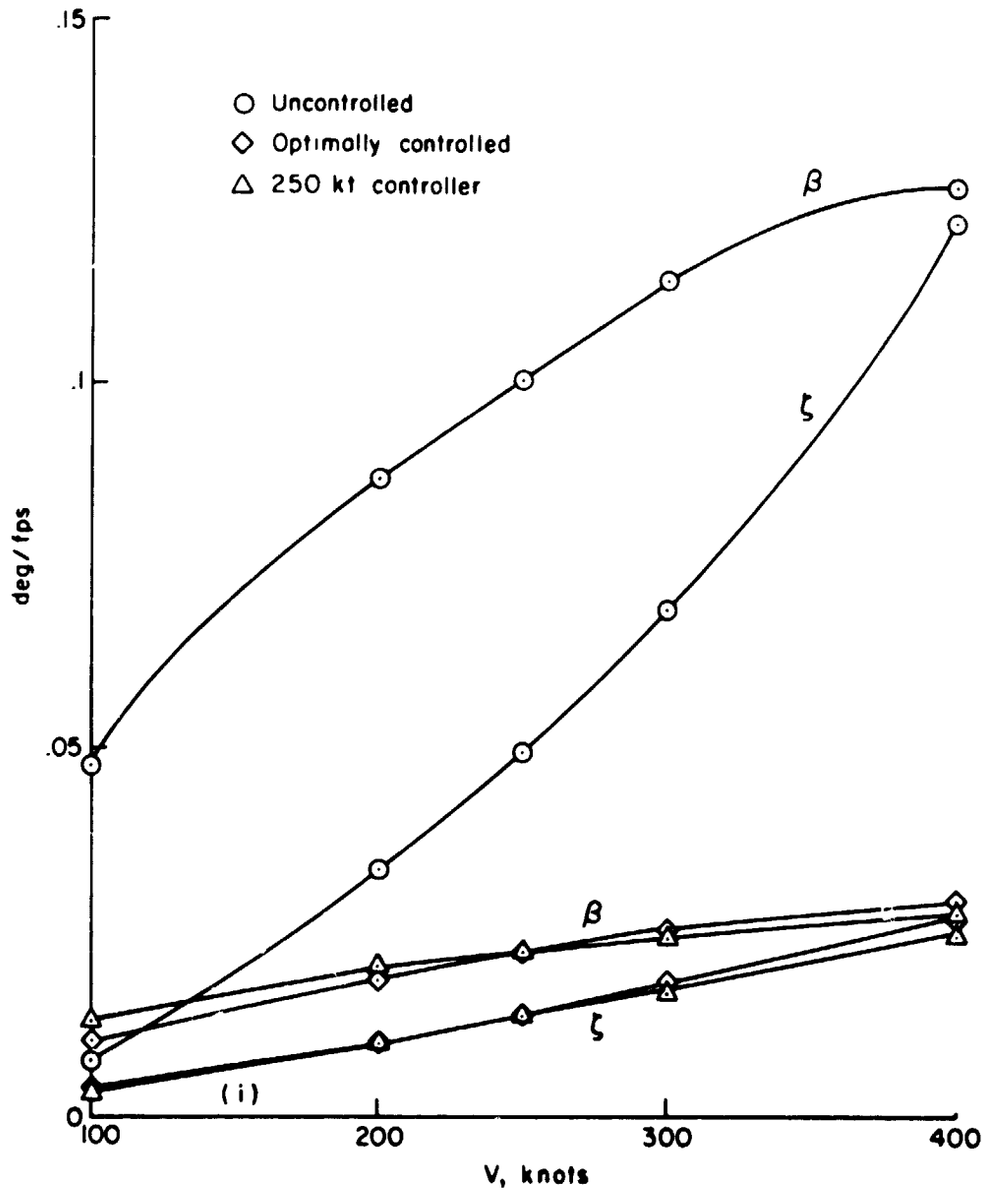

(i) Rms response of flap and lag motion.

Figure 13.– Continued.

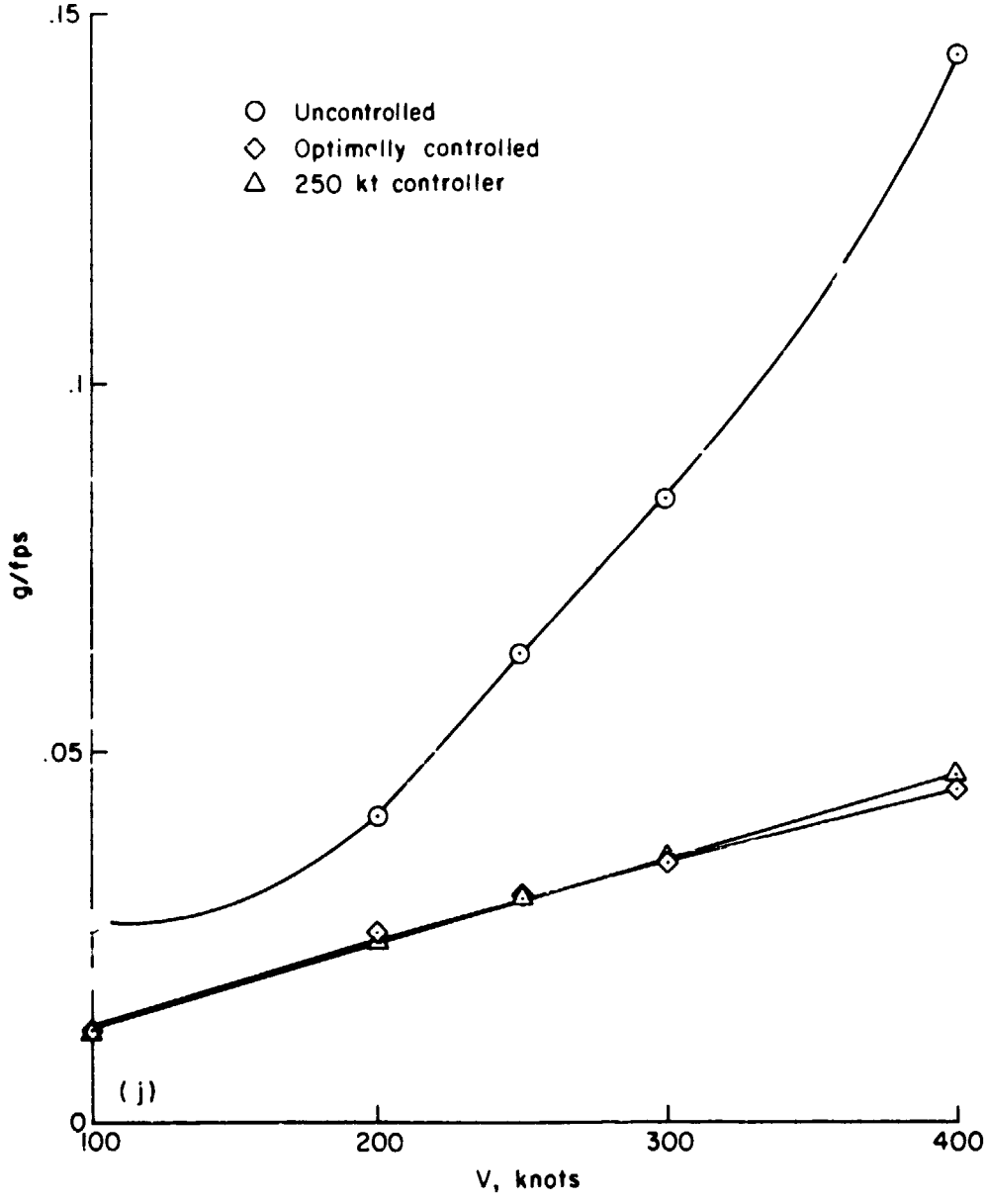

(j) Rms acceleration of wing vertic 1 bending motion.

Figure 13.– Concluded.

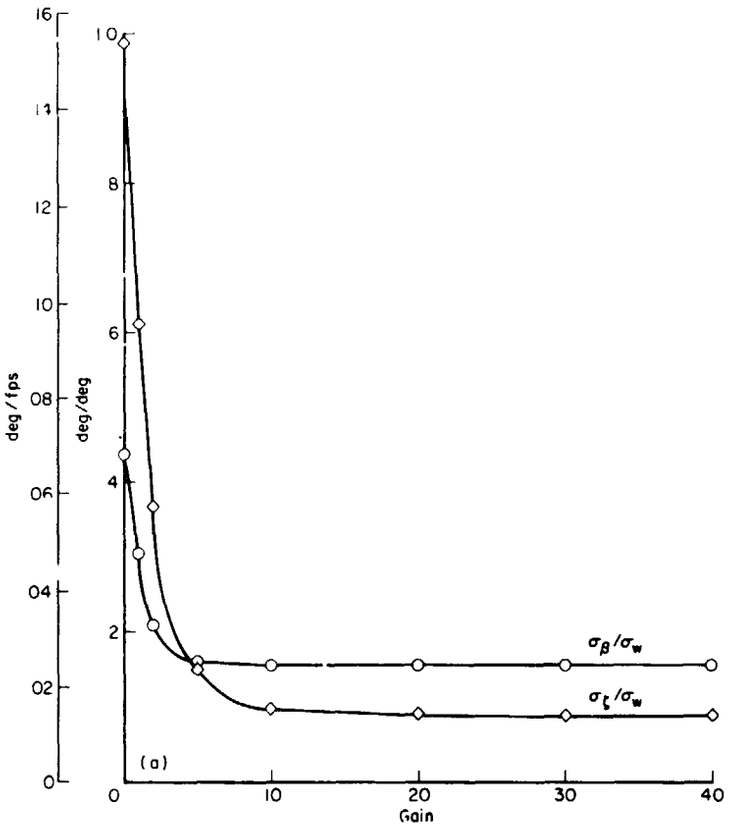

(a) Rms rotor flap and lag response (closed loop/open loop).

Figure 14.— Optimal control for Boeing rotor at $V/\Omega R = 0.7$, gain sweep for Q = 5*.2, 10, 1, 10, 1.

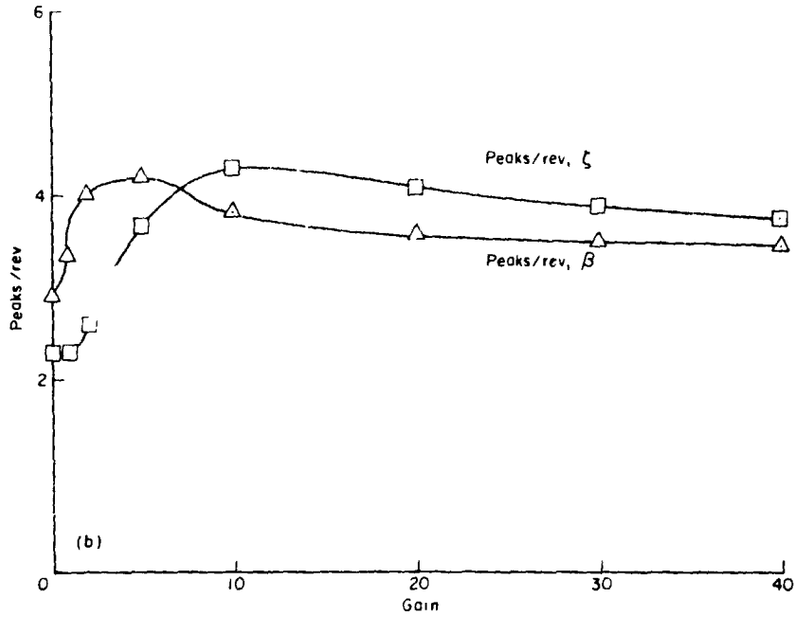

(b) Peak/rev for flap and lag.

Figure 14.– Continued.

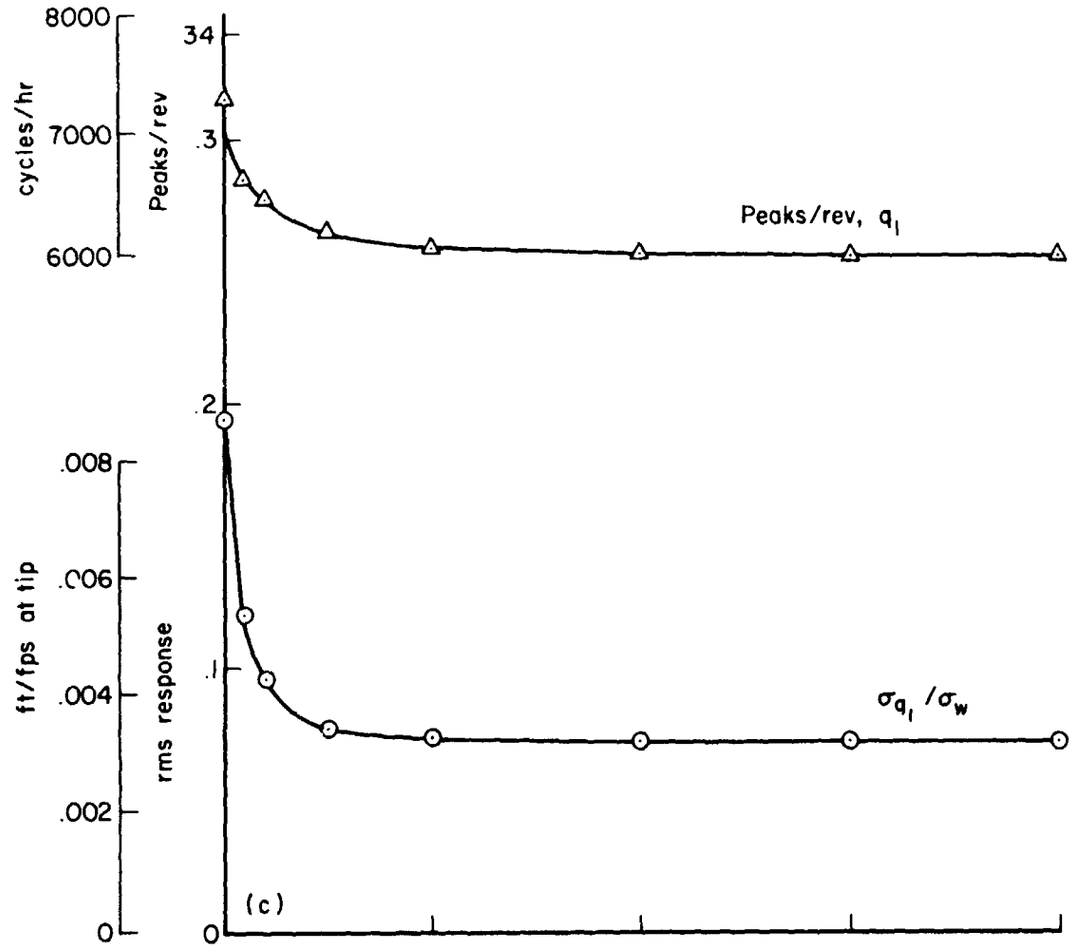

(c) Rms response (closed loop/open loop) and peaks/rev for wing vertical bending (q_1).

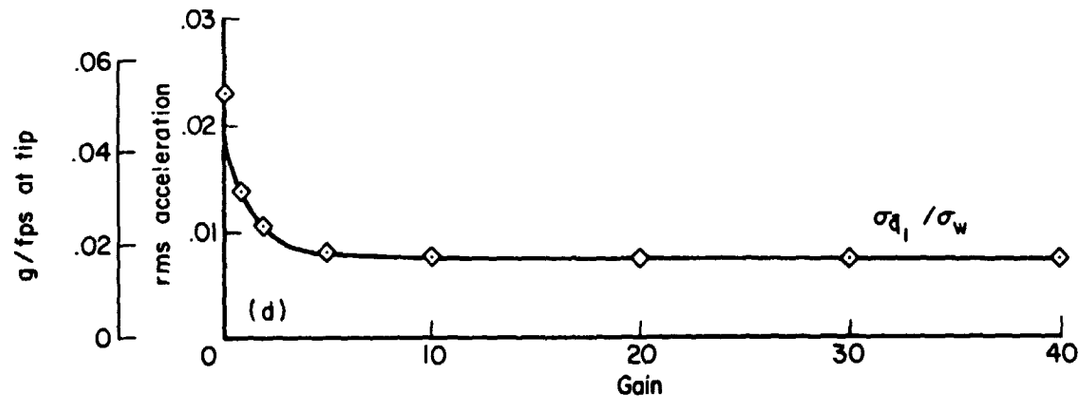

(d) Rms acceleration for wing vertical bending ($\ddot{q}_1$) (closed loop/open loop).

Figure 14.– Continued.

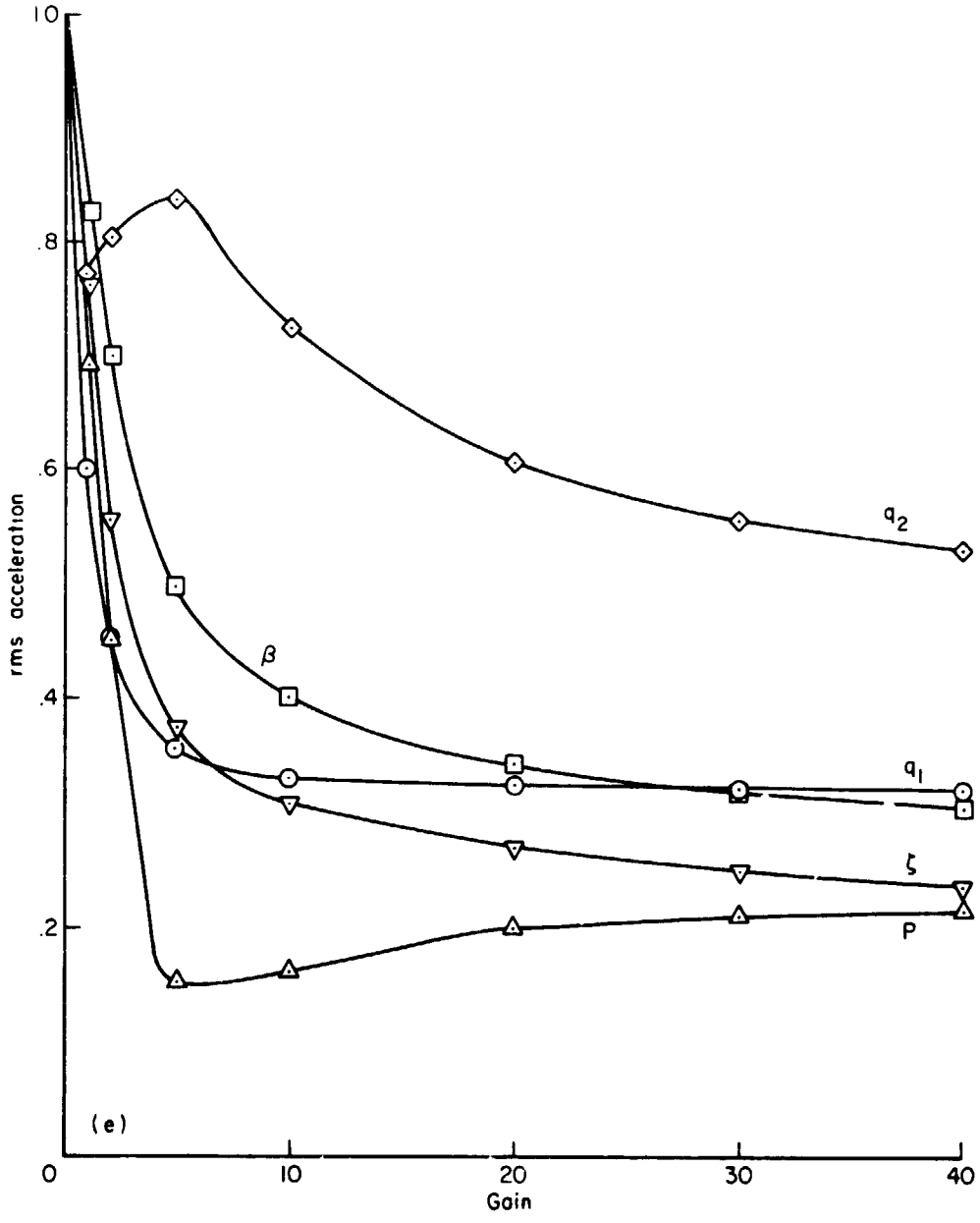

(e) Rms acceleration of wing and rotor motion (closed loop/open loop).

Figure 14.– Continued.

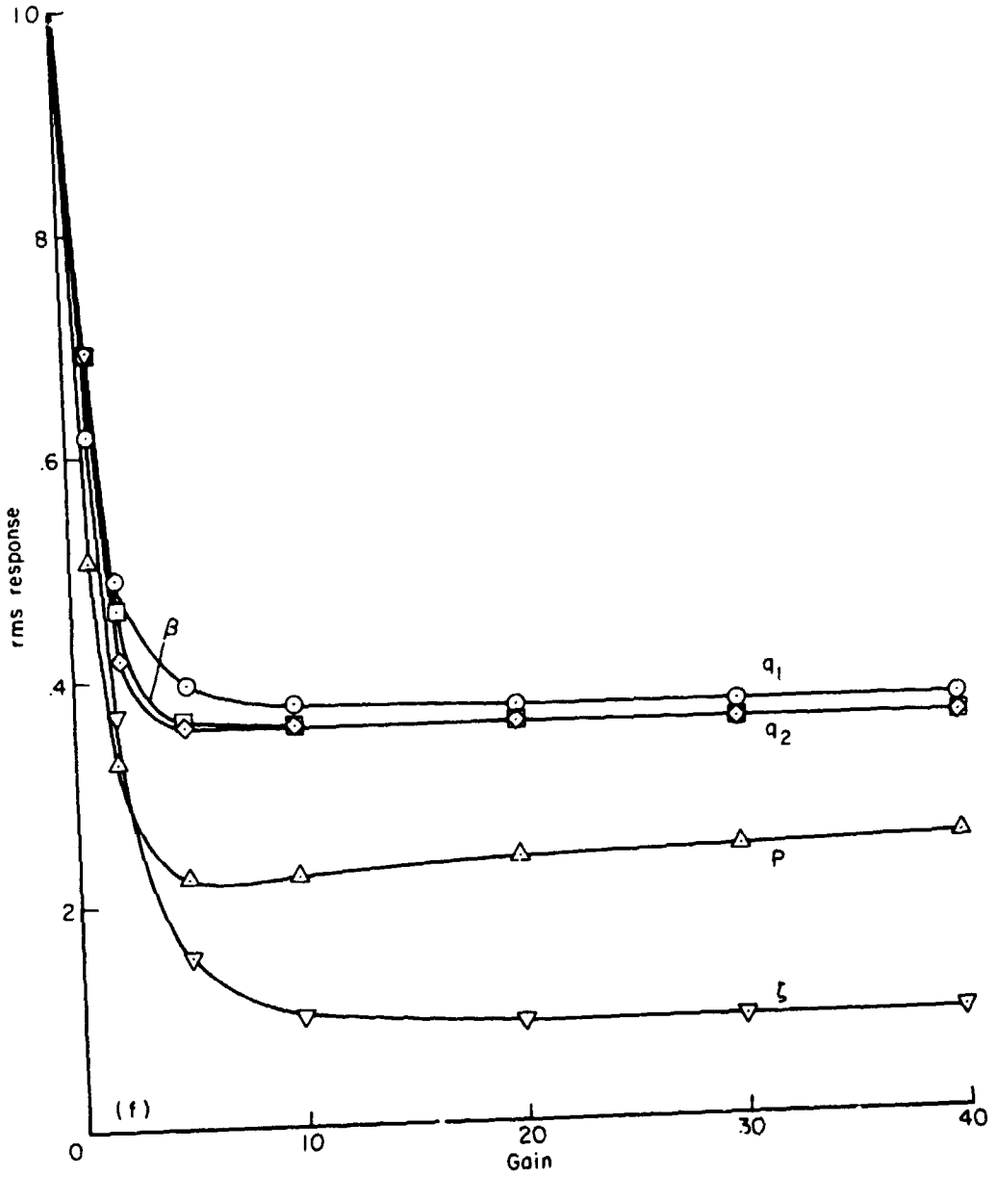

(f) Rms response of wing and rotor motion (closed loop/open loop).

Figure 14.— Continued.

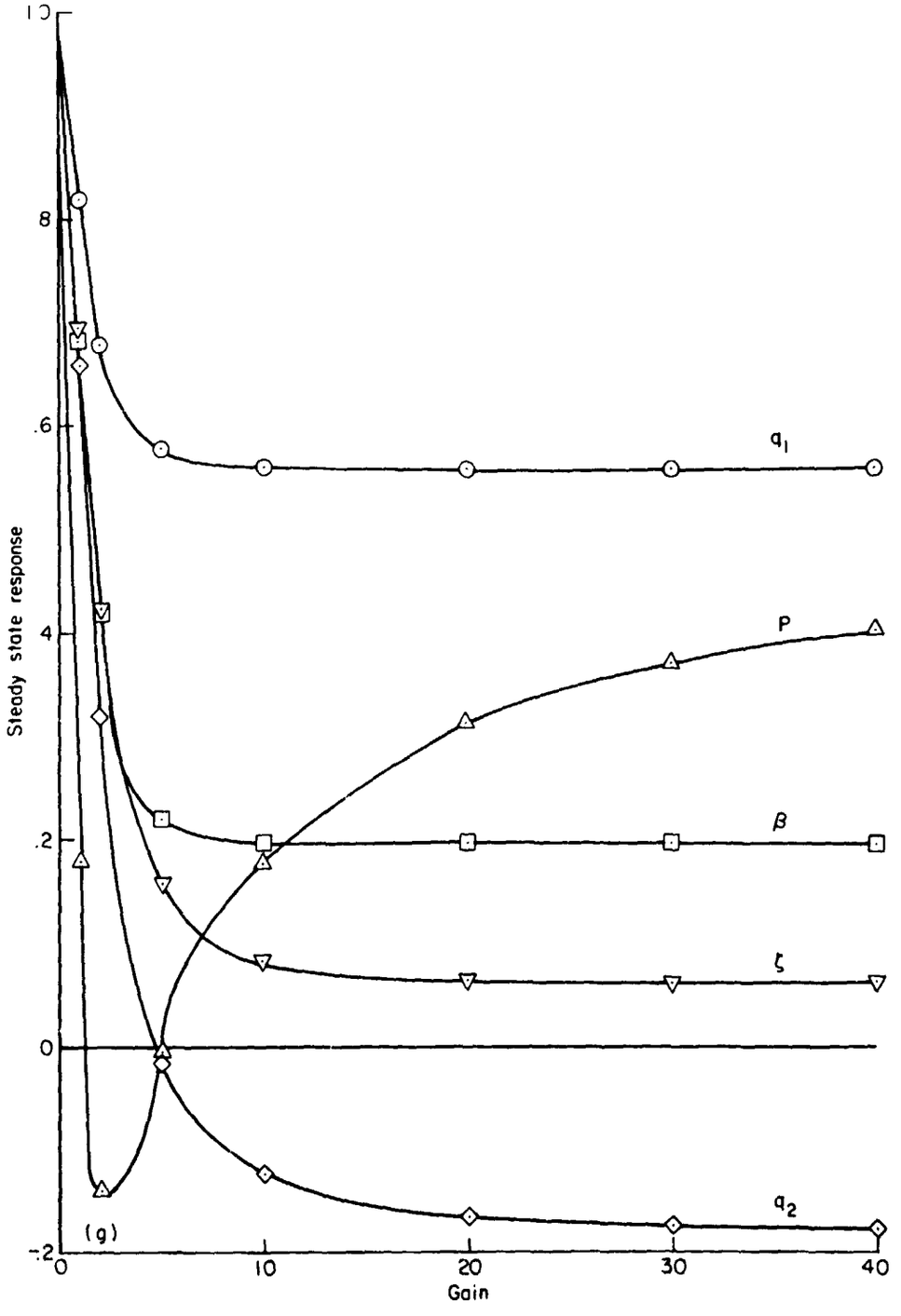

(g) Steady state response of wing and rotor (closed loop/open loop).

Figure 14.– Continued.

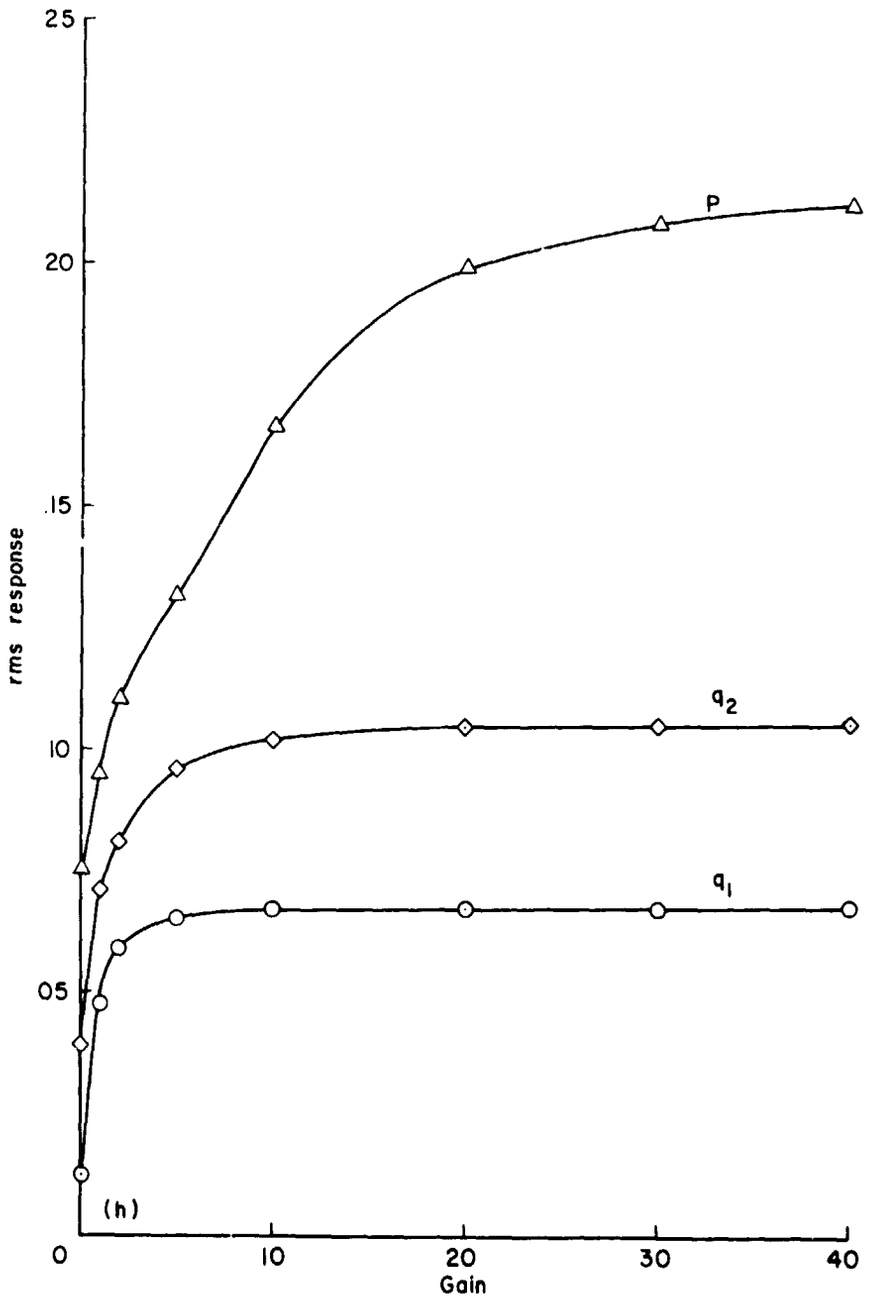

(h) Damping ratio of wing modes.

Figure 14.– Concluded.

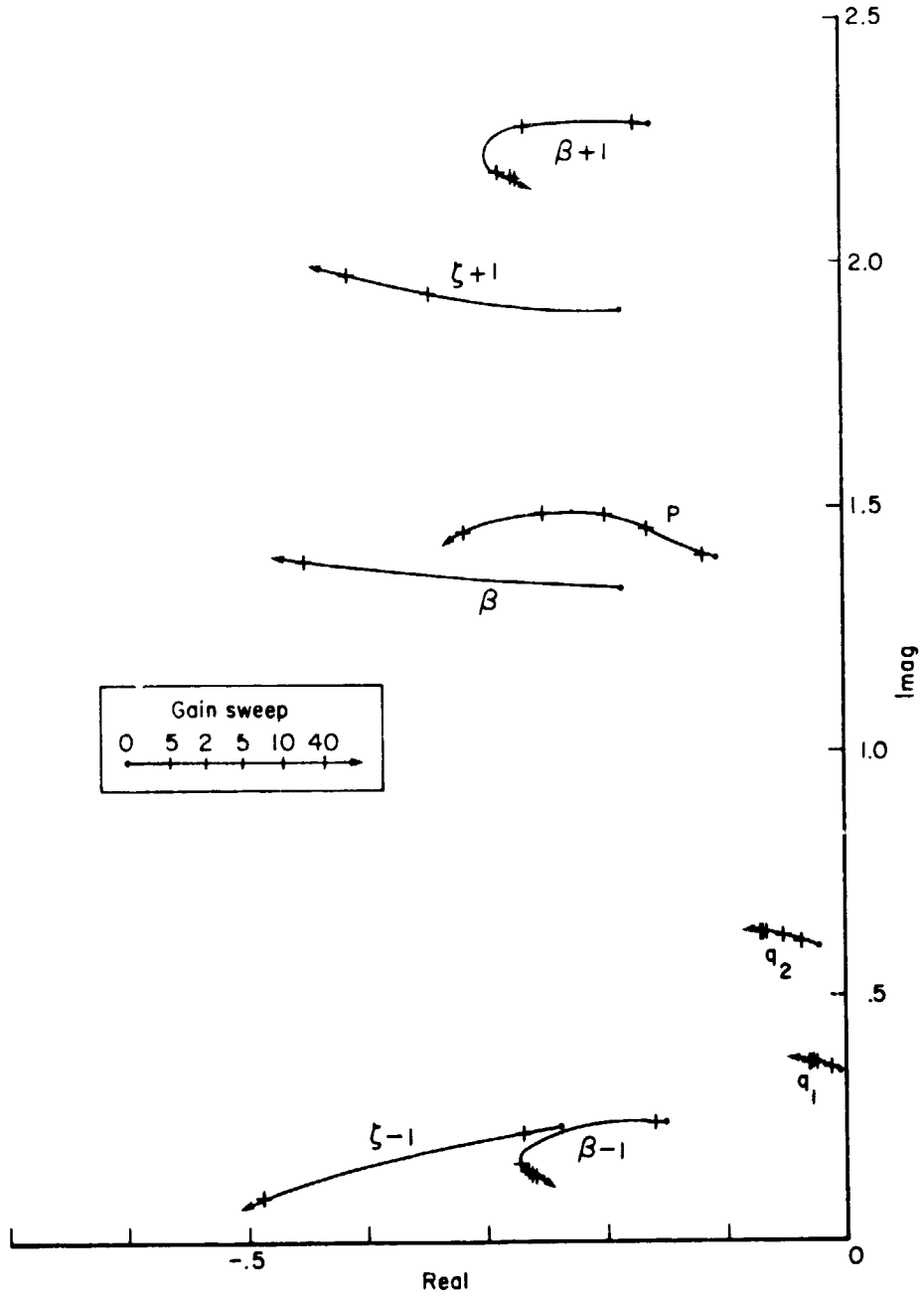

Figure 15.— Root locus for Boeing rotor, gain sweep for Q = 5*.2, 10, 1, 10, 1.

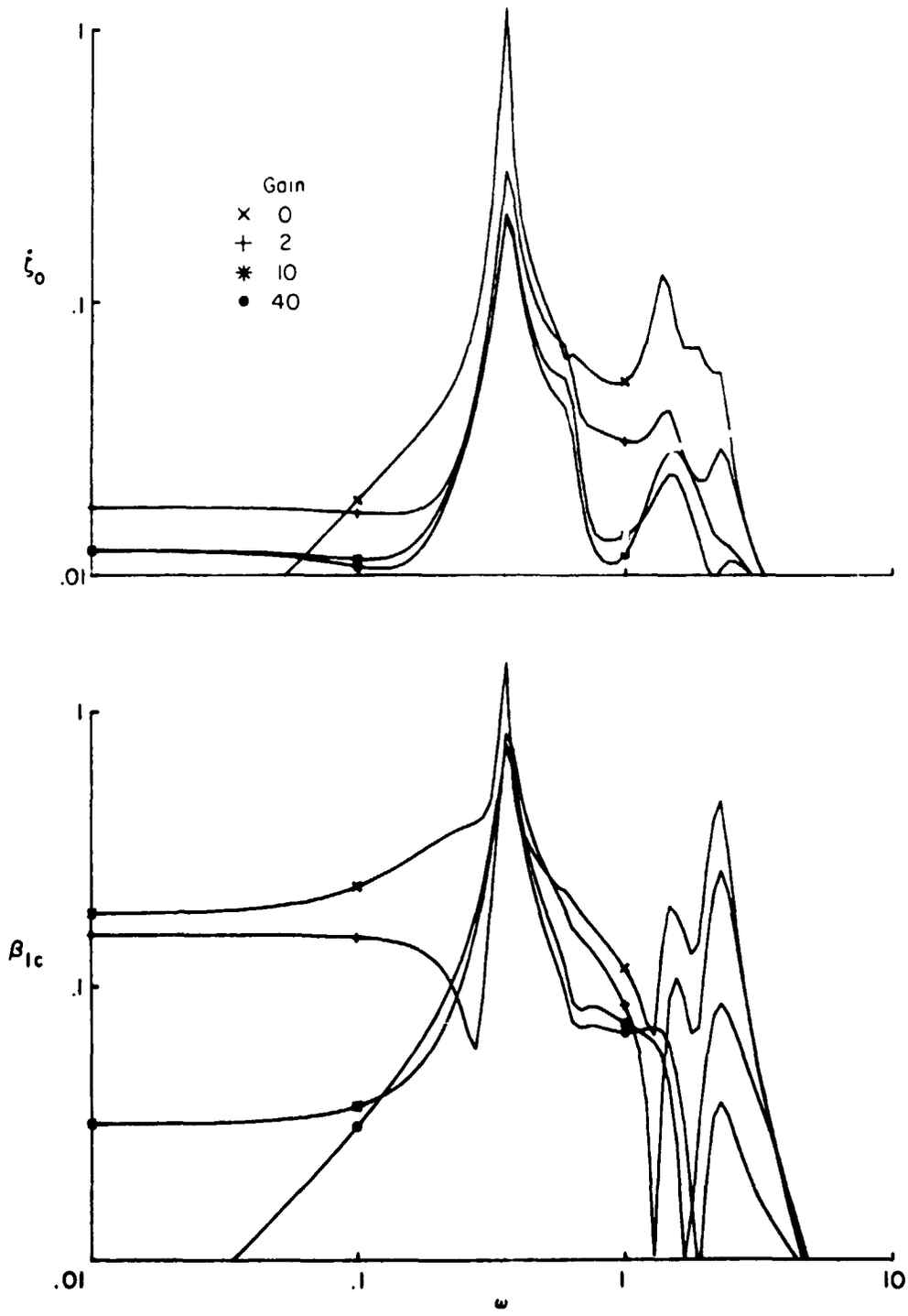

Figure 16.— Transfer function for Boeing rotor, gain sweep for Q = 5*.2, 10, 1, 10, 1.

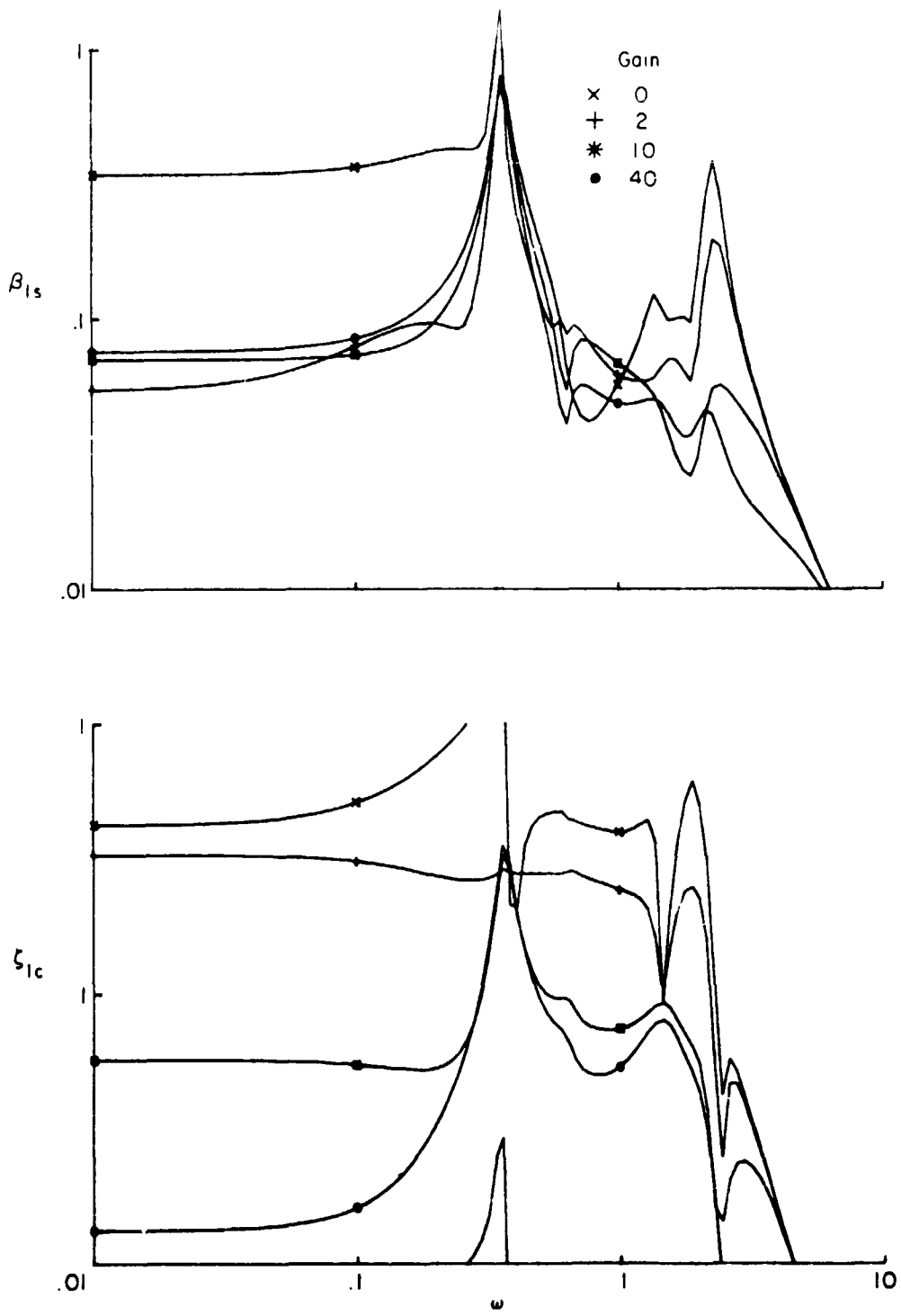

Figure 16.– Continued.

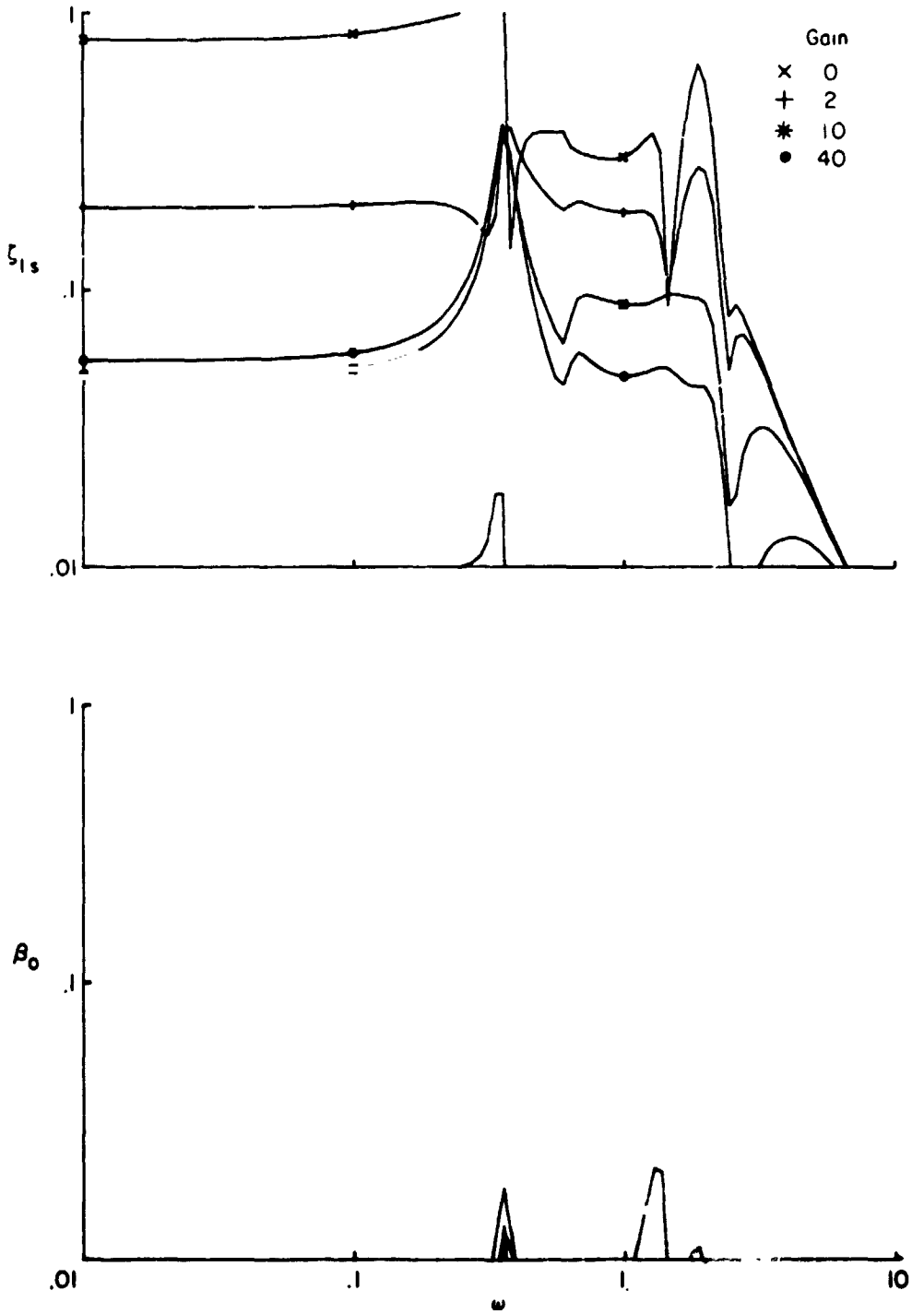

Figure 16.— Continued.

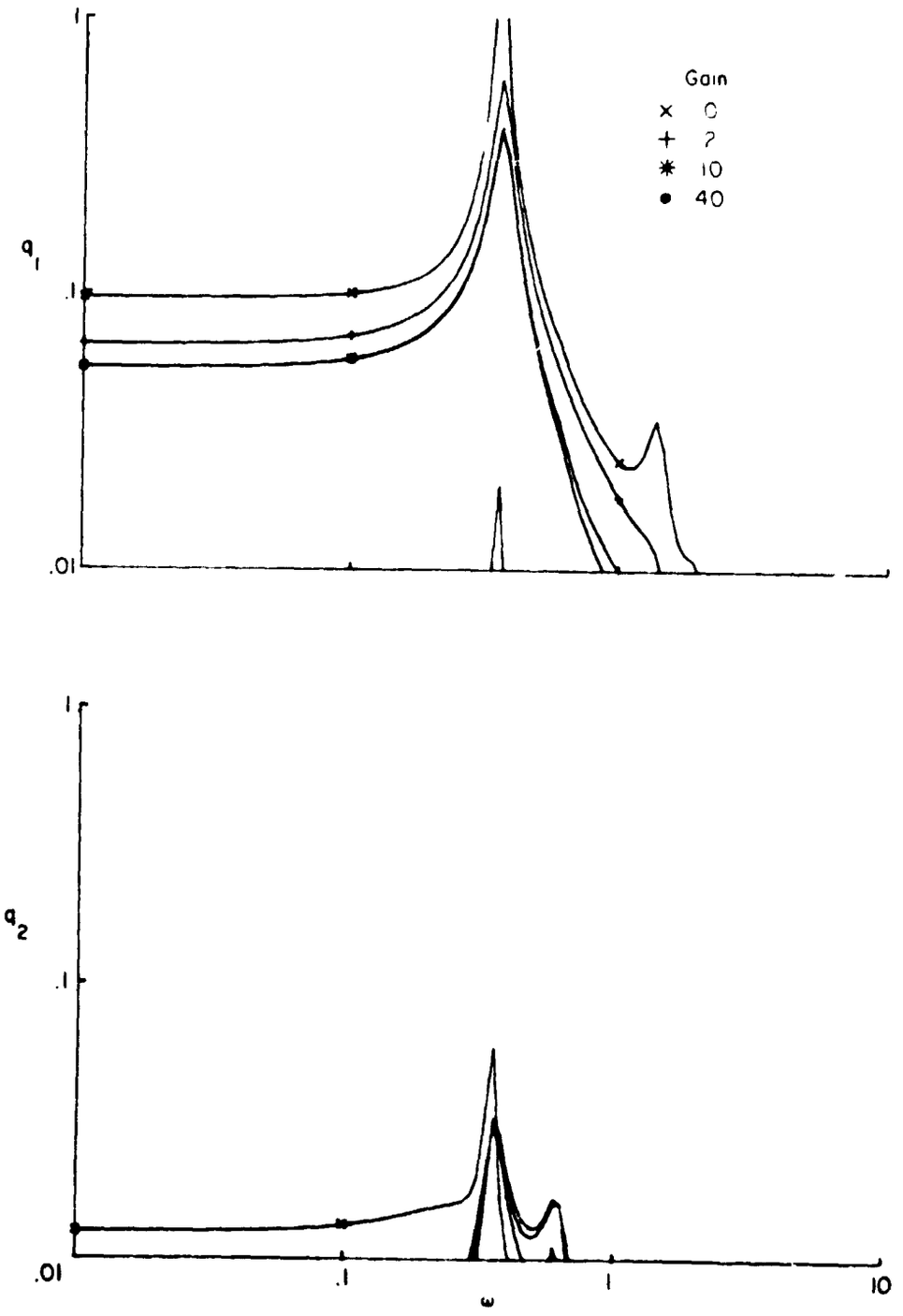

Figure 16.– Continued.

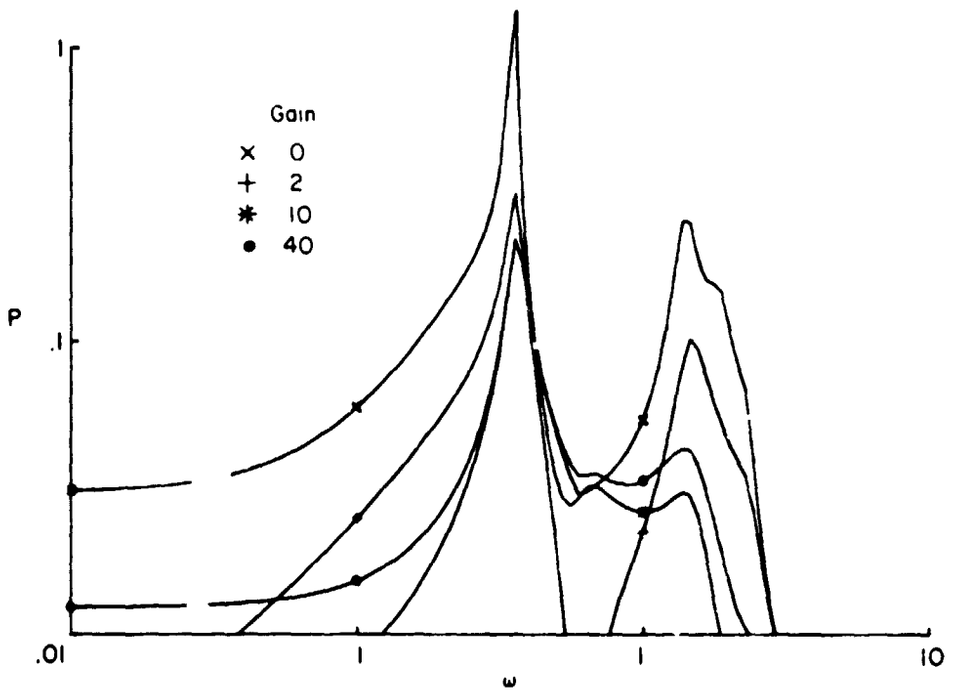

Figure 16.– Concluded.

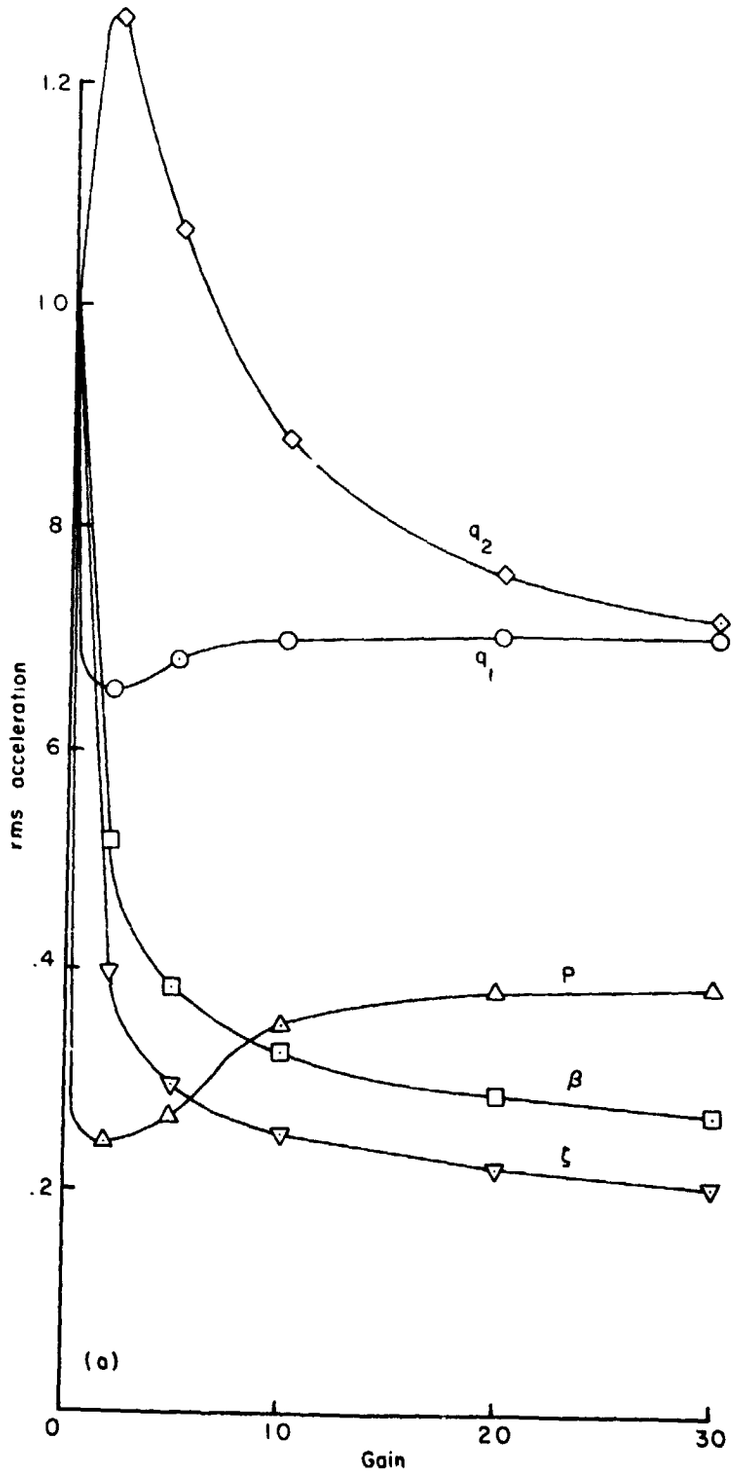

(a) Rms acceleration of wing and rotor motion (closed loop/open loop).

Figure 17.— Control of Boeing rotor with constraint on rotor motion only, Q = 6*1, 3*0.

C.2

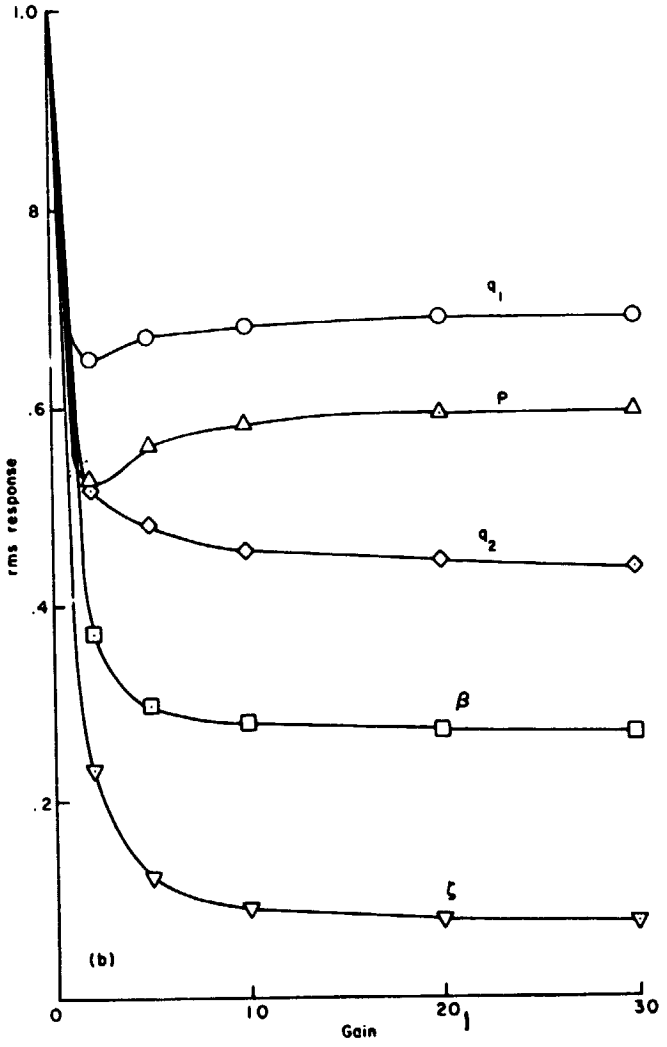

(b) Rms response of wing and rotor motion (closed loop/open loop).

Figure 17.— Continued.

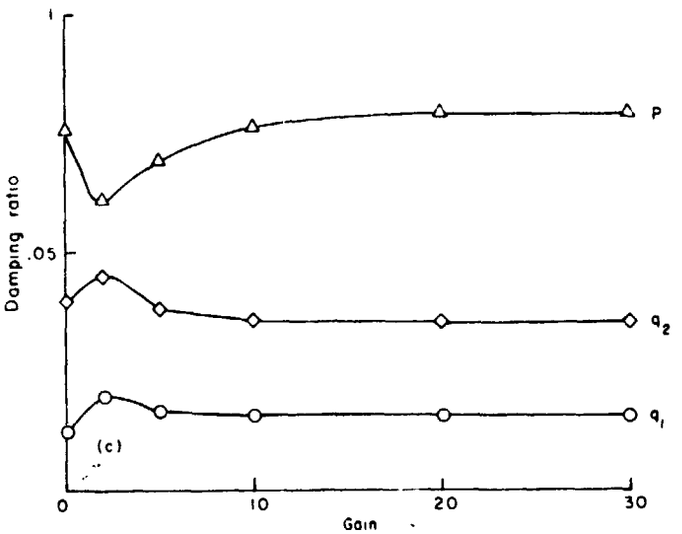

(c) Damping ratio of wing modes.

Figure 17.– Continued.

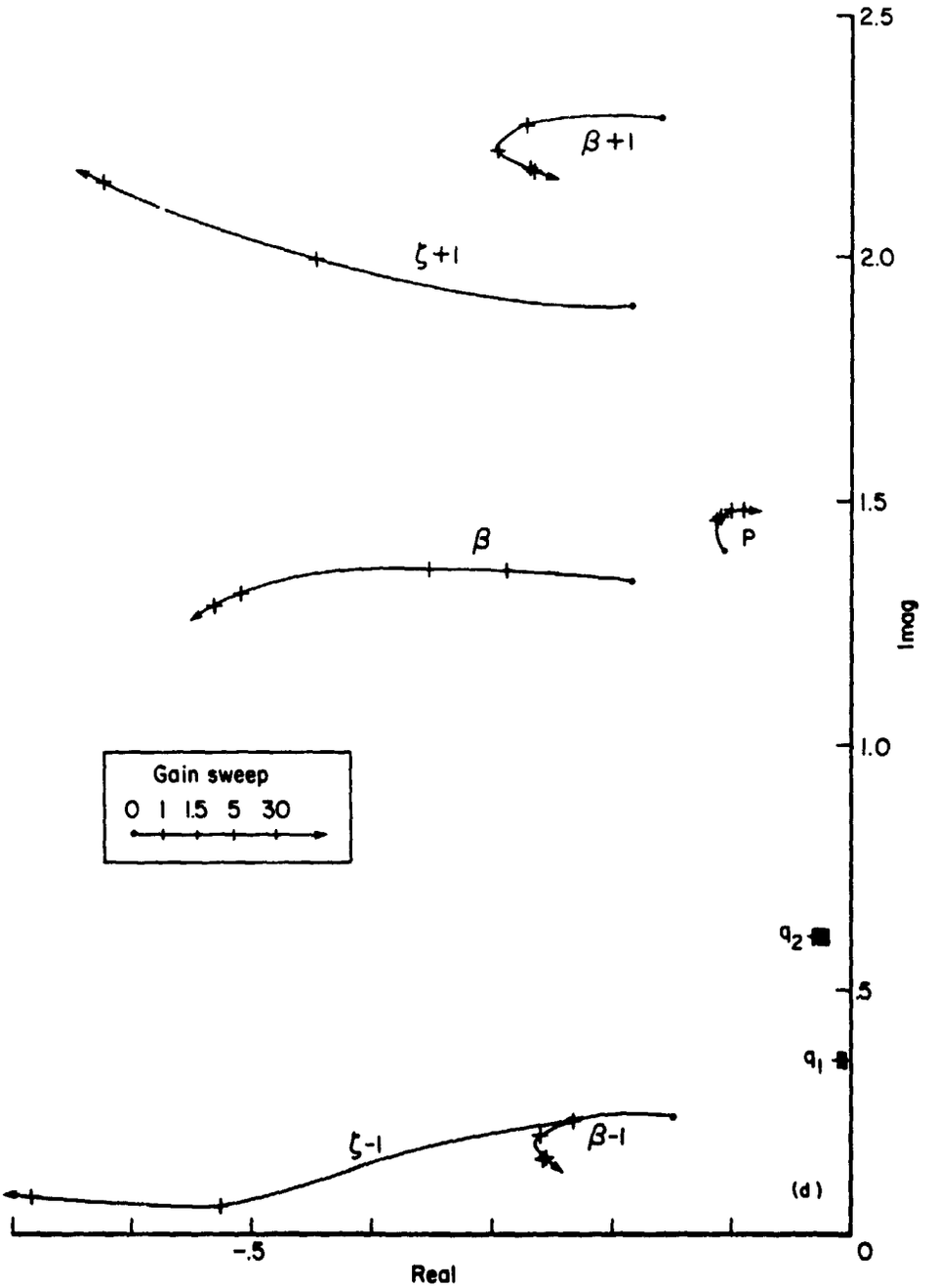

(d) Root locus.

Figure 17.– Concluded.

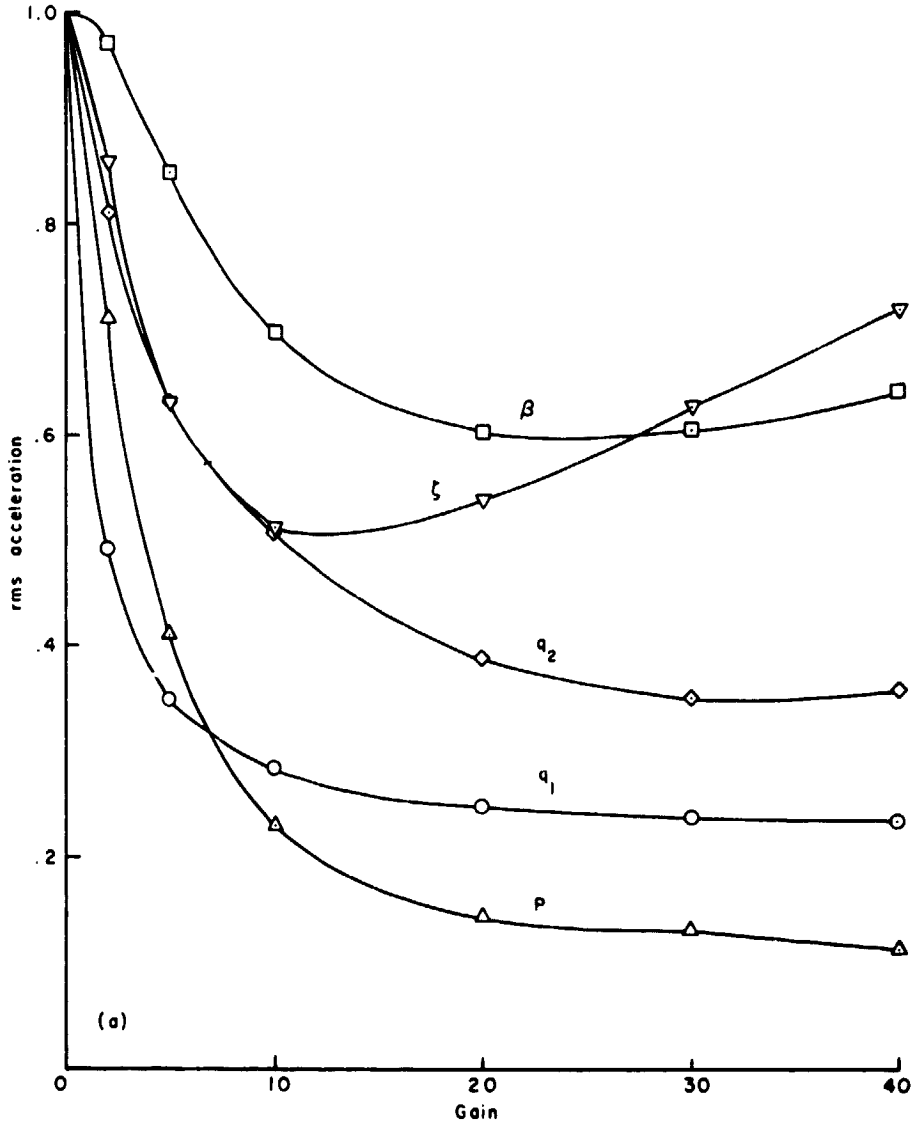

(a) Rms acceleration of wing and rotor motion (closed loop/open loop).

Figure 18.– Control of Boeing rotor with constraint on wing motion only, Q = 6*0, 3*1.

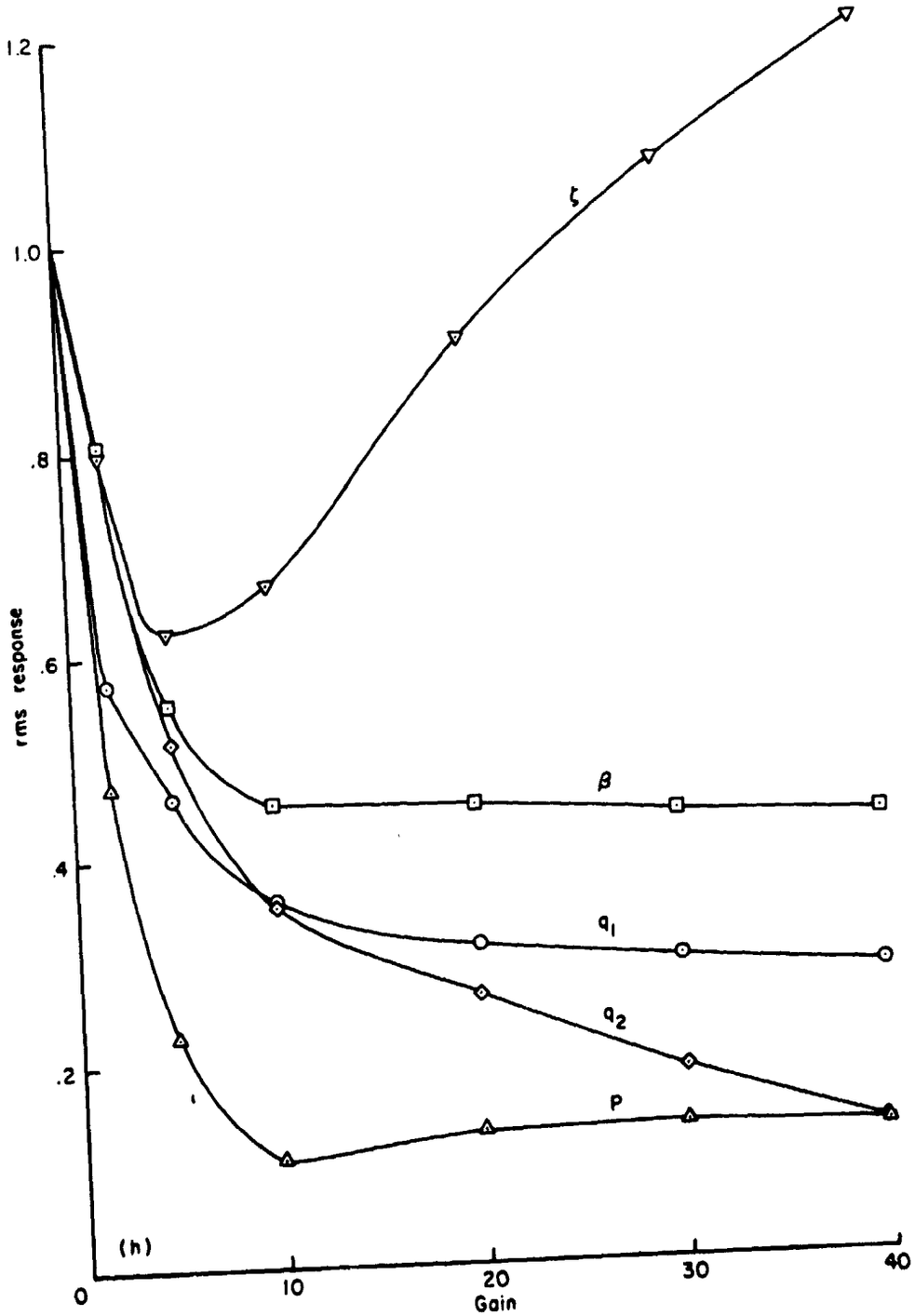

(b) Rms response of wing and rotor motion (closed loop/open loop).

Figure 18.– Continued.

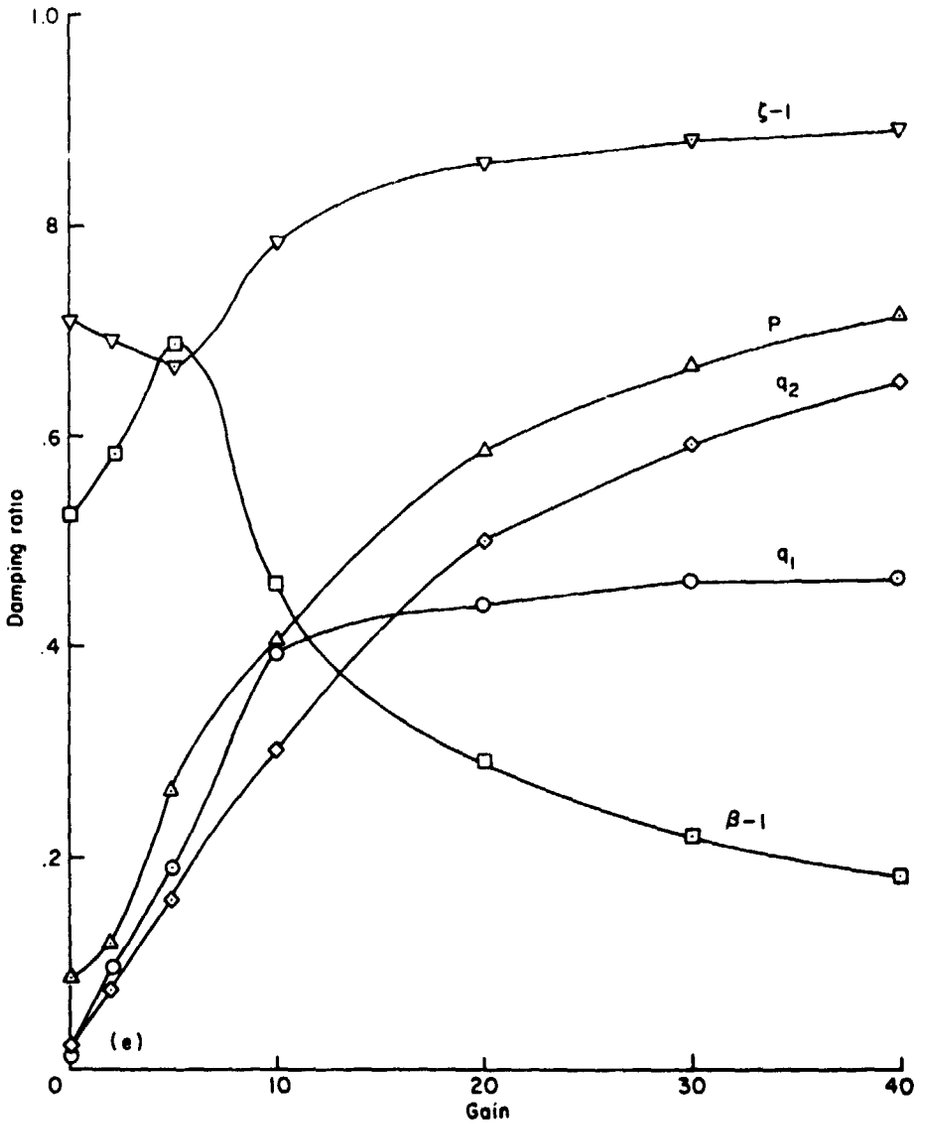

(c) Damping ratio of wing modes.

Figure 18.— Continued.

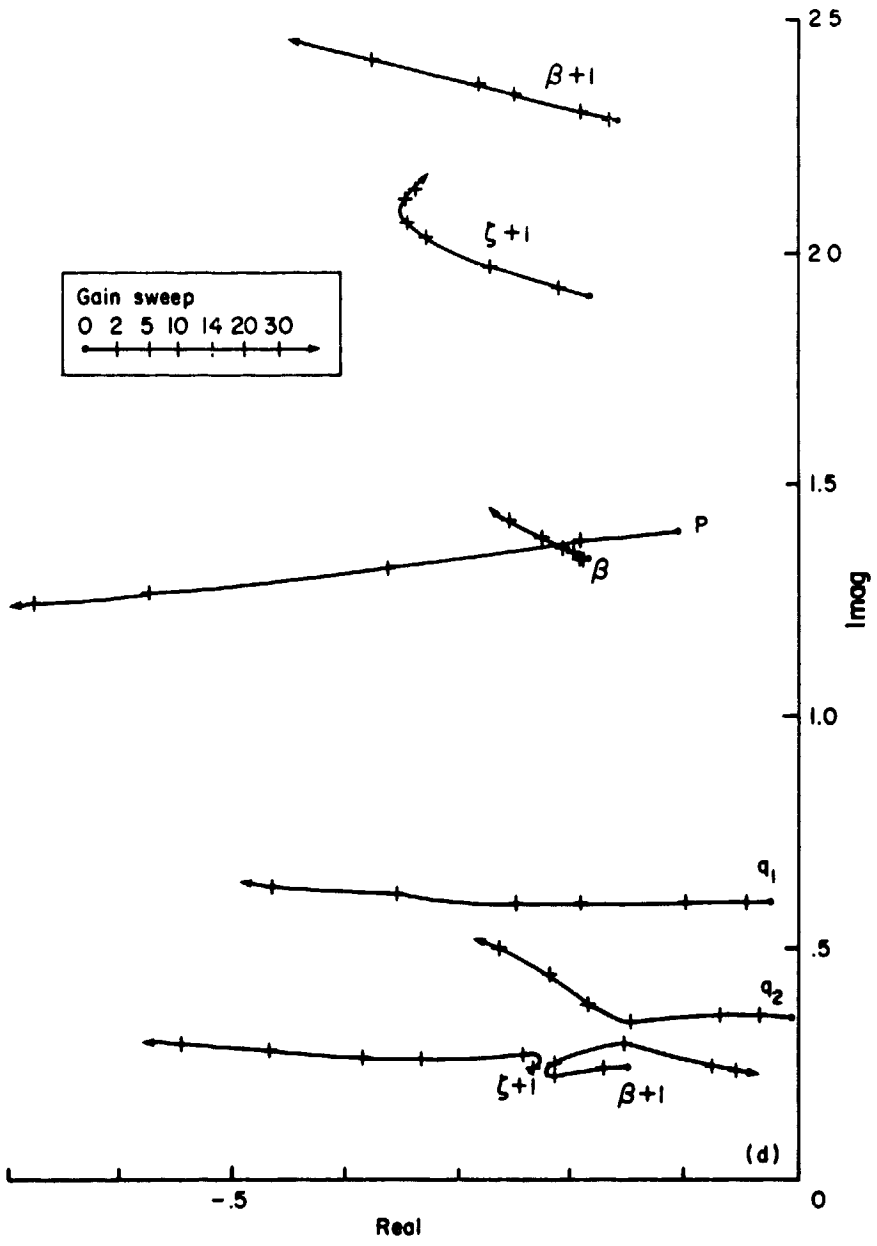

(d) Root locus.

Figure 18.– Concluded.

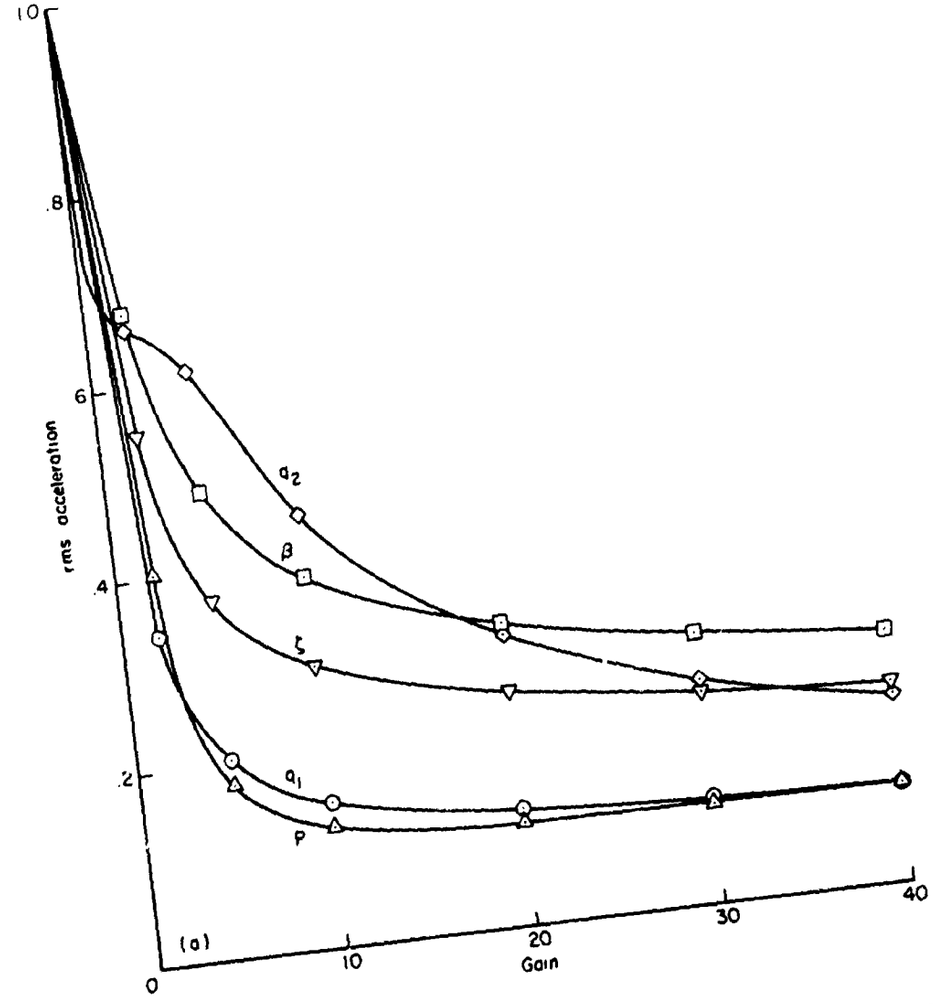

(a) Rms acceleration of wing and rotor motion (closed loop/open loop).

Figure 19.— Optimal control of Boeing rotor including wing flap control input, Q = 5*.1, 4*1.

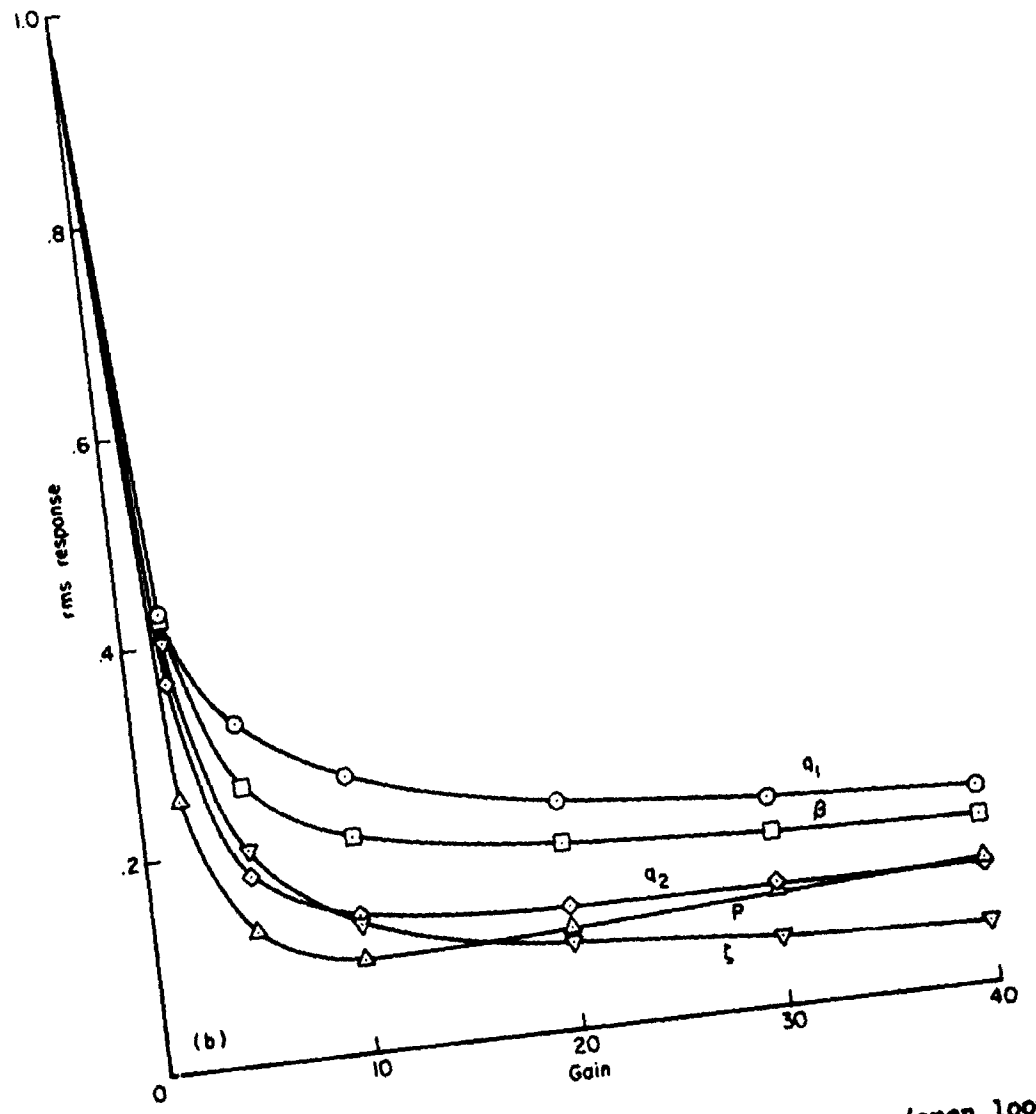

(b) Rms response of wing and rotor motion (closed loop/open loop).

Figure 19.– Continued.

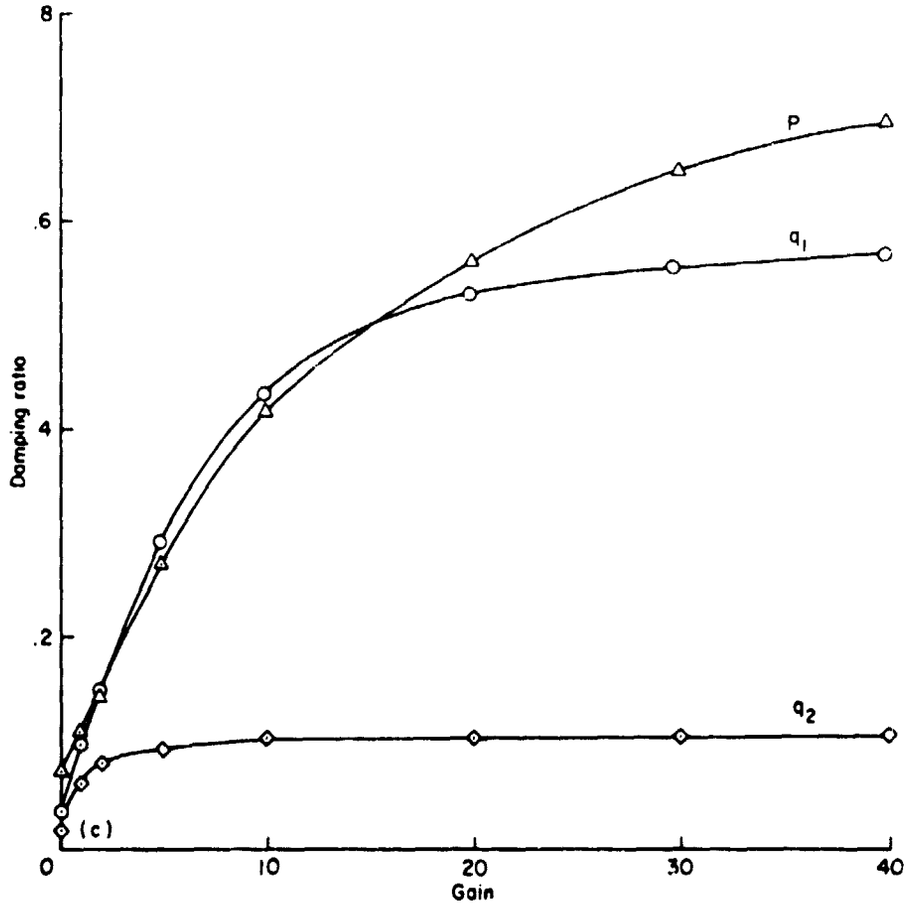

(c) Damping ratio of wing modes.

Figure 19.— Continued.

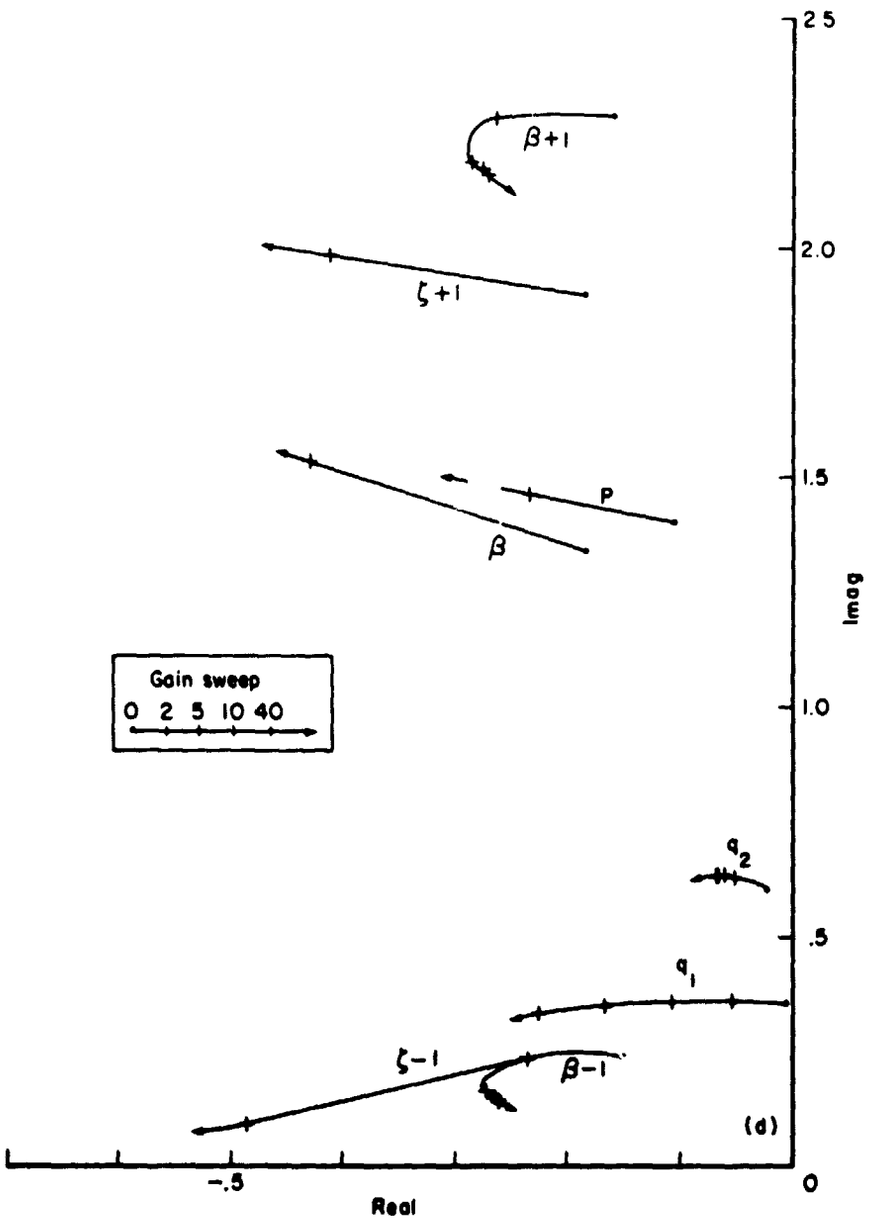

(d)' Root locus.

Figure 19.— Concluded.

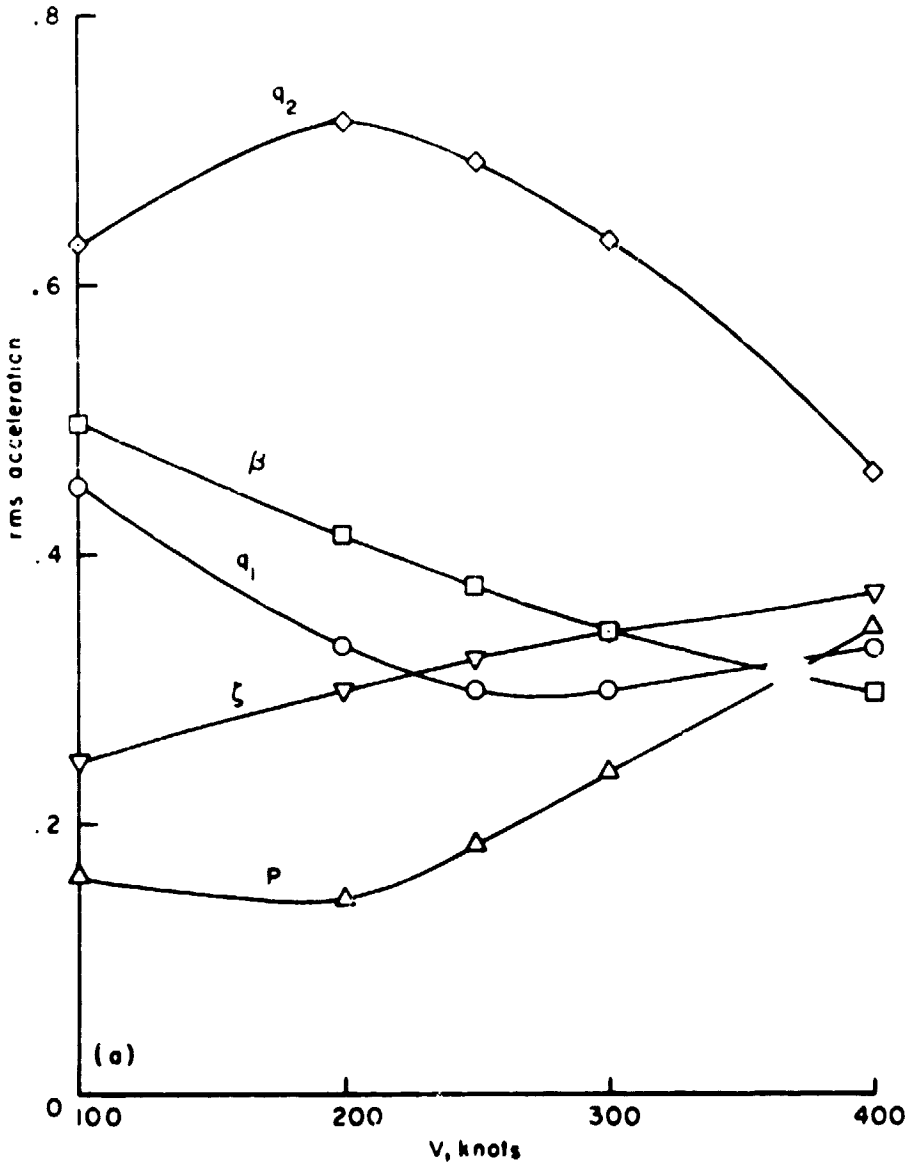

(a) Rms acceleration, optimum controller (closed loop/open loop).

Figure 20.— Control of Boeing rotor for velocity sweep, with optimum controller for each speed and with controller designed for 250 knots (Q = 5*.2, 10, 1, 10, 1).

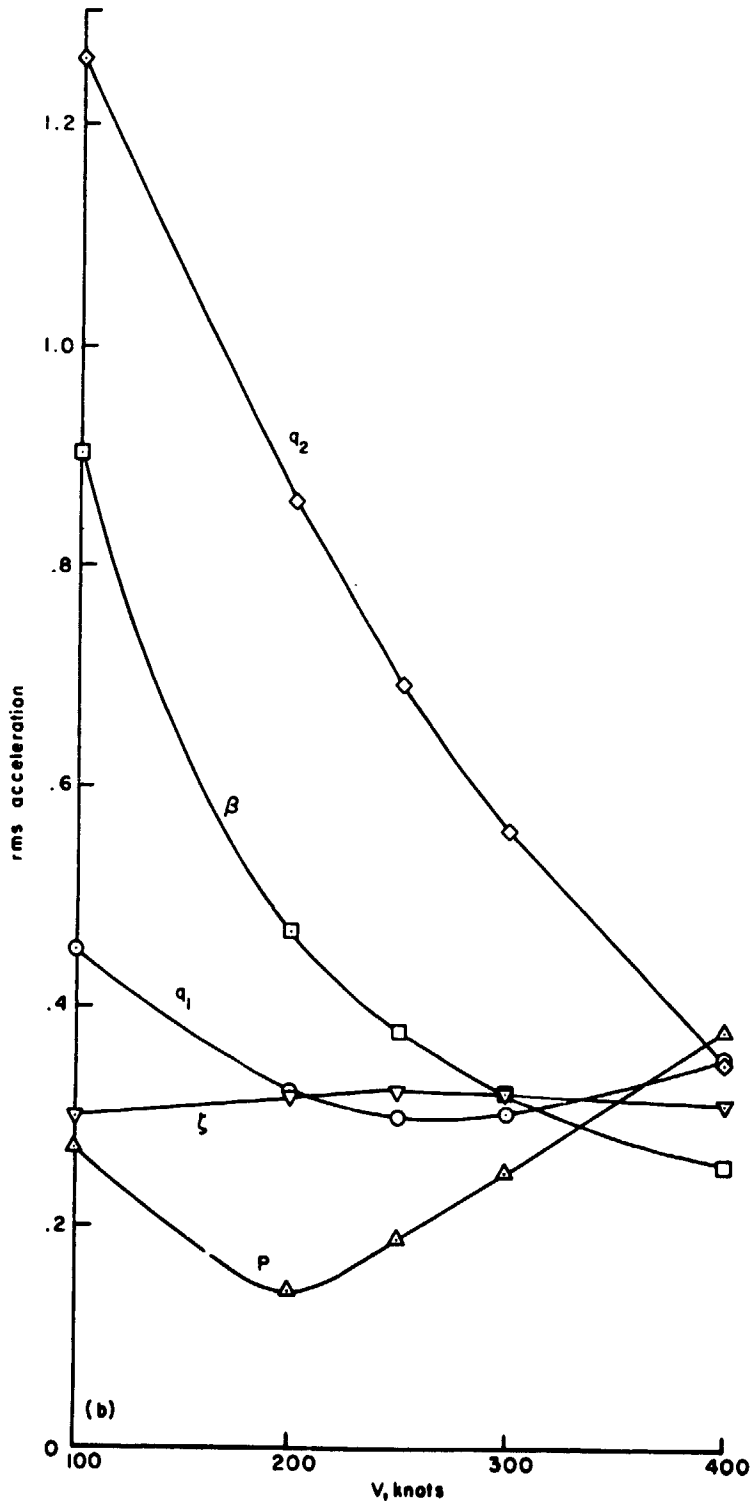

(b) Rms acceleration, 250 knot controller (closed loop/open loop).

Figure 20.— Continued.

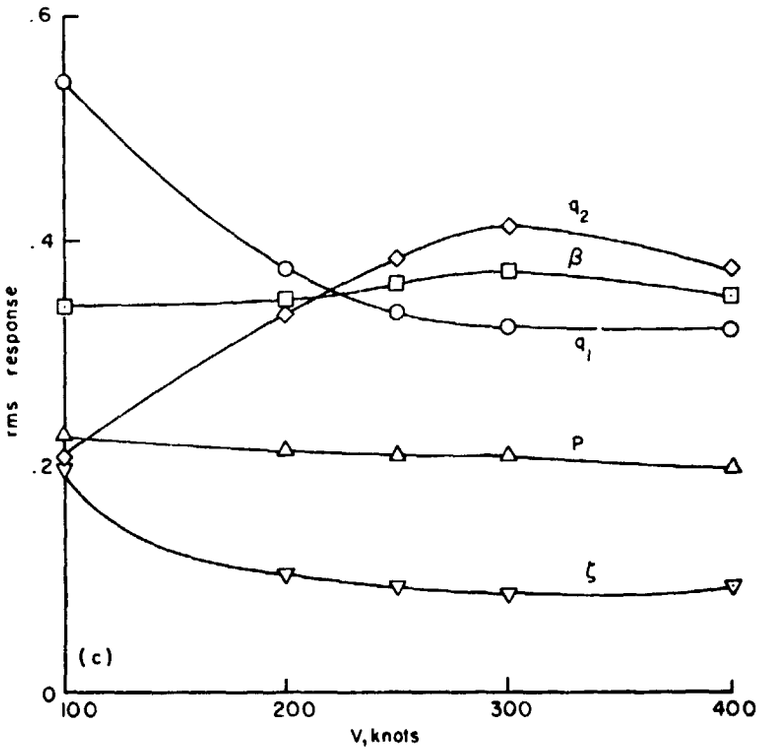

(c) Rms response, optimum controller (closed loop/open loop).

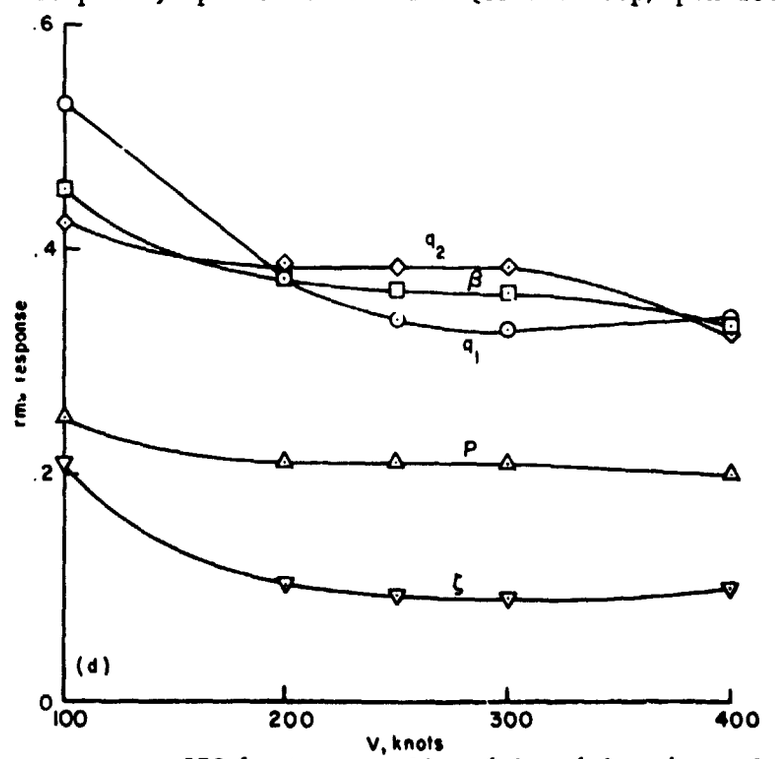

(d) Rms response, 250 knot controller (closed loop/open loop).

Figure 20.— Continued.

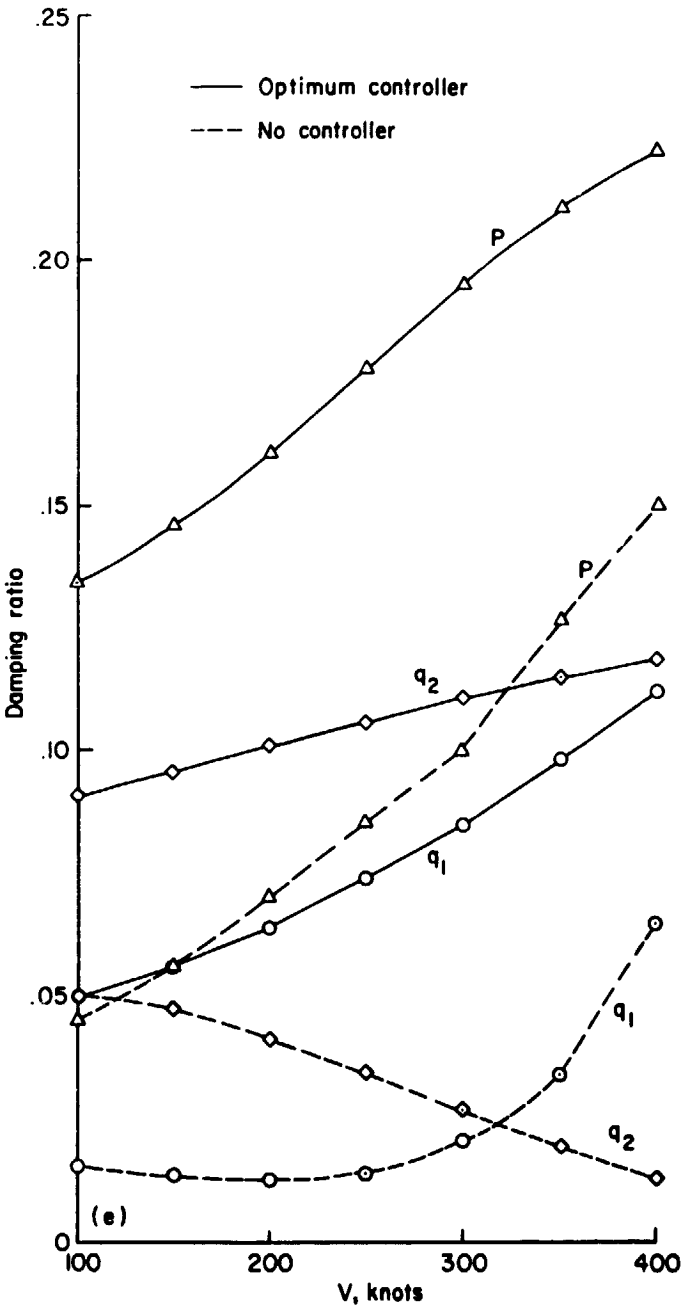

(e) Damping ratio, optimum controller.

Figure 20.– Continued.

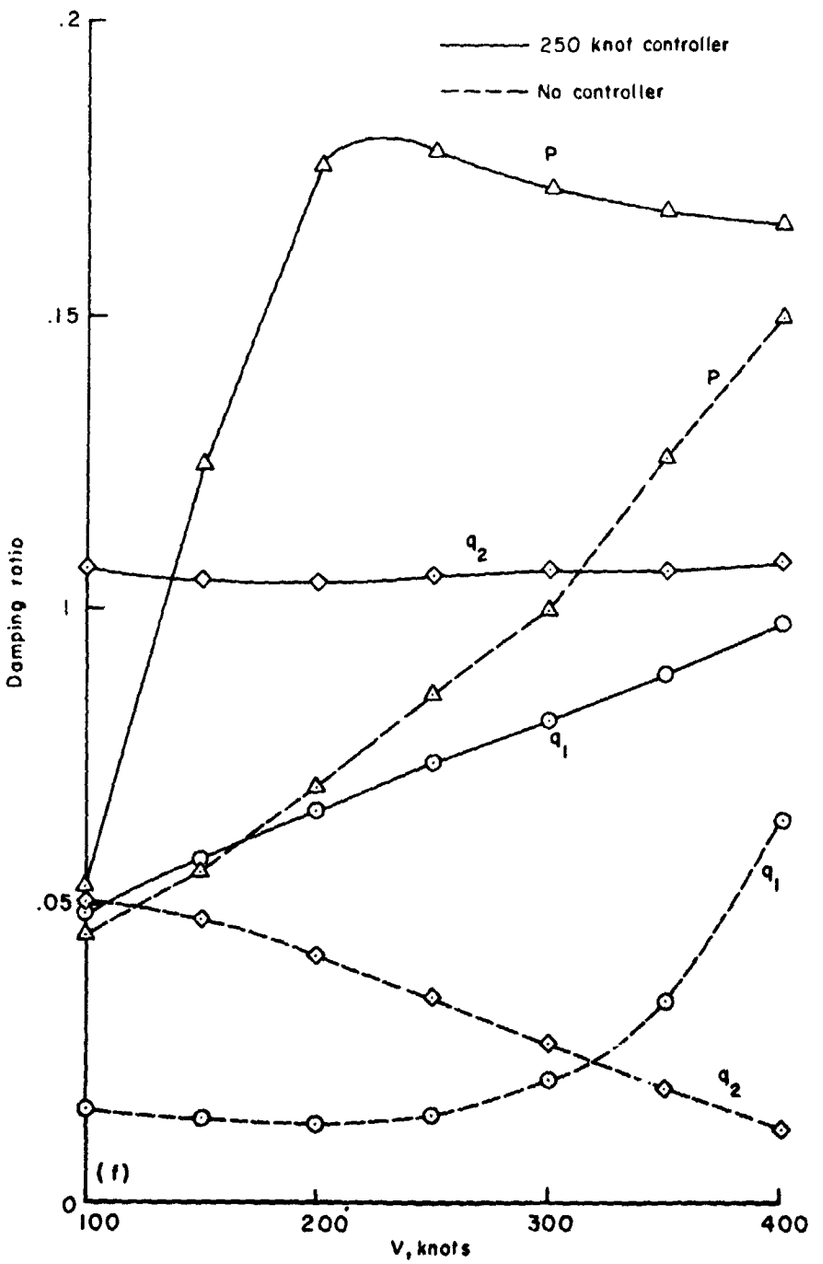

(f) Damping ratio, 250 knot controller.

Figure 20.— Continued.

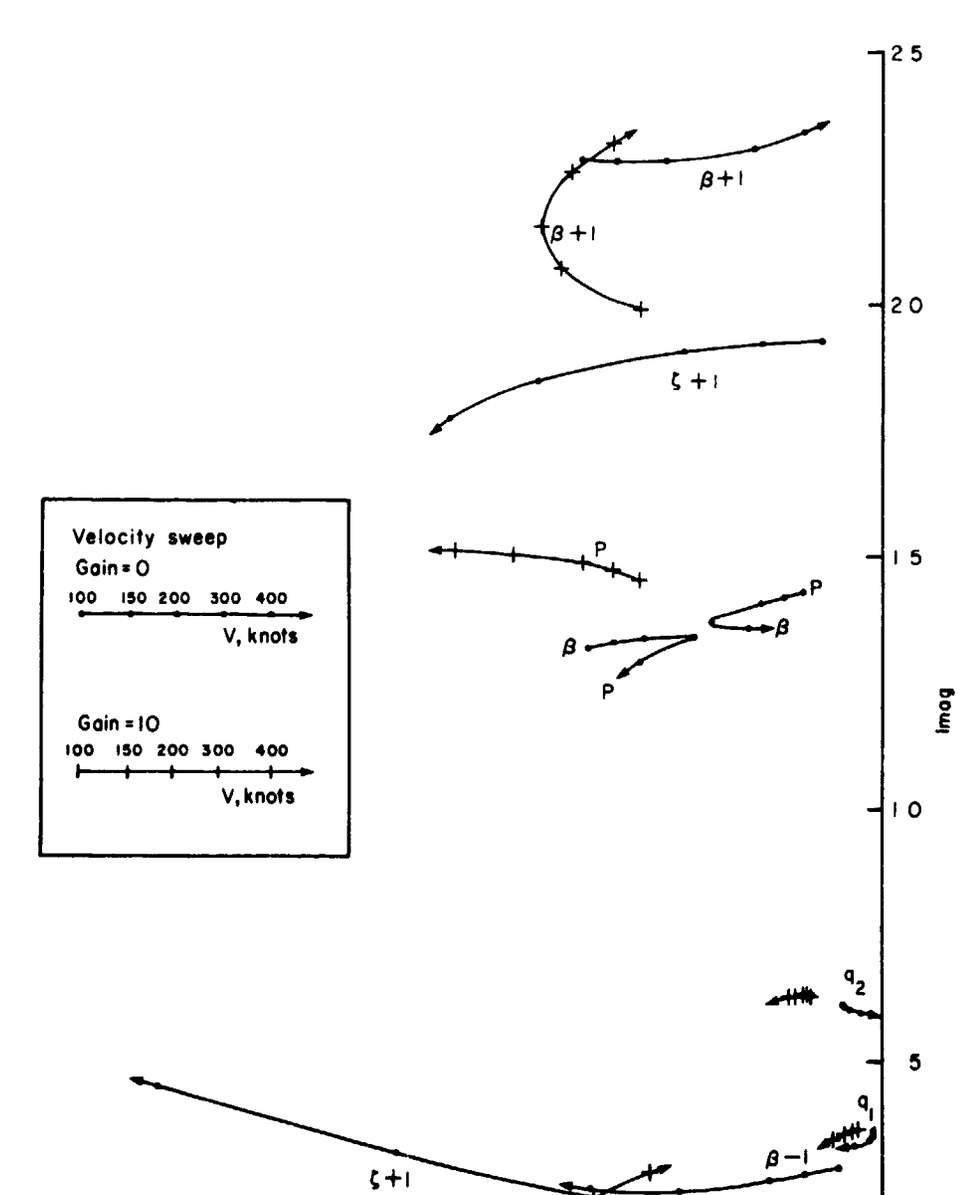

(g) Root locus, optimum controller.

Figure 20.— Continued.

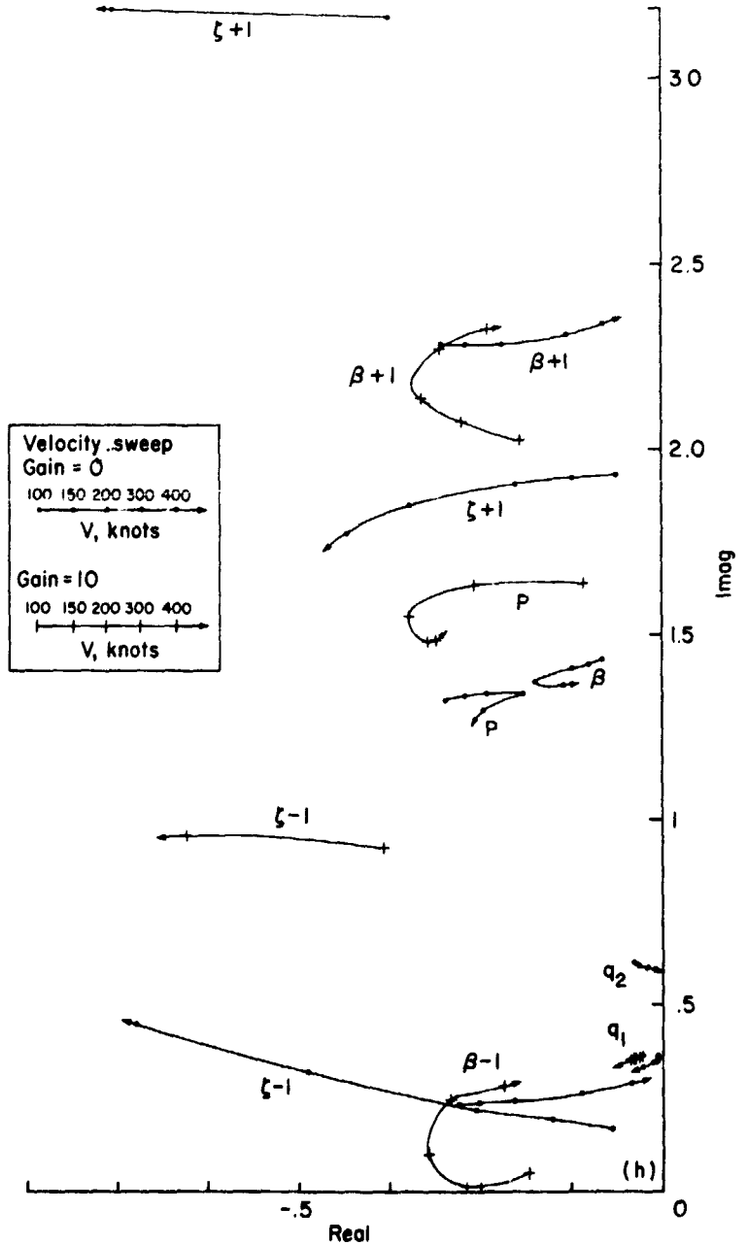

(h) Root locus, 250 knot controller.

Figure 20.– Continued.

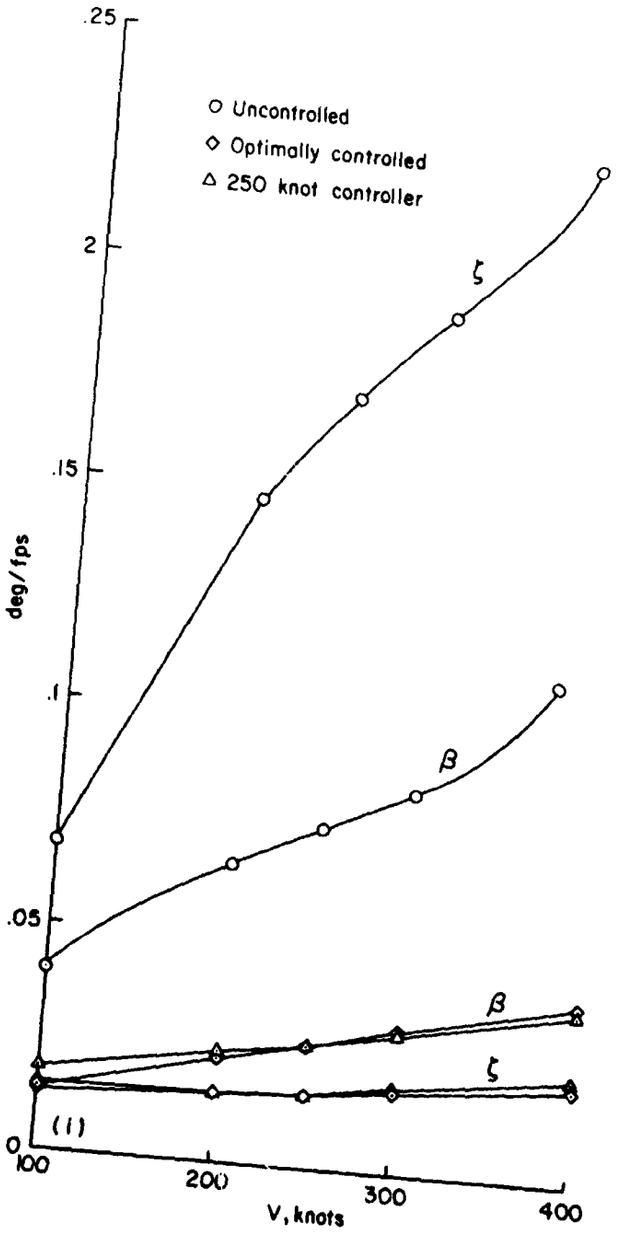

(i) Rms response of flap and lag motion.

Figure 20.– Continued.

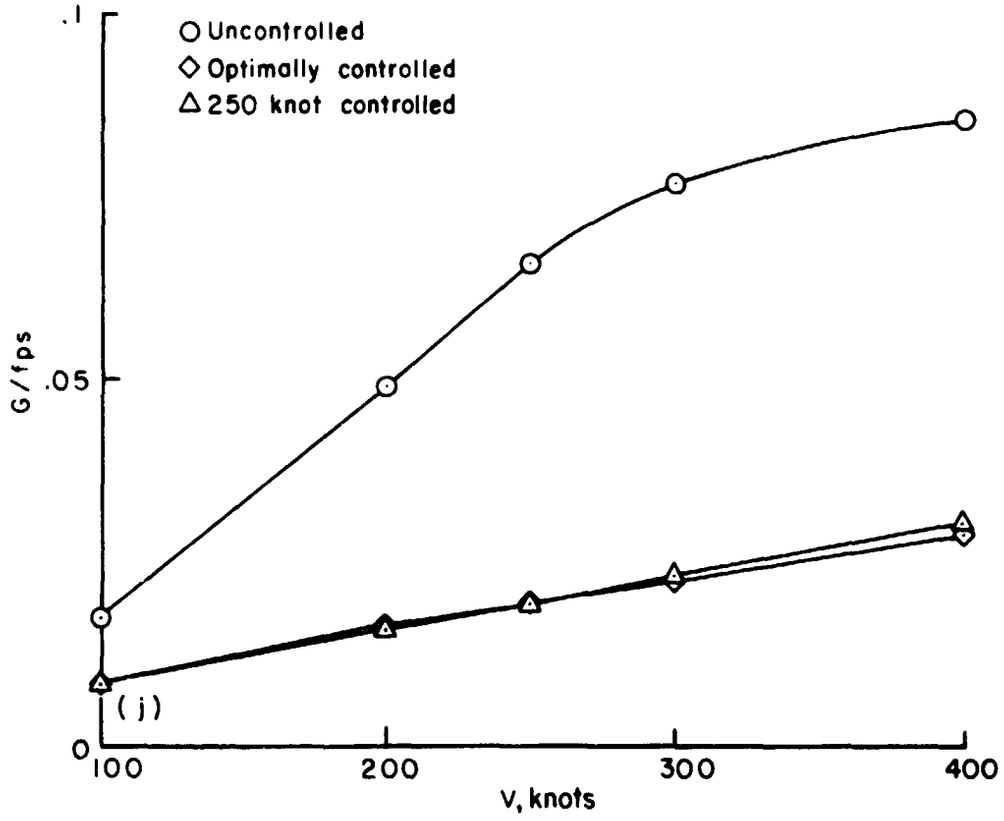

(j) Rms acceleration of wing vertical bending motion.

Figure 20.– Concluded.